# Virtual Screening and Experimental Validation of Bioactive Constituents from Selected Medicinal Plants of Western Ghats Region against Hepatitis B Virus and its Associated Complications

**Thesis submitted to**

**KLE ACADEMY OF HIGHER EDUCATION AND RESEARCH**

**BELAGAVI**

**(KLE DEEMED UNIVERSITY)**

**[Declared as Deemed-to-be-University u/s3 of the UGC Act, 1956 vide Govt. of India Notification No. F.9-19/2000-U.3(A)]**

**(Accredited 'A$^{+}$' Grade by NAAC) (3$^{rd}$ cycle)**

**[Placed in Category 'A' by MoE (GoI)]**

***For the award of the degree of***

## Doctor of Philosophy

## In the Faculty of Pharmacy

**By**


**Mr. Vishal Shivalingappa Patil M. Pharm,**

**(Registration No: KLEU/Ph.D./2020-21/DO1220056)**


**Under the Guidance of**


**Dr. Harish. D. R. Ph.D.**

**Scientist C, ICMR-National Institute of Traditional Medicine, Belagavi – 590010, Karnataka, India**


**Under the Co-Guidance of**


**Prof. (Dr.) Sunil S. Jalalpure Ph.D.**

**Principal, KLE College of Pharmacy, Belagavi, KLE Academy of Higher Education and Research, Belagavi – 590010, Karnataka, India**


**November 2023**

## UNDERTAKING

I, Mr. **Vishal Shivalingappa Patil** hereby declare that the information and the data mentioned in my thesis entitled **"Virtual Screening and Experimental Validation of Bioactive Constituents from Selected Medicinal Plants of Western Ghats Region against Hepatitis B Virus and its Associated Complications"** belongs to me and is original.

I am aware of definition of plagiarism as detailed below:

- An act or instance of using or closely imitating the language and thoughts of another author without authorization and the representation of that author's work as one's own, as by not crediting the original author.
- A piece of writing or other work reflecting such unauthorized use or imitation.
- The deliberate or reckless representation of another's words, thoughts or ideas as one's own without attribution in connection with submission of academic work, whether graded or otherwise.

I hereby declare that the thesis prepared by me is original-one and does not involve plagiarism anywhere. In case at a later stage it is found that I have indulged in plagiarism, then I am solely responsible for the same and the Institution is at liberty to take any disciplinary action against me including cancellation of dissertation or any other penalties imposed by the university.

**Place:** Belagavi
**Date:**

**Mr. Vishal Shivalingappa Patil**
Full time Ph.D. Research Scholar
Reg. No.: DO1220056
KAHER, Belagavi-590010

# PLAGIARISM REPORT

KLE ACADEMY OF HIGHER EDUCATION AND RESEARCH
(Formerly known as KLE University)
(Deemed-to-be-University established u/s 3 of the UGC Act, 1956)
Accredited A+ Grade by NAAC (3rd Cycle) Placed in Category 'A' by MoE (GoI)
*JNMC Campus, Nehru Nagar, Belagavi-590 010, Karnataka State, India*
☎: 0831-2444444 Web: http://www.kledeemeduniversity.edu.in E-mail: info@kledeemeduniversity.edu.in

Ref. No. KAHER/AA/23-24/D- 313 16th November 2023

Sir,

The soft copy of Ph.D. research thesis of **Mr. Vishal S. Patil, Faculty of Pharmacy, KAHER, Belagavi** has been submitted for anti-plagiarism check at the office of the undersigned through "Turn-it-in" package. The scan has been carried out and the scanned output reveals a match percentage of **6%** which is within the acceptable limit of 10%.

To obtain the comprehensive report of the plagiarism test, research scholar can send a mail to **diracademic@kledeemeduniversity.edu.in** along with the Registration Number, Name of the Scholar, Name of Guide/Co-guide and title of the thesis.

DIRECTOR * Deemed-to-be University * ACADEMIC AFFAIRS

for **Dr.(Mrs.) Roopa M. Bellad**
**Director, Academic Affairs**

**To,**

**Mr. Vishal S. Patil**
Full-Time Ph.D. Scholar,
2020-21 Batch,
Faculty of Pharmacy,
KAHER, **Belagavi.**

Cc to :

1. The Principal, KLE College of Pharmacy, KAHER, Belagavi
2. Dr. Harish D R, Scientist C, ICMR-NITM, Belagavi – Guide
3. Dr. Sunil S Jalalpure, Professor, KLE College of Pharmacy, KAHER, Belagavi – Co-Guide

**KLE ACADEMY OF HIGHER EDUCATION AND RESEARCH**

**(KLE DEEMED UNIVERSITY)**

**[Declared as Deemed-to-be-University u/s3 of the UGC Act, 1956 vide Govt. of India Notification No. F.9-19/2000-U.3(A)]**

**(Accredited 'A$^{+}$' Grade by NAAC) (3$^{rd}$ cycle)**

**[Place in Category 'A' by MoE (GoI)]**


# COPYRIGHT DECLARATION

***We hereby declare that* KLE ACADEMY OF HIGHER EDUCATION AND RESEARCH (KAHER), BELAGAVI-590010, KARNATAKA, INDIA, *shall have the rights to preserve, use and disseminate this thesis in print or electronic format for academic/research purpose.***

**Mr. Vishal S. Patil**
Full time Ph.D. Research Scholar Reg. No: DO1220056
KLE College of Pharmacy Belagavi,
KAHER, Belagavi-590010, India.

**Dr. Harish D. R.**
Scientist C,
ICMR National Institute of Traditional Medicine, Belagavi-590010, India.

**Prof. (Dr.) Sunil S. Jalalpure**
Principal,
KLE College of Pharmacy Belagavi
KAHER, Belagavi-590010, India.

**Place:** Belagavi
**Date:**

**KLE ACADEMY OF HIGHER EDUCATION AND RESEARCH**

**(KLE DEEMED UNIVERSITY)**

**[Declared as Deemed-to-be-University u/s3 of the UGC Act, 1956 vide Govt. of India Notification No. F.9-19/2000-U.3(A)]**

**(Accredited 'A$^{+}$' Grade by NAAC) (3$^{rd}$ cycle)**

**[Place in Category 'A' by MoE (GoI)]**


# DECLARATION

***I hereby declare that the thesis entitled*** **"Virtual Screening and Experimental Validation of Bioactive Constituents from Selected Medicinal Plants of Western Ghats Region against Hepatitis B Virus and its Associated Complications"** ***is a bonafide and original research carried out by me under the guidance of Dr. Harish D. R., Scientist C, ICMR-National Institute of Traditional Medicine, Belagavi-590010 and co-guidance of Prof. (Dr.) Sunil S. Jalalpure, Principal, KLE College of Pharmacy Belagavi, KAHER, Belagavi-590010. The thesis or any part of thereof has not formed the basis for the award of any degree/fellowship or similar title to any candidate of any University.***

**Place:** Belagavi
**Date:**

**Mr. Vishal Shivalingappa Patil**
Full time Ph.D. Research Scholar
Reg. No: DO1220056
KLE College of Pharmacy, Belagavi
KAHER, Belagavi-590010

.

**KLE ACADEMY OF HIGHER EDUCATION AND RESEARCH**

**(KLE DEEMED UNIVERSITY)**

**[Declared as Deemed-to-be-University u/s3 of the UGC Act, 1956 vide Govt. of India Notification No. F.9-19/2000-U.3(A)]**

**(Accredited 'A$^{+}$' Grade by NAAC) (3$^{rd}$ cycle)**

**[Place in Category 'A' by MoE (GoI)]**


# CERTIFICATE

***This is to certify that the thesis entitled* "Virtual Screening and Experimental Validation of Bioactive Constituents from Selected Medicinal Plants of Western Ghats Region against Hepatitis B Virus and its Associated Complications"** ***is a bonafide record of original research carried out by Mr. Vishal Shivalingappa Patil under the guidance of Dr. Harish D. R., Scientist C, ICMR-National Institute of Traditional Medicine, Belagavi-590010 and co-guidance of Prof. (Dr.) Sunil S. Jalalpure, Principal, KLE College of Pharmacy Belagavi, KAHER, Belagavi-590010.***

**Place:** Belagavi
**Date:**

**Prof. (Dr.) M. S. Ganachari**
Dean, Faculty of Pharmacy
KAHER, Belagavi-590010

**KLE ACADEMY OF HIGHER EUCATION AND RESEARCH**

**(KLE DEEMED UNIVERSITY)**

**[Declared as Deemed-to-be-University u/s3 of the UGC Act, 1956 vide Govt. of India Notification No. F.9-19/2000-U.3(A)]**

**(Accredited 'A$^{+}$' Grade by NAAC) (3$^{rd}$ cycle)**

**[Place in Category 'A' by MHRD (GoI)]**

# CERTIFICATE

***This is to certify that the thesis entitled* "Virtual Screening and Experimental Validation of Bioactive Constituents from Selected Medicinal Plants of Western Ghats Region against Hepatitis B Virus and its Associated Complications"** ***is a bonafide record of original research carried out by Mr. Vishal Shivalingappa Patil for the award of degree of DOCTOR OF PHILOSOPHY IN FACULTY OF PHARMACY under my supervision and guidance.***

**Place**: Belagavi
**Date**:

**Guide Signature**
**Dr. Harish D. R.**
**Scientists C,**
ICMR-National Institute of Traditional Medicine,
Belagavi-590010, India

**Co-Guide Signature**
**Prof. (Dr.) Sunil S. Jalalpure**
**Principal,**
KLE College of Pharmacy
Belagavi, KAHER,
Belagavi-590010, India.

**KLE ACADEMY OF HIGHER EDUCATION AND RESEARCH**

**(KLE DEEMED UNIVERSITY)**

**[Declared as Deemed-to-be-University u/s3 of the UGC Act, 1956 vide Govt. of India Notification No. F.9-19/2000-U.3(A)]**

**(Accredited 'A$^{+}$' Grade by NAAC) (3$^{rd}$ cycle)**

**[Place in Category 'A' by MoE (GoI)]**

# CERTIFICATE

***This is to certify that the thesis entitled* "Virtual Screening and Experimental Validation of Bioactive Constituents from Selected Medicinal Plants of Western Ghats Region against Hepatitis B Virus and its Associated Complications"** ***is a bonafide record of original research carried out by Mr. Vishal Shivalingappa Patil under the guidance of Dr. Harish D. R., Scientist C, ICMR-National Institute of Traditional Medicine, Belagavi-590010 and co-guidance of Prof. (Dr.) Sunil S. Jalalpure, Principal, KLE College of Pharmacy Belagavi, KAHER, Belagavi-590010.***

**Place:** Belagavi
**Date:**

**Signature**
**Prof. (Dr.) Sunil S. Jalalpure**
Principal, KLE College of Pharmacy Belagavi,
KAHER, Belagavi-590010, India

## ACKNOWLEDGEMENTS

It is with great hat tip that I express my sincere gratitude to my advisor, **Dr. Harish D. R.**, for the constant support, for his patience, motivation, and immense knowledge during my Ph.D. research. Having him as my advisor and mentor during my Ph.D study was a great experience. He guided me throughout the entire research and writing process. I'd like to thank to **Dr. Sunil S. Jalalpure,** Co-guide and Principal, KLE College of Pharmacy, Belagavi for his constant support and guidance. I'd like to thank to **Dr. Subarna Roy**, Director, ICMR-National Institute of Traditional Medicine for their insightful comments and encouragement during my Ph.D. research. I thank to Indian Council of Medical Research, Department of Health Research, New Delhi (Grant No. ISRM/12(61)2019) for extramural funding and ICMR-National Institute of Traditional Medicine, Belagavi for intramural funding and facilities. Thanks to the Retired Director, **Dr. Dinakar M. Salunke** and **Dr. Ravinder Kumar**, International Centre for Genetic Engineering and Biotechnology, New Dehli, for providing HepG2.2.15 cell line.

Apart from my advisors, I'd like to thank the rest of my Ph.D. committee: **Prof. (Dr.) P. A. Patil**, **Prof. (Dr.) Roopa Bellad**, **Dr. M. S. Ganachari, Dr. Shankar Alegaon, Dr. P. M. Dandagi** Director of Academic Affairs, KAHER, and thank to **Dr. N.A. Khatib**, **Dr. Harsha V. Hegde** and **Dr. Umashankar Vetrivel** for their insightful comments and encouragement.

In the last three years, I have enjoyed discussions with my colleagues (**Mrs. Rajitha, Ms. Rajashree, Dr. Priyanka, Dr. Pukar, Dr. Anushree, Mr. Sanjay D, Dr. Vishwambhar, Mr. Shamanand, Mr. Akshay, Dr. Himani, Mr. Veerkumar, Mr. Sandeep, Mr. Ganesh, Mr. Kashinath, Mr. Jagadeesh, Ms. Sanjana, Mrs. Chaitanya, Dr. Faizan, Mr. Swarup, Ms. Aarati, and Mr. Sathgowda**), restless nights as we worked on deadlines, and had many laughs and tears together. For their direct and indirectsupport in completing this study, I am also grateful to the teaching and non-teaching faculties of ICMR-National Institute of Traditional Medicine and KLE College of Pharmacy, Belagavi.

Last but not least, I want to thank my family for supporting me both mentally and emotionally during the writing of this thesis and in general.

**Place:** Belagavi Mr. Vishal Shivalingappa Patil

**Date:**

# CONTENTS

# LIST OF TABLES

# LIST OF FIGURES

# LIST OF SUPPLEMENTARY TABLES

14. Supplementary Table 14: (1) Column 1: List of genes/protein molecules regulated by the Hepatitis B virus (2) Column 2 and 3 Peer review of Hepatitis B protein induced hepatitis and its effect on protein molecules (3) Column 4: References.
15. Supplementary Table 15: (1) Column 1: List of genes/protein molecules regulated by the Alcohol (2) Column 2: Peer review of Alcohol induced hepatotoxicity and its effect on protein molecules (3) Column 3: References.
16. Supplementary Table 16: (1) Column 1: List of genes/protein molecules regulated by the Acetaminophen (2) Column 2: Peer review of Acetaminophen induced hepatotoxicity and its effect on protein molecules (3) Column 3: References.
17. Supplementary Table 17: (1) Column 1: List of genes/protein molecules regulated by the Isoniazid (2) Column 2: Peer review of Isoniazid induced hepatotoxicity and its effect on protein molecules (3) Column 3: References.
18. Supplementary Table 18: (1) Column 1: List of genes/protein molecules regulated by the D-Galacotosamine (2) Column 2: Peer review of D-Galacotosamine induced hepatotoxicity and its effect on protein molecules (3) Column 3: References.
19. Supplementary Table 19: (1) Column 1: List of genes/protein molecules regulated by the Lipopolysaccharide (2) Column 2: Peer review of Lipopolysaccharide induced hepatotoxicity and its effect on protein molecules (3) References.
20. Supplementary Table 20: (1) Column 1: List of genes/protein molecules regulated by the Rifampicin (2) Column 2: Peer review of Rifampicin induced hepatotoxicity and its effect on protein molecules (3) Column 3: References.
21. Supplementary Table 21: (1) List of genes/protein molecules regulated by the Thioacetamide (2) Peer review of Thioacetamide induced hepatotoxicity and its effect on protein molecules (3) Column 3: References.

22. Supplementary Table 22: Molecular pathways modulated by HBV. 1546 genes modulated 220 molecular pathways. HBV associated pathways were highlighted with yellow color.
23. Supplementary Table 23: Molecular pathways modulated by Acetaminophen. 152 genes modulated 185 molecular pathways. HBV associated pathways were highlighted with yellow color.
24. Supplementary Table 24: Molecular pathways modulated by Isoniazid. 72 genes modulated 184 molecular pathways. HBV associated pathways were highlighted with yellow color.
25. Supplementary Table 25: Molecular pathways modulated by Alcohol. 434 genes modulated 200 molecular pathways. HBV associated pathways were highlighted with yellow color.
26. Supplementary Table 26: Molecular pathways modulated by D-Galactosamine. 72 genes modulated 185 molecular pathways. HBV associated pathways were highlighted with yellow color.
27. Supplementary Table 27: Molecular pathways modulated by Lipopolysaccharide 278 genes modulated 202 molecular pathways. HBV associated pathways were highlighted with yellow color.
28. Supplementary Table 28: Molecular pathways modulated by Thioacetamide. 57 genes modulated 167 molecular pathways. HBV associated pathways were highlighted with yellow color.
29. Supplementary Table 29: Molecular pathways modulated by Rifampicin. 54 genes modulated 172 molecular pathways. HBV associated pathways were highlighted with yellow color.

## LIST OF SUPPLEMENTARY FIGURES

# ABBREVIATIONS

**APHA,** *Andrographis paniculata* hydroalcoholic; **ANOVA**, Analysis of variance; **BE,** Binding energy; **BPHA**, *Bidens pilosa* hydroalcoholic; **BPM**, *Bidens pilosa* methanolic; **CAHA**, *Centella asiatica* hydroalcoholic; **cccDNA**, Covalently closed circular DNA; **$CC_{50}$**, Cytotoxic concentration 50; **DMEM**, Dulbecco's Modified Eagle Medium; **DLS**, Druglikeness score; **DNA Pol**, DNA polymerase; **FBS**, Fetal bovine serum; **FDR**, False discovery rate; **GSH**, Glutathione; **HBeAg**, Hepatitis B e-antigen; **HBsAg**, Hepatitis B surface antigen; **HBV**, Hepatitis B virus; **HBx**, HBV X protein; **HCC**, Hepatocellular carcinoma; **IBSC**, Institutional Biosafety Committee; **$IC_{50}$**, Inhibitory concentration 50; **ICGEB**, International Centre for Genetic Engineering and Biotechnology, **KEGG**, Kyoto Encyclopedia of Genes and Genomes; **LC-MS**, Liquid chromatography-mass spectrometry; **locPREFMD**, local Protein structure REFinement *via* Molecular Dynamics; **LPO**, lipid peroxidase; **MAPK**, Mitogen-activated protein kinases; **MD**, Molecular dynamics; **MF**, Molecular formula; **mg**, Milligram; **mL**, Milliliter; **MM-GBSA**, Molecular mechanics with generalised Born and surface area solvation; **MTT**, 3-[4,5-dimethylthiazol-2-yl]-2,5 diphenyl tetrazolium bromide; **MW**, Molecular weight; **NFKB**, Nuclear factor kappa B; **NRTI**; Nucleotide Reverse Transcriptase Inhibitors; **NTCP**, Sodium taurocholate co-transporting polypeptide; **Pa**, Pharmacological activity; **PBS**, Phosphate buffer saline; **PCIDB**, PhytoChemical Interactions DB; **PE**, Potential energy; PGG, Pentagalloylglucose; pgRNA, Pregenomic RNA; **rcDNA**, Relaxed circular DNA; **RCSB**, Research collaboratory for structural bioinformatics; **RMSD**, Root-mean-square-deviation; **RMSF**, Root-mean-square-fluctuation; **RT**, Reverse transcriptase; **SGOT**, Serum glutamic-oxaloacetic transaminase; **SGPT**, Serum glutamic pyruvic transaminase; **SOD**; Superoxide dismutase; **STRING**, Search Tool for the Retrieval of Interacting Genes/Proteins; **TCN**, *Terminalia chebula* n-butanol fraction; **TCW**, *T. chebula* water fraction; **TDF**, Tenofovir Disoproxil Fumarate; **TP**, Total protein, **TPHA,** *Thespesia populnea* hydroalcoholic; **YMDD**, Tyrosine (Y)-Methionine (M)-Aspartic acid (D)-Aspartic acid (D).

# ABSTRACT

**Introduction:** Traditional medicines are widely utilized in the Western Ghats region of India to treat various liver diseases and viral-like infections. However, such practices lack scientific evidences and mechanisms of actions at the molecular level. To date, HIV-reverse transcriptase (RT) inhibitors are used to manage hepatitis B virus (HBV) infection due to its functional similarity and conserved active site motif with HBV-RT, and these inhibitors pose severe side effects, development of drug resistance, and are also expensive.

**Objective:** This study intends to identify phytocompounds having druggability and non-toxic profiles with potential activity against HBV protein targets and HBV-induced hepatocellular carcinoma (HCC) by *in silico, in vitro, and in vivo* studies.

**Methods:** The details of phytocompounds form selected plants used in the Western Ghats region were collected from phytochemical databases and publications. The druggability and toxicity of these compounds were predicted using MolSoft and ADVERpred, respectively. The probable targets of these phytocompounds were predicted using BindingDB. Moreover, compound-gene set-pathways, cellular processes, and functional enrichment analyses were also performed using STRING and KEGG pathway databases. Subsequently, plant-compound-target-disease pathway networks were constructed using Cytoscape. Homology modeling of HBV-RT and HBx was executed through Phyre2, Modeller, and virtual screening of the shortlisted phytocompounds was performed using AutoDock vina executed through POAP pipeline. Finally, molecular dynamics (MD) simulations of the most potential protein-ligand complexes were performed using Schrödinger Desmond. LC-MS analysis of prepared plant extracts/enriched fractions was performed and followed by RT inhibitory activity, time-dependent HBsAg and HBeAg secretion, and intracellular HBV DNA, and pgRNA by qRT-PCR, HBx-HBXIP inhibition was performed in HBV expressing HepG2.2.15 cell line. Finally, the prioritized plant extract and fraction by *in vitro* studies were tested for hepatoprotective potential in an alcohol-induced liver injury model in rats (model which mimics the pathophysiology of HBV infection that is identified through system biology approach). Serum lipid profile and liver function tests; tissue anti-oxidant and pro-inflammatory markers, and histology of liver were examined.

**Results:** Firstly, 15 molecules from 3 plants (*Terminalia chebula* (6 compounds), *Bidens pilosa* (5 compounds), and *Centella asiatica* (4 compounds)) were identified as potential inhibitors of YMDD and RT1 motif of HBV-RT. MD simulation demonstrated stable interactions of these 15 phytocompounds with HBV-RT, of which 1,2,3,4,6-Pentagalloyl Glucose (PGG) was identified as a lead molecule. Secondly, flavonoids and diterpenoids from *Andrographis paniculata* (11 compounds) and *Thespesia populnea* (3 compounds) were identified to modulate multiple targets and pathways involved in HBV-induced HCC. Thirdly, flavonoids from *Andrographis*

*paniculata* were identified as potential compounds against HBV HBx protein. Fourthly, the study identified alcohol- and LPS-induced hepatitis (out of seven chemically induced hepatitis) to resemble the molecular mechanisms involved in HBV-induced hepatitis. LC-MS analysis revealed the presence of *in silico* identified compounds in the prepared extract/fraction. *T. chebula* n-butanol fraction (TCN), water fraction (TCW), A. paniculata hydroalcoholic extract (AP) (500µg/mL) showed potent RT inhibition, decreased intracellular HBV DNA, and pgRNA, and time-dependent inhibition of HBsAg and HBeAg levels compared to pentagalloyl glucose (PGG) and Tenofovir Disoproxil Fumarate (TDF). In the hepatoprotective animal study, observed a significant amelioration of the liver and kidney function by all doses of TC, a moderate dose of AP, and a moderate dose of combination which was evidented by decreased levels of SGPT, SGOT, ALP, BUN, and creatinine levels; regulating the inflammation by inhibiting TNF-α and IL6 secretions; and regulation of anti-oxidant biomarkers in the liver tissue viz., GSH, SOD, and LPO; which was followed by histological restoration of the liver.

**Conclusion:** Theoretical knowledge combined with predicted and validated results of this study confirms TCN, TCW, AP, and PGG as valuable resources for the management of HBV infection and associated complications like HCC.

**Keywords**: *Andrographis paniculata*, Bioinformatics, Hepatitis, HepG2.2.15, Reverse Transcriptase, *Terminalia chebula*

# INTRODUCTION

Viral hepatitis is characterized as the inflammatory response of the liver resulting from infection by viral pathogens. There are five distinct hepatitis viruses (A–E) that specifically target and multiply inside the hepatocytes of the liver.[1] All five viruses are from different viral families and have diverse molecular properties, although they all cause similar clinical symptoms.[1,2] Amongst them, the Hepatitis B virus (HBV) is a most common and serious public health threat that can trigger a variety of hepatic diseases ranging from acute illness to hepatocellular carcinoma.[3] The HBV infected more than 400 million individuals throughout the globe and accounted for one million deaths every year due to its significant complications such as cirrhosis and HCC.[4] HBV belongs to the family Hepadnaviridae and that enters into the host cell by using the sodium taurocholate co-transporting polypeptide (NTCP) hepatocyte receptor. HBV is classified as a hepatotropic DNA virus and has a circular, double-stranded genome of about 3.2 kilobases in length. The viral capsid is enveloped, providing further protection, and it replicates via reverse transcription of an RNA intermediate, the pregenomic RNA (pgRNA).[5]

HBV genome carries 4 major genes (i) HBsAg - codes for the three envelope proteins (The PreS1 (Large), PreS2 (Medium), and Surface (Small) genes), which are crucial in the formation of Dane particles, viral morphogenesis, infection, and propagation[6,7] (ii) The polymerase (P) gene- codes for its 4 domains i.e. terminal protein (TP), spacer (SP), reverse transcriptase (RT), and ribonuclease H (RNase H) for viral RNA packaging and replication[8,9], (iii) The core gene - codes for the nucleocapsid protein and the pre-core protein for synthesis and secretion of hepatitis B e antigen (HBeAg)[10] and (iv) The X gene - codes for the regulatory X protein, an important regulatory protein responsible for viral infection, replication, pathogenesis, and carcinogenesis.[11] Among

these genes, HBV polymerase, and X protein gained high intense interest because of their multifunctional role in the HBV replication cycle. Researchers demonstrated HBV DNA polymerase RT domain is the major drug target due to its major functional role in the protein priming and HBV cDNA synthesis activity. Further, the TP domain is another potential drug target because residue Y63 and T3 motif from the TP domain are necessary for "RNA binding, RNA packaging, and protein priming".[9] Similarly, RNaseH is also a novel therapeutic target because it packages and primes RNA throughout viral synthesis of DNA. Blocking RNaseH causes capsids to accumulate RNA:DNA heteroduplexes, that prematurely block minus-polarity DNA strands and prevent plus-polarity DNA synthesis. At present, no medicines have been produced to inhibit RNaseH activity because of a lack of suitable screening tests.[12]

Current treatment for chronic HBV infection includes five nucleoside RT inhibitors (NRTIs) i.e. "Lamivudine (Epivir), Adefovir dipivoxil (Hepsera), Entecavir (Baraclude), Telbivudine (Tyzeka), and Tenofovir disoproxil fumarate (Viread)" and two immune modulators i.e. Pegasys (Pegylated Interferon) and Intron A (Interferon Alpha).[13] To date, Entecavir and Tenofovir are the most effective hits to inhibit HBV DNA synthesis by targeting priming (minus-strand DNA synthesis) and DNA strand elongation.[14] Recently, Clevudine (thymidine analog) was identified to inhibit all stages of DNA synthesis which target DNA chain elongation via reverse transcription of pgRNA by the viral polymerase.[9] NRTIs have a potential effect against HBV replication but are associated with drug resistance, and side effects such as nephrotoxicity, myopathy, and neuropathy and require life-long therapy.[9,14–16] Compared to NRTIs, interferon therapy is more effective but requires careful evaluation due to greater adverse drug reactions and is highly contraindicated in pregnancy and patients with decompensated cirrhosis.[17] For these reasons, the World Health Organization (WHO) has

recommended a continuous search for new drugs that are cheaper, safer, and greater effective against complex diseases like HCC. An appropriate source for such goals is the wide range of bioactive phytoconstituents that are present in the medicinal plants that are used in different traditional / folklore medicinal practices.

To date, India, China, Egypt, South America, and many other countries are still utilizing traditional medicines/ herbal formulations/ plant-based remedies for the treatment, control, and management of cancer, hypertension, diabetes, jaundice, skin diseases, neurological disorders, tuberculosis, and various infections of unknown etiology. As per the WHO, 60% of the worldwide population uses herbal/traditional medicine for primary health care and about 80% of the population in developing countries relies almost mostly on it for their primary health care needs.[18] The Western Ghats region in India is a treasure house for various medicinal plants and is ranked among the 34 global biodiversity hotspots. The majority of the population in the Western Ghats region mainly rely on traditional/folklore for their medical care.[19]

Thus, in the current research, 18 medicinal plants that are practiced and utilized to treat various diseases resembling viral hepatitis and their complications by local/tribal healers in the Western Ghats area of North Karnataka, India were selected to identify the anti-HBV and hepatoprotective compounds/extracts/fractions by utilizing computational, *in vitro*, and *in vivo* studies.

# AIM AND OBJECTIVES

## AIM

Identification of anti-HBV and hepatoprotective bioactive constituents from Traditional medicinal plants from the Western Ghats region of Karnataka.

## OBJECTIVES OF THE STUDY

1. To perform virtual screening of phytocompounds from selected TMs against potential targets of HBV by molecular docking, molecular dynamic simulation, and network pharmacology.
2. To evaluate the anti-HBV and hepatoprotective activity of selected phytocompounds/enriched fractions by *in vitro* studies.
3. To evaluate the selected phytocompound(s)/enriched fraction(s) for hepatoprotective potential in laboratory animal model.

# REVIEW OF LITERATURE

Hepatitis disease was long known before its discovery as catarrhal jaundice in 1865 which was later redefined as hepatic inflammation in the 1930s.[20] The major causes of hepatitis includes "(1) hepatotropic viruses: hepatitis A-E (2) toxins: alcohol, $CCl_4$, others, (3) medication: acetaminophen, anti-tuberculosis drugs, antibiotics, many other, (4) systemic viral infections: adenoviruses, herpesviruses, arboviruses (yellow fever, Crimean–Congo haemorrhagic fever, Rift Valley fever), (5) severe sepsis: gram negative bacteria, (6) ischaemic hepatitis: shock, including hypovolaemic shock due to trauma, and (7) auto immune hepatitis: type 1 and type 2".

## 3.1. Viral Hepatitis

Viral hepatitis is liver inflammation induced by hepatitis viruses (A-E); that replicate in liver cells and are from different viral families and have diverse molecular properties, although they all cause similar clinical symptoms.[2] Table 1 provides the characteristics of different hepatitis viruses.

**Table 1: Features and clinical characteristics of hepatitis viruses**

| **Types of nucleic acid** | HAV | HBV | HCV | HDV | HEV |
|---|---|---|---|---|---|
| | RNA | DNA | RNA | RNA | RNA |
| **Transmission** | Fecal-oral | Blood; sexual; mother to child | Blood and its products & Sexual | Blood and its products | Fecal-oral |
| **Risk factors** | Low socio-economic status | Sexual contact; IV injections of drugs. | Sexual contact; IV injections of drugs. | Sexual contact; IV injections of drugs. | Consuming polluted water, consuming shellfish or pork, and visiting endemic areas. |
| **Vaccine** | Yes | Yes | No | Yes | Yes |
| **Chronic infection** | No | Yes | Yes | Yes | Yes |

### 3.2. Hepatitis B virus

HBV is one of five types of hepatitis viruses that pose a serious public health risk by triggering a wide range of liver disorders.[3] HBV was identified in the 1960s. According to the International Committee on Taxonomy of Viruses classification, it belongs to the family of the hepadnaviridae and Orthohepadnavirus genus. The hepatitis B virion is known as a Dane particle having a size of 42nm diameter.[21] The virion consists of a viral envelope composed of surface proteins, hepatotropic DNA virus with a circular, double-stranded genome (~3.2kb) and enclosed in a nucleocapsid made of 120 core protein dimmers.[22,23] The replication of the virus takes place *via* an RNA intermediate RNA reverse transcriptase. "The transcription is controlled by 4 ORFs that code for 7 proteins (3 surface proteins, core and e-antigens, polymerase, and X transactivator); four promoters and two enhancers coordinate the expression of these genes to generate six unique mRNAs (two 3.5kb transcript core and e-antigens, the polymerase, and for pregenomic RNA (pgRNA); one 2.4kb transcript for the large surface protein; two 2.1kb transcripts for the middle and small surface proteins; and one 0.7kb mRNA for the X transactivator protein".[22,24] Figure 1 and Figure 2 represents the HBV structure and its life cycle, respectively.

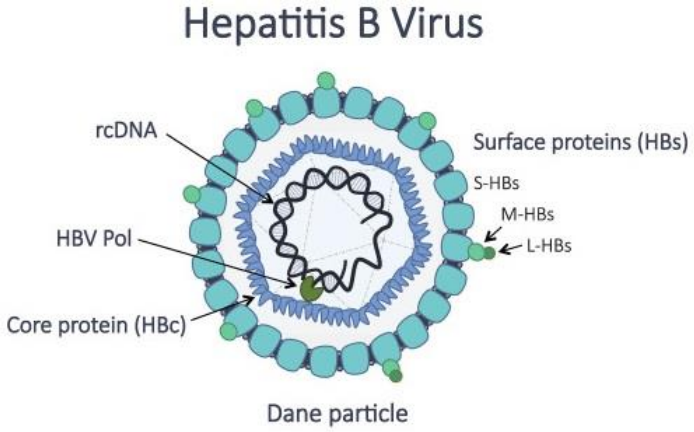


**Figure 1: HBV particle structural diagram.[25]**

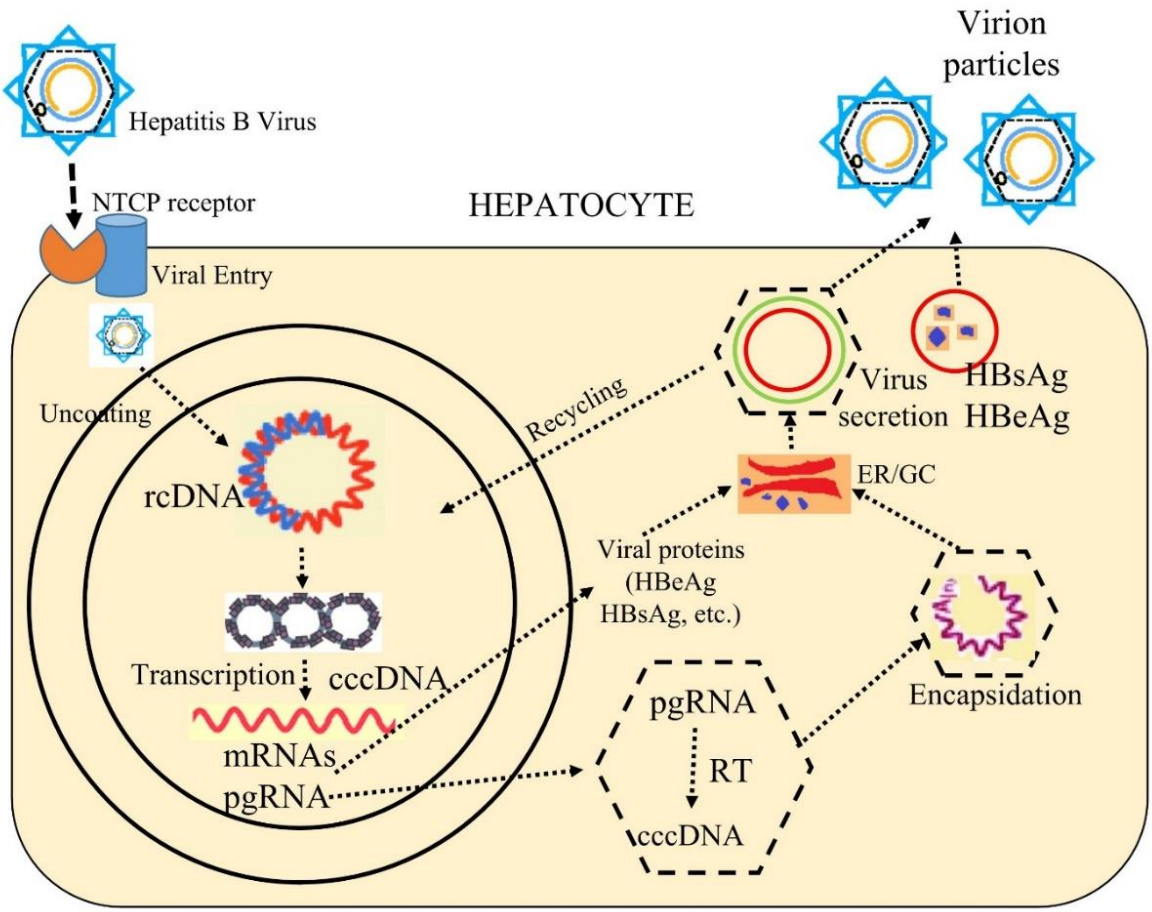


**Figure 2: Brief outline of HBV life cycle.**[26]

### 3.2.1. Epidemiology

According to the WHO, 296 million individuals worldwide have chronic HB infection as of 2019 (WHO_01/07/2023). According to reports, the prevalence of HBsAg is 3.5%. With 116 million cases of illnesses, the area of the Western Pacific had the highest incidence, which is followed by Africa (81 million), the Eastern Mediterranean (60 million), and the Southeast Asian region (60 million). Europe has 14 million people, but the United States and Canada only have 5 million. The frequency of HBsAg in India is estimated to be between 3.4% and 4.2%, while there are an estimated 40 million HBV carriers in the country.[27]

### 3.2.2. HBV proteins

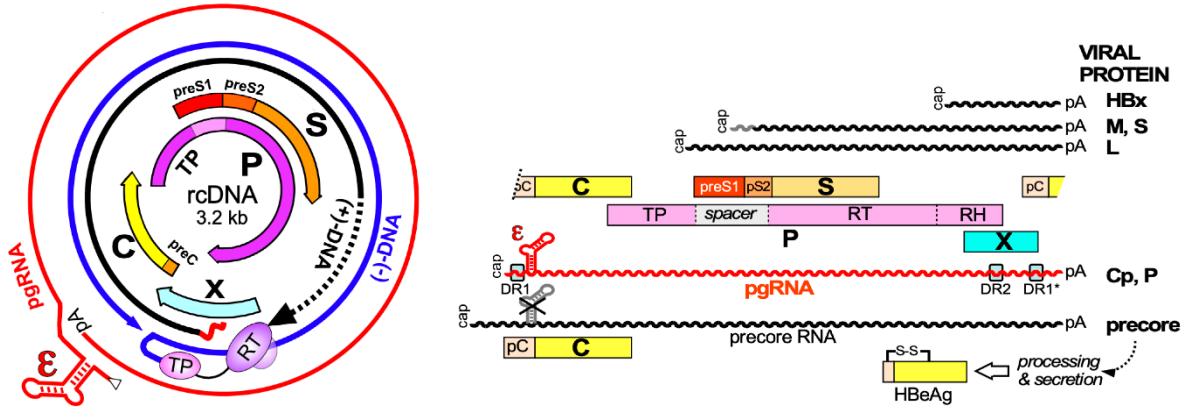


**Figure 3: Structural information of HBV.**[28]

#### 3.2.2.1 HBV surface antigen (HBsAg)

The HBV encodes the three proteins namely SHBsAg, MHBsAg, and LHBsAg of HBsAg to form a viral polypeptide envelope. Two HBV subgenomic mRNA transcripts (1) preS1 and (2) preS2, are responsible for translating these proteins in the ER. Each of the three envelope proteins has a glycosylated form that aids in the release of infectious virus particles. The virion contains a majority of S proteins and an equal amount of M and L proteins. M and L proteins envelop and secrete HBsAg particles. The S protein reveals a low affinity-binding site for HSPG and is essential for infection. The high-affinity attachment point of HBV to NTCP is located on the L protein with the preS1 domain, which aids in the envelopment of the core particles. HBsAg helps in viral binding and entry into the susceptible cells.[29]

HBsAg consists of a polyprotein with three distinct regions: the PreS1, PreS2, and S domains. The PreS1 (aa1-aa108), PreS2 (aa109-aa163), and S (aa364-aa389) domains together code for 389 residues (39 kDa) that make up the LHBs.[30] Whereas, MHBs have a polypeptide encoded by both PreS2 and S, whereas SHBs only include the S domain.

LHBs are present in the 4 putative transmembrane (I-IV) segments. The PreS1 and PreS2 domains have been revealed to play an important role in viral entrance in prior studies. For HBV morphogenesis to occur, the PreS1 domain is essential, in which recognition of a hepatocyte receptor is mediated by amino acids 2-78 (77 residues) in the PreS1 domain of the LHBs protein. The region of this protein between aa122 and aa147, known as the determinant, is essential for the binding of antibodies to HBsAg. Several different mutations have been traced to this area and as a result, this region is not a good fit for medication development.[7]

#### 3.2.2.2 HBV DNA POL

The HBV DNA is circular and partially double-stranded, and the DNA polymerase is attached by a covalent bond to the 5' end of the minus strand. The DNA of HBV is copied by generating a pgRNA RNA-intermediate by reverse transcription.[31] Briefly, HBV entry into hepatocytes by NTCP host cellular receptors. After entering the nucleocapsid, rcDNA is taken to the nucleus, where it undergoes converting to become episomal cccDNA and is eventually incorporated into a minichromosome. The viral mRNA transcription process begins with this cccDNA as the template. DNA polymerase attaches to the epsilon (stem-loop structure) in the 5' region of pgRNA, starting the process of packaging into nucleocapsids and allowing for the production of viral proteins. This is where the pgRNA is converted into its offspring rcDNA. Additional rcDNA becomes encapsulated and released from the cell as virion particles. Therefore, DNA polymerase's participation in the synthesis and intracellular amplification of cccDNA is crucial for the development and persistence of infection.[32]

#### 3.2.2.3 HBV Capsid Protein (HBc)

The HBc plays a critical role in the life cycle virus. HBc is separated into 3 distinguished regions, an N- and C-terminal domain (NTD and CTD), and NTD and CTD linker region. NTD is responsible for the capsid assembly and CTD plays a significant role in the pgRNA packaging and reverse transcription.[33] HBc aids in the reverse transcription of the pgRNA to produce the minus and plus strands of HBV DNA. The electron-microscopic and chromatin immunoprecipitation techniques have been employed to show that HBc is a component of cccDNA minichromosome and that its binding to the cccDNA aids in regulating the rate of HBV transcription. The current research on HBV therapeutics aimed at preventing HBV transcription could focus on preventing HBc from attaching to cccDNA.[34,35]

#### 3.2.2.4 HBV e Antigen (HBeAg)

Pre-core, core, and HBeAg are all products of PreC-C gene translation that occur during HBV replication. HBeAg protein is released as an auxiliary of HBV during viral replication and during chronic HBV infection, HBeAg plays a crucial role as an immunomodulator by establishing host immunological tolerance.[36] HBeAg doesn't involved in the replication process, it plays a vital role in the modulation of the immune response of human hosts. Researchers found that elevated viral loads, which in turn triggered a more serious proinflammatory response and liver damage, resulted from HBeAg's ability to decrease IL-1 mediated NF-κB activation by inhibiting TRAF6-dependent K63-linked ubiquitination of e NF-κB essential modulator (NEMO).[37] The tumor suppressor protein p53 plays a crucial role in the HCC for cell differentiation, cell cycle regulation, and apoptosis. Loss of function of p53 causes hepatocarcinogenesis. HBeAg enhances the p53 degradation and can promote liver tumorigenesis.[37,38]

However, HBeAg's potential therapeutic role in blocking NF-κB activation in HBV-infected cells and prevention of p53 degradation could be the new therapeutic approach.

#### 3.2.2.5 Hepatitis B X Protein (HBx)

HBX is a protein with several different functions; it is involved in the control of many different cellular transcriptional products, including AP-1, AP-2, NF-κB, and cAMP. "Gene transcription, cell cycle progression, DNA damage repair, cell proliferation, and apoptosis" are just some of the biological processes that HBX has been shown to influence in previous studies.[39] HBX causes the overexpression and activation of different cell signaling pathways, 1) Activation of Ras-Raf-MAPK results in the pro-apoptotic effects, which leads to the HCC and also causes the degeneration of cell cycle checkpoint control and leads to the cell cycle stimulation. 2) Overexpression of PKC results in the stimulation of NFKB and AP-1 leading to abnormal cell formation and transformation. 3) Activation of SAPK/JNK causes the HCC through tyrosine phosphorylation of various STATs, raises STAT-dependent DNA binding as well as transcriptional initiation. 4) Activation of PI3K-PKB/Akt pathway accompanying the Fas-mediated apoptosis and causes the deactivation of caspase-3. HBX is the first potent caspases-3 inhibitor and it can inhibit the TGF-beta-induced cell apoptosis. Hence, from above mentioned mechanisms, HBX plays a crucial role in the cause of HCC (Figure 4).[40–44]

### 3.2.3. HBV infection and regulation of signaling pathways

#### 3.2.3.1 PI3K signaling pathway

PI3K-Akt pathway controls cell propagation, differentiation, and cell survival. This pathway gets activated in numerous kinds of human cancer including HBV-mediated HCC. HBV favors its replication by activating the PI3K-Akt pathway, which blocks apoptosis and increases cell survival.[45] HBx serves as a regulator of HBV

replication and cell survival and LHBsAg behaves as a carcinogenesis factor by stimulating the PI3K-AKT pathway.[46]

#### 3.2.3.2 Jak-STAT and IFN signaling pathway

The host cell secretes cytokines termed "Interferons" in response to HBV infection. The JAK/STAT signaling pathway is utilized by all three types of interferons to activate the transcription of Interferon Stimulated Genes (ISGs). Inactive JAKs bind the cytoplasmic domain of all IFN receptors and once IFN binds to its receptor, a conformational change occurs in the receptor that brings nearby inactive JAKs into active proximity. As a consequence, JAKs undergo auto-phosphorylation and activation. Specific STATs (STAT1-5) are activated when JAKs are turned on by phosphorylating their own tyrosine residues. Translocation to the nucleus of activated STATs occurs by homo/hetero-dimerization and the Importin-RanGDP complex. ISG transcription is initiated when STATs bind to consensus DNA motifs in the ISG promoter region. Among all STATs, STAT1 is essential for the signal transduction process of all IFNs (type I, II, and III). Chronic HBV infection reduces STAT1 transcription and other immune responses associated with type I, II, and III IFN signalling.[47]

#### 3.2.3.3 NFkB signaling pathway

Antiviral immunity in the host is a critical line of defense in warding off virus invasion and curing illness. Numerous RNA and DNA viruses can modulate antiviral immunity by controlling the stimulation of the non-canonical NF-κB signaling via a variety of adaptor proteins. However, certain viruses can avoid antiviral defenses by interfering with the non-canonical NFKB pathway. HBV DNA encodes multiple proteins that inhibit the activation of the non-canonical NK-B pathway.[48] TBK1 is a main positive and negative regulator of the non-canonical NFKB pathway and evidently, HBV DNA

POL suppresses TBK1/IKK-mediated phosphorylation, dimerization, and nuclear translocation of IRF3 (positive regulator of NFKB pathway).[48,49]

#### 3.2.3.4 MAPK signaling pathway

HBx's regulated MAPKs are involved in a variety of cellular signaling pathways and activate transcriptional factors to cause HCC. HBx does not directly interact with the Fos and Jun proteins that make up the transcription factor AP-1, many studies have shown that it may stimulate their activation. This led to the realization that HBx promotes the activation of Ras, a GTP-binding protein that is upstream in the MAPK signaling cascade. Therefore, HBx activates AP-1 through Ras-MAPK signalling.[50]

#### 3.2.3.5 Ras-Raf-MAPK signaling pathway

HBx directly stimulates Ras via Src. When upstream signals are aberrant, RTKs are activated and then activated Ras interacts directly with the target effectors by exchanging GTP for GDP. To activate MAPK, the Raf kinase inhibitor protein must be deactivated. This protein blocks PKC's ability to inhibit GPCR-kinases and prevents Raf-1 kinase from regulating the Ras/Raf/MAPK signaling pathway. KSR, MEK-partner 1, Sef, and Paxillin are scaffold proteins that aid in the spatial and temporal activation of the Ras/Raf/MAPK signaling. In addition, HBx induces Ras-dependent NFKB activation. This happens because p105 is depleted in the cytoplasm and the IB protein is phosphorylated. The nuclear import of NF-κB is blocked by both IB and p105. HBx's presence in the cytoplasm, rather than the nucleus, is required for the activation of Ras-MAPK signaling and NF-κB/AP-1-dependent transcription.[50]

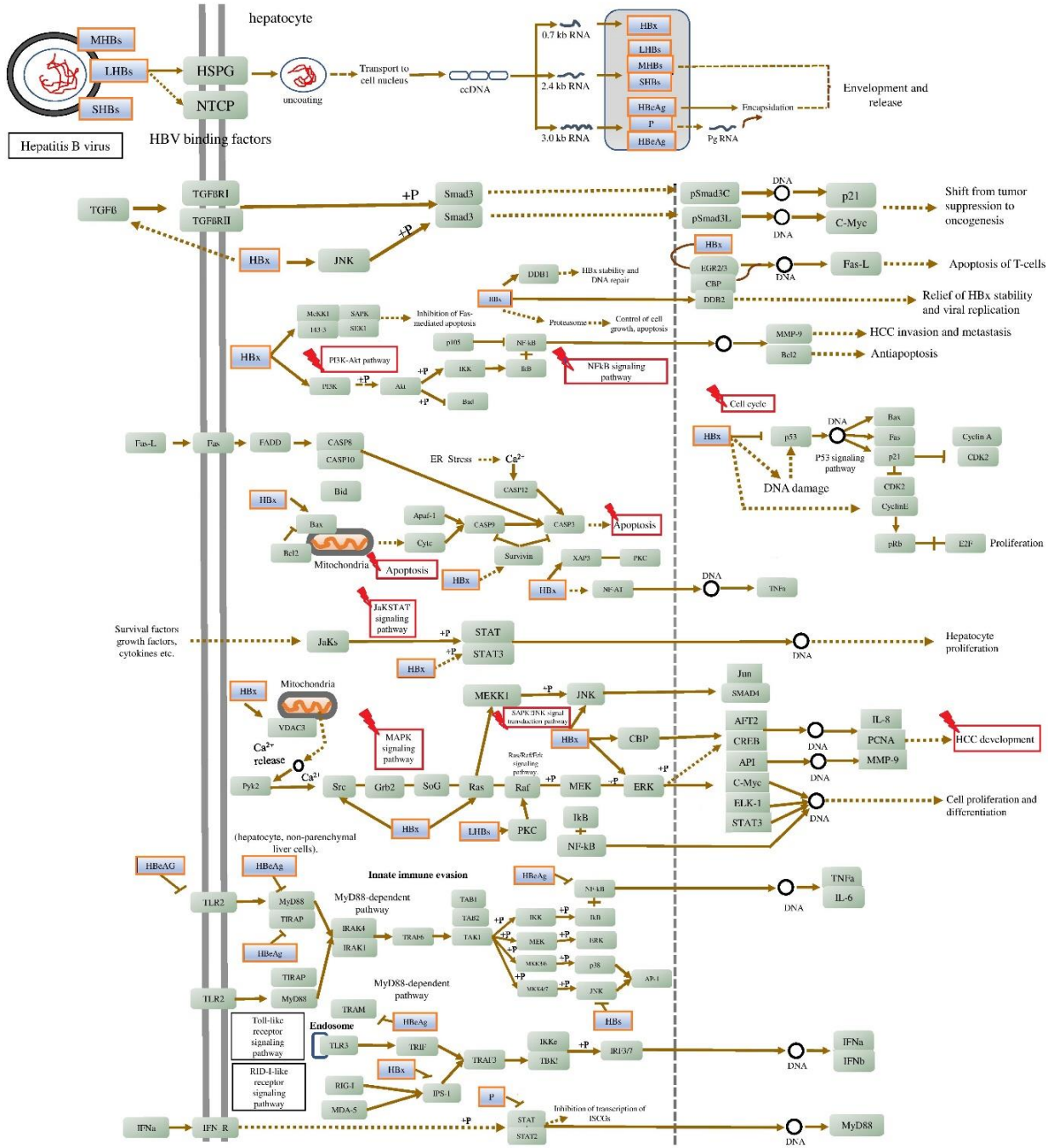


**Figure 4: HBV proteins triggered molecular pathways to cause HCC. The Figure is adapted from KEGG pathway database with accession number hsa05161 (https://www.genome.jp/pathway/hsa05161).**

### 3.3. Liver inflammation

The liver is the largest glandular organ in the body and is responsible for the metabolism of haematological, biochemical, and enzyme-related processes. The hepatotrophic viruses cause various degrees of inflammation ranging from fibrosis to cirrhosis in many cases which leads to HCC and death.

Liver fibrosis is a hallmark of various chronic hepatic diseases and results from the continuous damage to the hepatic-related buildup of extracellular matrix molecules. Chronic hepatitis virus infection, excessive alcohol and drug use, and nonalcoholic steatohepatitis (NASH) are the primary causes of liver scarring in industrialized countries.[51] Hepatic fibrosis was formerly thought to be a discrete and irreversible cycle due to the collapse of the hepatic parenchyma and subsequent replacement by collagen-rich tissue.[52,53] Hepatic transplantation is often required in cases of severe hepatic fibrosis, which is characterized by cirrhosis, hepatic damage, and HCC. Hepatic fibrosis is a complex disease, the cellular and molecular components of which we now understand in great detail. Crucial collagen-generating cells in the damaged liver include hepatic stellate cells, portal fibroblasts, and bone marrow myofibroblasts. In addition, "fibrogenic cytokines" including serum albumin, fibroblast growth factor 1, angiotensin II, and leptin are responsible for the initial development of these cells. Recent archival evidence suggests that patients' growing hepatic fibrosis may be reversed, which has encouraged scientists to develop antifibrotic medications.[54]

Cirrhosis of the liver is a chronic condition characterized by the formation of persistent fibrotic tissue, resulting in impaired liver structure and functionality. The potential outcome of this condition is the development of liver failure. Cirrhosis is a pathological condition that arises as a consequence of prolonged and continuous liver injury. The most prevalent etiological variables including alcohol and drug use, viral

infections, and metabolic dysregulation are widely recognized as the primary causative agents. The advancements in the treatment, quality of life, and prognosis of individuals with cirrhosis may be attributed to the continuous progress in our understanding of the normal progression and underlying mechanisms of cirrhosis, as well as the intricate nature of its therapeutic interventions. Hepatic fibrosis progresses to cirrhosis when it is accompanied by hepatic vascular distortion. As a result, the liver's gateway and artery blood supply is redirected directly into the liver surge, severing contact between the sinusoids and the surrounding hepatic parenchyma. The liver sinusoids are lined by fenestrated endothelia and a porous connective tissue layer including hepatic stellate cells and some mononuclear cells.[55] Cirrhosis-related underlying inflammatory condition has been linked to enhanced bacterial migration across the digestive system, weakened immune capability, and an excessive release of pro-inflammatory cytokines in its pathogenesis.[56] Different people with the same risk factors develop cirrhosis at different rates. Recent years have seen the identification of a growing number of helpful genetic variants that likely increase the risk of fibrosis progression. Over time, cirrhosis causes the liver to replace healthy tissue with scar tissue. As a result, fewer healthy liver cells. Similarly, the rate at which blood moves through the liver slows back down. This prevents the liver from doing its work properly.[57] Cirrhosis is most often brought on by long-term infections with the hepatitis B virus (HBV). The progression from viral hepatitis to cirrhosis might take anywhere from ten to twenty years. Cirrhosis is the end result of a process that begins with inflammation, necrosis, and regeneration of the liver tissue. This inflammation is induced by infections that are intermediately active. CD8+ T cells and NK cells are responsible for the damage caused to the liver because they directly target the infected hepatocytes and then release pro-inflammatory cytokines and chemokines. Through the secretion of fibrosis-related substances, hepatic stellate cells

are actively involved in the process of fibrogenesis. In an inflammatory environment, viruses go through a process of mutation, selection, and adaptation in order to avoid being eliminated by the immune system (Figure 5).[58,59]

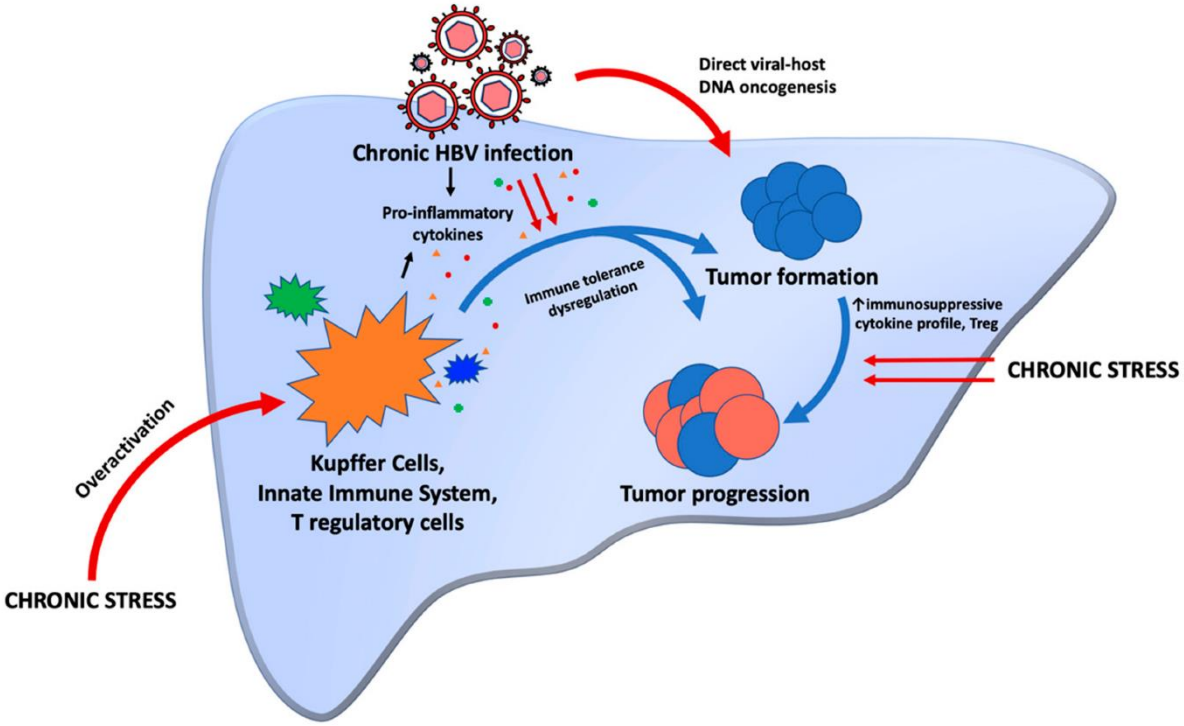


**Figure 5: Brief outline of HBV induced liver cirrhosis.[58]**

### 3.4. Pharmacotherapy of HBV treatment

Acute hepatitis B infections often clear up without any treatment but patients with CHB who have developed compensated cirrhosis need to undergo therapy.[60] Currently there are no known effective treatments for HBV infection and the objective of prescription therapy is to establish a functional cure by blocking HBV replication, reducing liver inflammation, and halting the development of the disease to cirrhosis and hepatocellular cancer.[61] The current treatment of CHB includes the use of (a) interferon or (b) nucleoside/nucleotide analogues.[62]

Signaling proteins called interferons (IFN) may suppress HBV activity while also stimulating the immune system. Since the 1980s, interferon alpha (IFN-a) has been the primary therapy for chronic hepatitis B (CHB), its benefits include (i) a limited duration of treatment, (ii) an improved rate of HBsAg and HBeAg seroconversion, and (iii) efficacy in drug-resistant mutants.[63,64] The biggest problem of IFN-α is that the antiviral must be injected subcutaneously three times a week for six weeks, which may be difficult and painful for patients. Injections were reduced from twice weekly to once weekly by pegylation of IFN-α, which lengthens the half-life of the protein in circulation. There are also negative side effects associated with this medication, such as weariness, flu-like symptoms, and nausea, in addition to the drug's modest antiviral impact.[64]

Inhibiting HBV polymerase with nucleoside/nucleotide analogs improves clinical outcomes by lowering the prevalence of cirrhosis and hepatocellular cancer. When it comes to treating HBV, lamivudine was the first drug of its kind to get official approval for usage.[65] The cytosine analog inhibits elongation by binding competitively to reverse transcriptase and serving as a chain terminator. Rapid inhibition of HBV replication, increased HBeAg seroconversion, and normalized blood ALT levels have all been seen in CHB patients treated with lamivudine. Patients with cirrhosis who take lamivudine had better liver function and a lower chance of developing hepatocellular carcinoma. Other advantages of using the drug include oral administration and minimal side effects. According to estimates, between 53 and 76 percent of CHB patients acquire resistance to lamivudine after 3 years, making the low barrier to resistance the main disadvantage of long-term use.[65] First-line monotherapies for chronic hepatitis B are tenofovir and entecavir. According to clinical investigations, both of these nucleoside/nucleotide analogs have been proven to have stronger antiviral effectiveness and better clinical outcomes in chronic hepatitis than lamivudine. Furthermore, both drugs show a better

barrier to resistance as compared to lamivudine, however, entecavir and tenofovir-resistant HBV strains have been identified in clinical samples.[65,66]

### 3.5. Models used in the HBV study

HBV belongs to the Hepadnaviridae family. Members of this family show high species specificity and tissue tropism. Although HBV has a unique mechanism of replication, it can be studied in different culture models and cell models. These models are essential to studying the viral host interactions as well as in deciphering the mechanisms involved by the virus to sustain its life cycle.[67]

#### 3.5.1. Animal models

Understanding the various disease processes of HBV and developing effective therapeutics is made even more challenging by the dearth of small animal models that exhibit human-like HBV infections.[68] Animal models such as chimpanzees, woodchucks, ground squirrels, tree shrews (*Tupaia belangeri*), and ducks have been established for *in vivo* HBV studies. However, the large life span of these animals makes them unsuitable and not routinely utilized as experimental hosts due to ethical and cost concerns.[69–71] While, the HBV mouse model could be useful, but possesses numerous disadvantages. The transgenic mouse model that has 1.3-HBV inserted into the murine genome is resistant to HBV infection, doesn't harm liver tissue, and doesn't make cccDNA.[72] Hydraulic injection (HDI)-based replication-competent HBV transgenic mice containing HBV replicons, including 1.2- or 1.3-HBV or HBV circular genomes, are hydrodynamically injected into mice to sustain cells for six months. They may induce liver fibrosis when the proper vector is used, and after injection, they are expressed in 10–25% of mouse hepatocytes.[72] Adenovirus vectors carrying the HBV genome were

injected into mice to create Adeno-HBV transgenic animals.[73] Both the lack of detectable cccDNA and an altered T cell profile—which is advantageous for immunotolerant studies—cause these mice to develop immunological tolerance to HBV.

### 3.5.2. Hepatic cell lines

Hepatic cell lines viz., HepG2, HuH7, etc. have been employed for research on hepatotoxicity, HBV, and HCC. Recently, these hepatitis cell lines were modified by introducing HBV DNA for stable expression of HBV virion and these include HepG2.2.15 and HepAD 38 cell lines. These cell lines are transfected with clones that are longer than the whole HBV genome in order to start the viral life cycle within the host cells since HBV has a circular genome.[74,75] One of the drawbacks associated with these cell lines is a huge amount of transfected DNA which interferes with the accurate quantification of replicative intermediates.[74,75] The HepG2.2.15 genome also has two copies of the HBV genome. HepAD 38 is a stable cell line that has been shown to produce HBV under Tetracycline-Off inducible control. Large amounts of pgRNA are produced when tetracycline is not present.[76] Understanding the processes of the HBV life cycle, drug analysis tests, and HBV pathogenesis are all greatly aided by the aforementioned cell culture models. HepaRG cells are another popular cell line. Their cells have the ability to passage in standard media and develop into hepatocyte-like cells. These are morphologically and functionally similar to Primary human hepatocytes (PHH). One disadvantage of using these cell lines is the time-consuming nature of the differentiation processes involved. In 2012, the HBV entry host receptor “NTCP” was discovered, leading to the development of NTCP-overexpressing hepatoma cell lines. In hepatocellular carcinomas, NTCP receptors are expressed exogenously. These have been used in the study of HBV infection etiology and the testing of potential antiviral

medicines. One limitation associated with this is these are distinct from hepatocytes in terms of mutations, chromosomal abnormalities, metabolic properties etc.[71,77]

### 3.5.3. Hepatotoxicants

Hepatotoxicity refers to chemically induced liver injury. The liver is especially susceptible to the toxicity of these drugs because of its central role in the processing and removal of toxins. When taken in large doses, and even infrequently when used appropriately, there is the possibility of organ damage from certain drugs. Other chemical agents, such as those found in industry and laboratories, natural chemicals (such as microcystins), and herbal treatments may also cause hepatotoxicity. Substances known as hepatotoxins are toxic to the liver. More than 900 drugs have been related to liver disease, making it the leading cause of drug recalls.[78] Toxic substances may cause subtle damage to the liver, which may not become apparent until an abnormal liver enzyme test is performed. Drug-induced liver damage (DILD) accounts for 50% of cases of acute liver failure and contributes to 5% of hospitalizations.[79]

## 3.6. Silymarin: An effective hepatoprotective agent

Milk thistle, or *Silybum marianum* (Family: Asteraceae/Compositae), is a plant that has been studied extensively for its potential to cure liver ailments. The dried seeds of the milk thistle plant contain the highest amounts of silymarin, which is subsequently extracted and used.[80] In the years 1968–1974, the active principle was initially isolated and structurally characterized. Four different flavonolignan isomers—silybin, isosilybin, silydianin, and silychristin—make up silymarin.[81] Silymarin's protein synthesis facilitative properties are thought to be due to its structural similarities to steroid hormones. For example, silybin accounts for 60–70% of the isomers, whereas silychristin and silydianin each account for 10% and isosilybin for 5%. The bioavailability of silybin

is greatly improved by its combination with phosphatidylcholine; this complex is known as silipide.[81,82] Researchers from all over the world have shown that silymarin protects the liver from "acetaminophen, diethyl nitrosamine, carbon tetrachloride, ethanol, D-galactosamine, Amanita phalloides toxin, and other toxins using partial hepatectomy models and toxic models in experimental animals". After 7 days of treatment with 100 mg/kg (p.o), silymarin significantly increased liver weight in mice compared to animals treated with $CCl_4$. In addition, silymarin protected the livers of 87.5% of mice against the hepatotoxicity caused by paracetamol. While silymarin did protect against $CCl_4$-induced liver necrosis, the proportion of protection was low.[83,84]

### 3.7. Traditional medicines of the Western Ghats for the management of hepatitis

Approximately 600 different herbal medicines claiming to have hepatoprotective effects are on the market today. In all, over 170 phytoconstituents extracted from 110 plants across 55 families have been proven to exhibit hepatoprotective effects. More than 93 medicinal plants are combined in 40 different ways to create herbal compositions that are patented in India.[85,86] However, there is a dearth of pharmacological assessments of the effectiveness and safety of hepatoprotective herbs and traditional medicine formulations. The primary acknowledged components of several herbal therapies are accessible as either pure compounds that are currently undergoing testing or as standardized extracts.[85]

The Western Ghats have a plethora of medicinal plants. It is estimated that there are ~700 different medicinal plants in the woods and hills of this area.[87] Which means that some of them are employed in alternative medicine. Many are used economically because of the active molecules they produce. There is a wide range of annual and perennial plant life represented among the Western Ghats' medicinal plant species. This

includes lichen, algae, herbs, shrubs, climbers, and trees. In addition, these plants are seasonal and dispersed from the canopy to the understorey. Understanding the auto-ecology and syn-ecology of traditional medicine species involves expertise in taxonomy, ethnobotany, and ecology. The Western Ghats, with their abundance of plant life, are a veritable pharmacy. Since not enough is known about the many medicinal plant uses, their availability, and their distribution, it is difficult to make the best use of these resources. Therefore, it is necessary to consolidate the data found in numerous locations. Ayurveda, Chinese medicine, and the Japanese Kampo system are just a few examples of classical traditional medical systems that make utilization of TMs, and TMs are also gaining significance in various areas of investigation, particularly in the fields of genetics and biotechnology. Approximately fifty of the Western Ghats' species have enormous importance in traditional and alternative medicine for the treatment of a wide range of illnesses and in the present study selected 18 medicinal plants (Figure 6) that are practiced by the local/tribal healers in the Western Ghats region of North Karnataka, India which are utilized for the treatment of viral infection and their complications like hepatitis.

**Table 2**: Brief literature on 18 medicinal plants for their hepatoprotective potency

| S. No. | Plant name | Family | Reported pharmacological activities |
|---|---|---|---|
| 1. | *Aerva lanata* | Amaranthaceae | It has hepatoprotection, nephroprotection, antiasthmatic, and antiamoebic properties. Its hydroalcoholic root extract showed hepatoprotective effects in acetaminophen-induced hepatitis.[88] |
| 2. | *Achyranthes aspera* | Amaranthaceae | It showed Hepatoprotective, Hypoglycaemic, Antiparasitic, Analgesic and antipyretic, Anti-inflammatory and anti-arthritic, Antimicrobial, Antimicrobial, Wound Healing, Immunomodulatory, Hypolipidemic, and antiviral activities.[89] |
| 3. | *Aloe vera* | Asphodelaceae | It possesses antioxidant, hepatoprotective, pain-relieving, and anti-inflammatory properties. Its polysaccharides reduce serum lipids and hepatic triglycerides; regulate the expression of lipolytic genes viz., AMPK-α2 and PPAR-α; down-regulate TNF-α, TLR-4, and MyD88 expression, and up-regulates I$\kappa$B-$\alpha$ expression.[90] Its anthraquinones possess anti-HBV activity.[91] |
| 4. | *Andrographis paniculata* | Acanthaceae | It is a key ingredient of many herbal formulations for the treatment of liver disease, hepatitis, diabetes, cancer, etc. Andrographolide downregulates EGFR expressed in epidermoid carcinoma (A-431) cells. Andrographolide and Neoandrographolide have protective effects against galactosamine and tert-butyl hydroperoxide intoxication-induced hepatotoxicity.[92,93] It has inhibitory activity against the HBV surface antigen. Dehydroandrographolide and Andrographolide showed potent inhibitory activity against HBV DNA replication. Neoandrographolide is a potent anti-inflammatory compound that inhibits iNOS and COX-2 expression by inhibiting p38 MAPK activation.[94,95] |
| 5. | *Bidens pilosa* | Asteraceae | It has anti-hyperglycemic, antihypertensive, antiulcerogenic, hepatoprotective, antipyretic, immunosuppressive, anti-inflammatory, anti-leukemic, anti-malarial, anti-bacterial, antioxidant, and antitumor properties. It showed hepatoprotective against $CCl_4$-induced hepatotoxicity.[96] |
| 6. | *Cassia auriculata* | Fabaceae | It possesses antipyretic, hepatoprotective, antidiabetic, antiperoxidative, anti-hyperglycaemic, microbicidal activity, antiviral activity, anti-spasmodic, etc, activities. |

| | | | |
|---|---|---|---|
| 7. | *Centella asiatica* | Umbelliferae/Apiaceae | Showed hepatoprotective potency against INH, GaIN, CCl4, and cyclophosphamide via restoring the cytokine production, inhibition of TGF-beta/Smad-assisted fibrogenesis, etc.[97] and also exhibits mild anti-HBV activity.[98] |
| 8. | *Diospyros Montana* | Ebenaceae | Selenium nanoparticles (SeNPs) using Diospyros montana showed antioxidant, antibacterial, and anticancer activities.[99] It also has antiviral, antitumor, antimalarial, anthelmintic, prostaglandin synthesis inhibitory, anti-inflammatory, hypolipidemic, and antileukemic activities.[100] |
| 9. | *Leucas aspera* | Lamiaceae | It exhibited hepatoprotection against d-GalN and $CCl_4$-triggered hepatotoxicity in rats via elevating SOD, CAT, GSH, etc.[101] |
| 10. | *Mangifera indica* | Anacardiaceae | It has anti-inflammatory, antibacterial, analgesic, antipyretic, antioxidant, anticancer, antiviral, immunomodulatory, anthelminthic, anti-aging, antidiabetic, lipometabolism regulating, cardioprotective, anti-hyperuricemic, neuroprotective and in obesity treatment properties. Its extracts protect the hepatocytes against all oxidative stress markers like lysis, ROS generation, lipid peroxidation, glutathione depletion, mitochondrial membrane potential decrease, lysosomal membrane oxidative damage, and cellular proteolysis.[102] It showed hepatoprotective against acetaminophen, mercuric chloride, etc chemicals induced hepatitis.[103] Mangiferin was considered as an antiviral agent for herpes simplex virus, HIV, and hepatitis B virus.[104] |
| 11. | *Phyllanthus niruri or Phyllanthus virgatus* | Phyllanthaceae | Along with its hepatoprotective nature, it showed inhibitory effects on HBV and woodchuck hepatitis virus DNA polymerase and also can bind to the surface antigen.[105] |
| 12. | *Pongamia pinnata* | Fabaceae | Traditionally used for their digestive, laxative, and anthelmintic properties, and have shown efficacy in treating diarrhea, leprosy, dyspepsia, and cough. Glabaarachalcone and isopongachromene exhibited binding affinity with the HBV DNA polymerase protein target. It possesses hepatoprotective and antiviral potential.[106] |
| 13. | *Ricinus communis* | Euphorbiaceae | Used for treating liver infections, stomach aches, flatulence, constipation, inflammation, warts, colic, enteritis, fever, headache, and as a counter-irritant. It possesses hepatoprotective, anti-nociceptive, antioxidant, antiulcer, anticancer, anti-inflammatory, central analgesic, antidiabetic, antimicrobial, |

| | | | |
|---|---|---|---|
| | | | antiviral, and wound healing activity. Showed antiviral against Coxsackie B virus type 4 (COXB4), HSV1, and HAV.[107] |
| 14. | *Solanum nigrum* | Solanaceae | Used in folkloric medicine as a remedy for hepatomegaly, splenomegaly, edema, gonorrhea, and epilepsy, as a diuretic, emmenagogue, and local application for painful swellings, abscess and ulcers, and for gastric ulcers. It has hepatoprotective, immunomodulatory, anticancer, antiviral, antimicrobial, etc. activities.[108] It showed HCV NS3 protease inhibition in a dose-dependent manner.[109] |
| 15. | *Strychnus nux-vomica* | Loganiaceae | Used for the treatment of neurodisorders, arthritis, and vomiting. It is validated for its effect on inflammation, hepatitis, microbial infections, gastrointestinal problems, the nervous system, bone cells, cardiovascular systems, cancer, and blood glucose levels. It also has antioxidant activity and antifeedant activity.[110] |
| 16. | *Terminalia chebula* | Combretaceae | It is known as King of Medicine or Arura because in Tibetan medicine it is considered to be a great panacea due to its beneficial effects on all diseases caused by Pitta, Vayu, and Kapha. It is also shown to cure diseases of all seven Dhatus viz., plasma, blood, muscle, fat, bone, marrow/nerve, and reproductive tissue. It possesses broad-spectrum activities, viz., antiviral, antiprotozoal, antibacterial, antifungal, etc., and has anticancer, antidiabetic, hepatoprotective, immunomodulatory, anti-inflammatory, wound healing, cardio-protective, anti-caries, etc., activities. Hydrolyzable tannins are documented for antiviral activities, viz., anti-HCV, anti-HSV-1, anti-HSV-2 (HSV, herpes simplex virus) activity via inhibiting entry and multiple viral targets.[111,112] |
| 17. | *Thespesia populnea* | Malvaceae | Ayurvedic physicians use bark decoction for skin and liver diseases. The bark and flower possess hepatoprotective, antioxidant, anti-inflammatory, memory-improving, and cholesterol-lowering activities. Methanolic flower extracts of *T. populnea* have a strong antiviral potency and possess nontoxic properties.[113] |
| 18. | *Vernonia cinerea* | Asteraceae | It possesses anti-inflammatory, antidiabetic, renoprotective, hepatoprotective, anticancer, antiviral, and antimicrobial activities.[114] The Ayurvedic Pharmacopoeia of India recommends the plant in intermittent fever, filariasis, pityriasis versicolor (tinea versicolor), blisters, boils, vaginal discharges, and in cases of psychoneurosis.[115] |

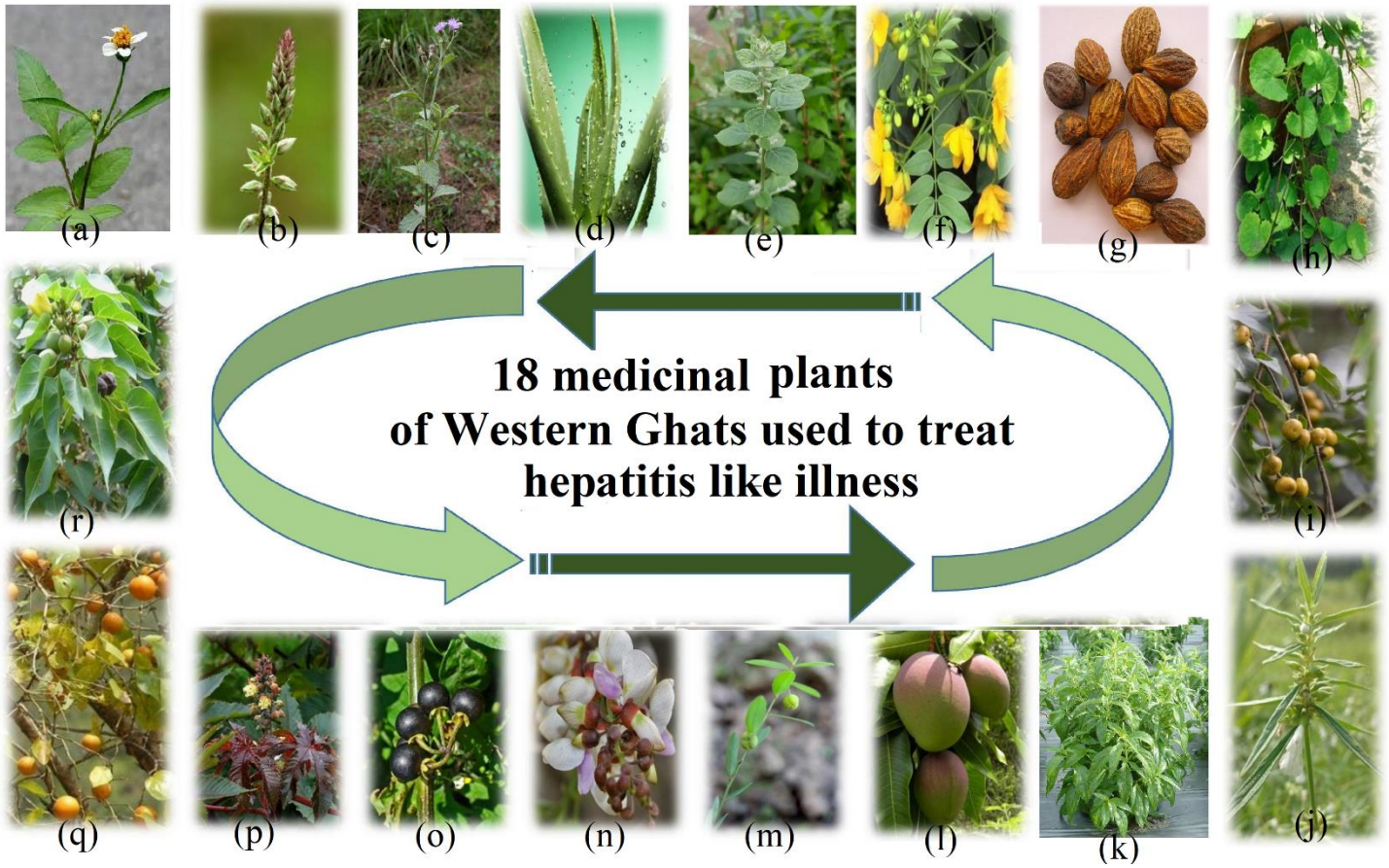


**Figure 6: Pictures of 18 medicinal plants selected in the current study.** a) *Bidens pilosa*, b) *Achyranthes aspera*, c) *Vernonia cinerea*, d) *Aloe vera*, e) *Aerva lanata*, f) *Cassia auriculata*, g) *Terminalia chebula*, h) *Centella asiatica*, i) *Strychnus nuxvomica*, j) *Leucas aspera*, k) *Andrographis paniculata*, l) *Mangifera indica*, m) *Phyllanthus niruri* or *Phyllanthus virgatus*, n) *Pongamia pinnata*, o) *Solanum nigrum*, p) *Ricinus communis*, q) *Diospyros montana*, r) *Thespesia populnea.*

# MATERIALS AND METHODS

The current study was designed to identify the potent medicinal plants of the Western Ghats region against HBV and its associated complications like HCC via implementation of *in silico*, *in vitro*, and *in vivo* studies (Figure 7)

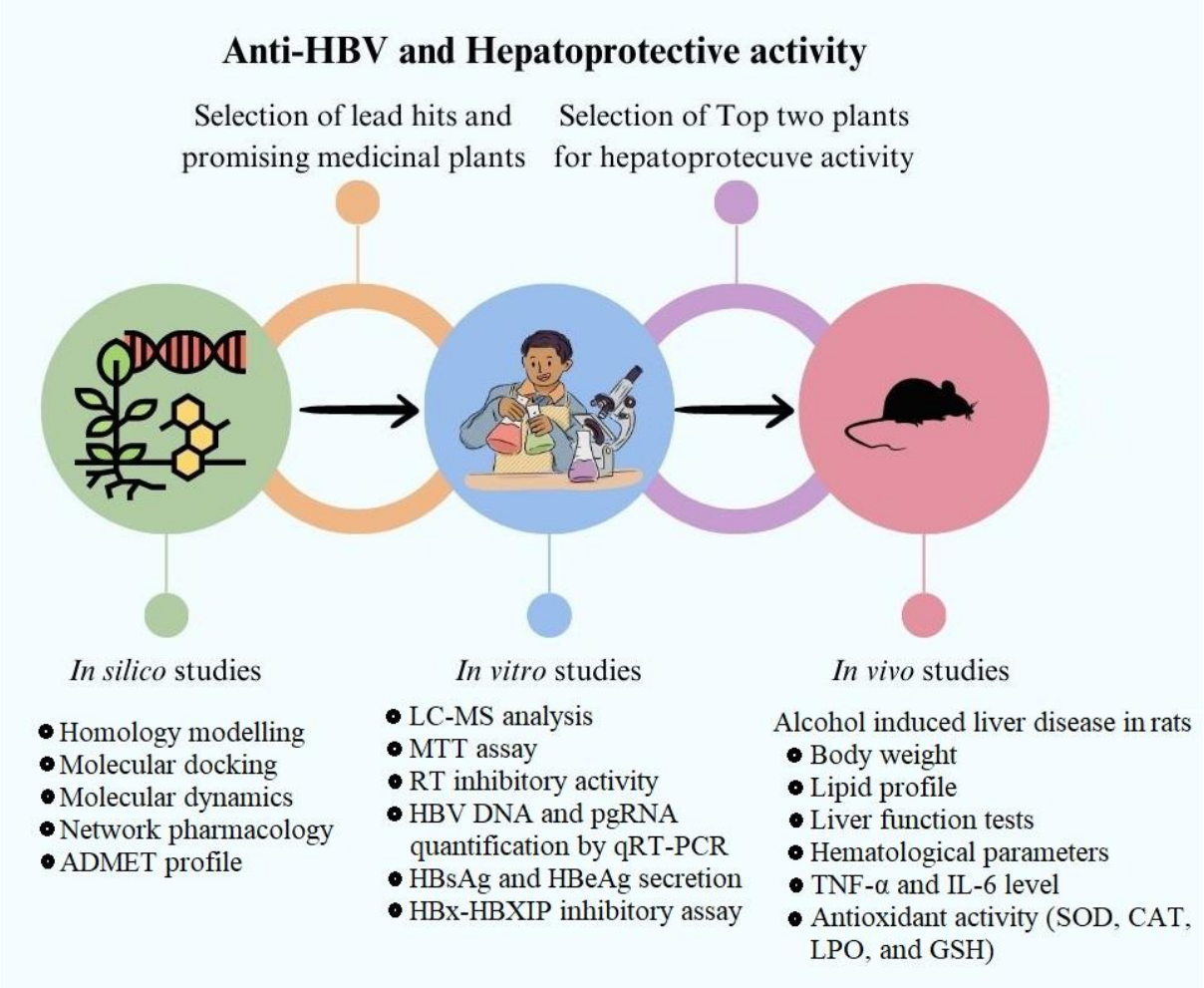


**Figure 7**: **Brief approach followed to identify the promising anti-HBV and hepatoprotective medicinal plants of the Western Ghats region.**

***In silico* pharmacology**

The *in silico* study is divided into four studies as shown in Figure 8.

**Study 1:** Identification of herbal drug candidates against HBV reverse transcriptase by homology modelling, molecular docking, and dynamics studies.

**Study 2:** Identification of drug candidates against HBV-induced hepatocellular carcinoma based on network pharmacology analysis: compounds interaction with host targets.

**Study 3:** Interaction of HBx with HBXIP and prioritized herbal drug candidates against HBx protein.

**Study 4:** Identification of a suitable chemical-induced hepatitis/HCC model that resembles to HBV pathogenesis.

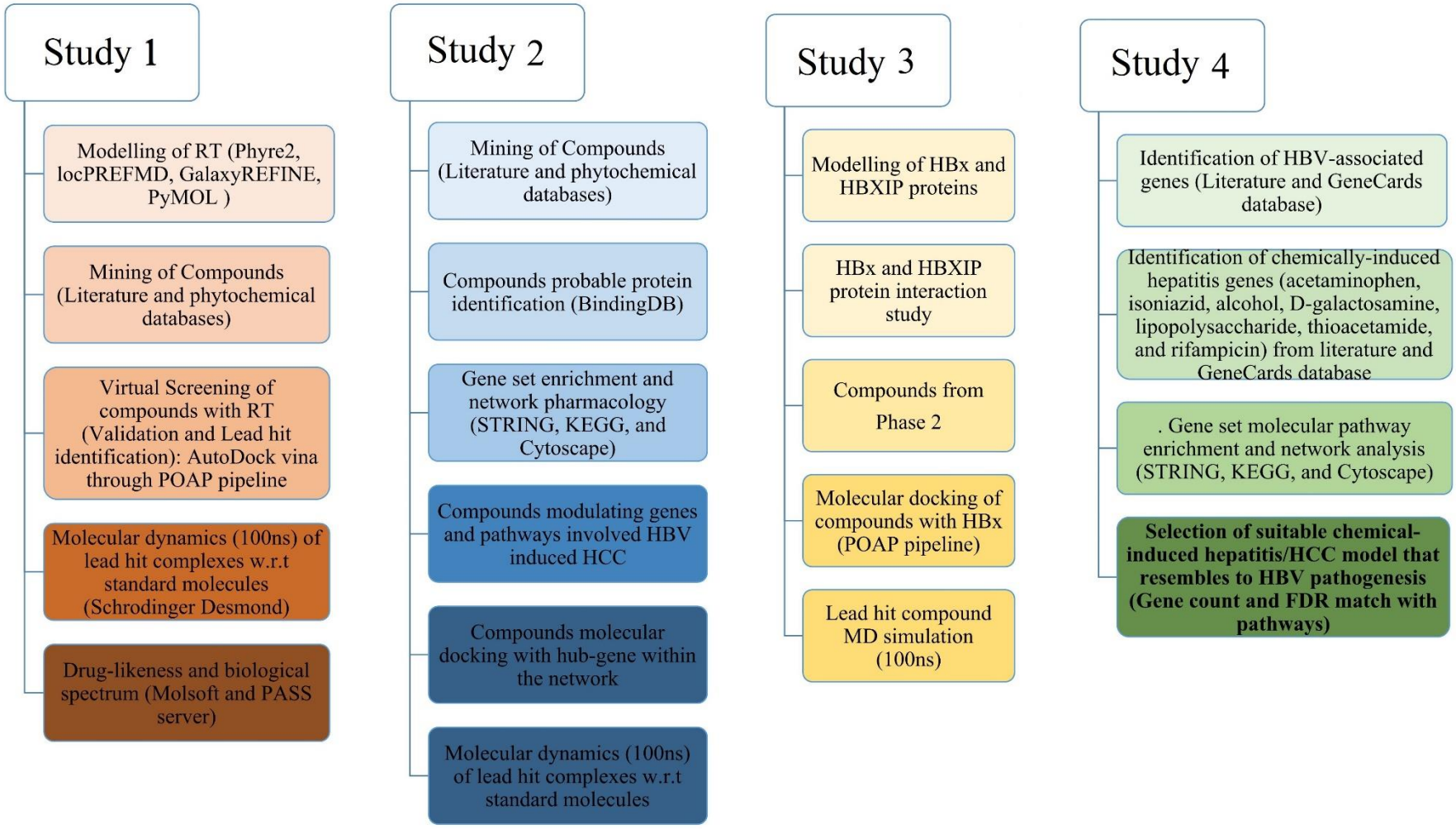


**Figure 8: Workflow for Study 1, Study 2, Study 3, and Study 4.**

## 4.1. Study 1 methodology: Identification of herbal drug candidates against HBV RT by homology modelling, molecular docking, and dynamics studies.

### 4.1.1. Modelling of HBV-RT by fold recognition

The structure of HBV-RT was modelled by Phyre2 online server[116], a fold recognition model. The Phyre2 server was provided with the HBV-RT sequence (ID: P03156; HBV genotype D; RT region aa 336-679) and an intensive model was chosen. Also, the Phyre2 server uses a heuristic approach to generate a model of the HBV-RT protein with a confidence of >90% by using 6 HIV-RT template models [3kk1_B, 5dmq_A, 1rth_A, 2zd1_A, 2opq_A, and 1mu2_A]. Further, the Phyre2 model structure was refined by two servers to improve stereochemical efficiency, bonds, angles, and torsion angles to within a statistically acceptable range, and side-chain refinement. Firstly, locPREFMD (local Protein structure REFinement through Molecular Dynamics)[117] was used and its output model was submitted to GalaxyREFINE (http://galaxy.seoklab.org/cgi-bin/submit.cgi?type=REFINE).[118]

### 4.1.2. Loop modeling

Protein priming is dependent on the structure of the HBV-RT, specifically, the YMDD motif (Y203, M204, D205, D206 motif) was identified as a structurally conserved loop on the template (PDB id: 3kk1).[119] HBV-RT's YMDD loop conformation was remodelled using ModLoop (https://modbase.compbio.ucsf.edu/modloop/)[120] to reduce the RMSD between the model and template. Additionally, PyMOL was used to re-evaluate the RMSD between the model and the template.

### 4.1.3. Lowest potential energy conformation by MD simulation

The dynamic behavior of molecular complexes and intermolecular interactions under physiologically mimicked conditions may be better understood via MD simulation,

which has become an essential tool in computational biology. The lowest PE for RT was retrieved from a 100ns MD simulation trajectory using Desmond 6.1v.[121] During MD simulation, the system was neutralized by adding 21 $Cl^-$ counter ions, and the system was solvated using the SPC water model with 10Å x 10Å x 10Å periodic boundary conditions. For a simulation time of 1000ps, the system was minimized. In the NPT ensemble, we used the "Nose- Hoover chain" Thermostat strategy with a relaxed time of 1.0 ns and the "Martyana-Tobias-Klein" Barostat strategy with a relaxed time of 2.0 ns to maintain a constant pressure of 1 bar and temperature of 300 K.

To the refined lowest potential energy conformation, the template coordinates "catalytic $Mg^{2+}$ and the known inhibitor" were transferred using the copy-ligand.py script in Modeller *ver.* 10.0. Further, a total of 100 different models were generated, and the one with the lowest discrete optimized protein energy (DOPE) score was chosen for further docking study.

### 4.1.4. Documentation and mining of phytocompounds

Traditional herbal medicines utilized for jaundice, fever, inflammation, and liver infection were chosen as they have a proven history of effectiveness amongst local/tribal healers in the Western Ghats region of North Karnataka, India. Plants that are rare, endangered, or otherwise difficult to locate were not included. Phytocompounds from the selected plants were retrieved from the Database of Ethnomedicinal Plants of Western Ghats[86] (https://nitmmedplantsdb.in/), Dr. Duke's Phytochemical and Ethnobotanical Databases, PhytoChemical Interactions DB (PCIDB; https://www.genome.jp/db/pcidb/), and public repositories. Phytochemicals from 18 plants were listed (268 in total, after deleting duplicates and ubiquitous) and provided in Supplementary Table 1.

### 4.1.5. Docking Studies

AutoDock Vina through the POAP pipeline[122] was used to re-confirm and validate the ligand-binding site by docking a known inhibitor ligand with HBV-RT (control docking). The grid box was set at the ligand-binding site having grid center x = 35.969, y = 79.743, z = 27.288 Å [size x = 18.985 Å, y = 24.983 Å, z = 20.812 Å] with grid spacing and exhaustiveness 1Å and 100, respectively. After docking, investigated the intermolecular interactions between HBV-RT, the native ligand, and the $Mg^{2+}$ cation at the atomic level using Discovery Studio Visualizer version 2019 (DSV v2019). Docked ligand conformation was compared to the reference molecule (ligand from model) using DSV v2019, which calculated the structural similarity between the two.

The known inhibitor (control) was docked with HBV-RT first, and then a library of phytochemicals was virtually screened against HBV-RT using the same grid size and docking conditions as the control docking. Finally, the DSV v2019 was used to examine the intermolecular interactions of the potential inhibitors.

### 4.1.6. Structural stability of docked complexes

The structural stability of **(1)** HBV-RT with catalytic $Mg^{2+}$ (RT-$Mg^{2+}$), **(2)** HBV-RT complexed with known HIV-RT inhibitor modelled as per PDB ID: 3KK1 [(2R,5R)-5-(6-aminopurin-9-yl)-4-fluoro-2,5-dihydrofuran-2-yl]oxymethyl-[hydroxy(phosphonooxy)phosphoryl]oxy-phosphinic acid (RT-$Mg^{2+}$-Std), **(3)** HBV-RT-$Mg^{2+}$-Std re-docked complex, and **(4)** HBV-RT- $Mg^{2+}$ with top screened phytocompounds with lower BE and higher number of intermolecular interactions with the active site than the known inhibitor (total 15 complexes) were validated by MD simulation for 100ns using Desmond 6.1v. The protein-Ligand interactions module of Desmond software was used to analyze the MD trajectories. The RMSD values of the

protein backbone and protein-ligand complexes, the RMSF of C-α, and the protein-ligand interaction fraction (in %) were analyzed as validation parameters.

### 4.1.7. Prime MM-GBSA

The relative binding-free energy (G bind) of screened phytochemicals with HBV-RT was computed using the Schrödinger Prime MM-GBSA module, using the equation $\Delta G_{GB}=\Delta E_{MM}+\Delta G_{solv}+\Delta G_{SA}$. The "$\Delta G_{GB}$ represents the electrostatic solvation energy; $\Delta E_{MM}$ is the difference between the minimized energies of the protein-ligand complex and the total energies of the protein and ligand in free form; $\Delta G_{solv}$ is the difference in the GBSA solvation energies of the protein-ligand complex and the sum of the solvation energies of protein and ligand in free form; $\Delta G_{SA}$ is the difference in the surface area energies for an unbound form of protein and ligand". The binding free energy was estimated using the last frame of the MD simulation.[123]

### 4.1.8. Gene set enrichment analysis and network construction

In order to identify the probable interaction of the above prioritized 15 compounds with host protein targets, BindingDB server[124] was with a search cut-off of Pa ≥ 0.7. STRING and KEGG pathway databases employed for molecular pathways enrichment and phytocompounds-targets-pathways interaction map were integrated using Cytoscape[125,126] *ver.* 3.6.1. The "edge count topological parameter" was applied for mapping node color and size from low to high.

### 4.1.9. Prediction of drug-likeness and biological spectrum

The drug-likeness and biological activities of 15 compounds were predicted using molsoft and PASS[127] servers, respectively. Hepatoprotectant, hepatic disease therapy and antiviral activities have been traced for pharmacological activities with a Pa score of 0.3 or above.

## 4.2. Study 2: Identification of drug candidates against HBV-induced hepatocellular carcinoma based on network pharmacology analysis

### 4.2.1. Selection of plants from Study-I study

From, Study 1, out of 18 plants, 3 plants were selected. Excluding these 3 plants, the remaining 16 medicinal plants were subjected to further evaluation.

### 4.2.2. Druggability and toxicity profile

The most frequent adverse drug reactions (ADRs) of drug molecules are hepatotoxicity, nephrotoxicity, arrhythmia, and myocardial infarction. First druggability was predicted by molsoft and compounds having a high drug-likeness score (DLS) were submitted to the ADVERpred[128] service for toxicity prediction using their canonical SMILES. We chose this server because it can forecast the hepatotoxicity, nephrotoxicity, arrhythmia, and myocardial infarction of unknown compounds, and during prediction pharmacological activity (Pa) value of $\leq 0.5$ proceeded for further studies.

### 4.2.3. Target identification

Prioritized compounds canonical SMILES were submitted in BindingDB[124] ($p>0.7$) to predict their probable host targets involved in HCC. UniProt (https://www.uniprot.org/) was manually queried for the Gene IDs of the predicted protein targets. Public repositories and the KEGG database[129] (https://www.genome.jp/kegg/) (Accessed on 09 April 2021) were also searched for information on the identified targets implicated in the pathogenesis of HBV-induced HCC.

### 4.2.4. Gene ontology and pathway enrichment analysis

A list of retrieved gene ID was entered into STRING 11.0 (https://string-db.org) to obtain molecular functions and processes of protein targets modulated by the

phytocompounds. A set of protein targets' molecular functions and processes were retrieved using STRING[130] GO, a program that performs Gene Ontology (GO)-based functional and process enrichment studies. The KEGG pathway (https://www.genome.jp/kegg/pathway.html) was used to retrieve the HBV-induced HCC-related enriched pathways. The false discovery rate (FDR) p-value cut-off of $p<0.05$ was used in this analysis to identify significantly enriched functions, processes, and pathways.

### 4.2.5. Network construction

Cytoscape v3.6.1, an open-source tool was utilized to visualize biological pathways and complex molecular interaction networks.[125,126] The edge count computation was utilized to represent the interconnectedness of the compound-protein pathways. The network was designed with "low values to small sizes" for node size and "low values to bright colors" for node color.

### 4.2.6. Structure refinement, homology modeling, and assessment of active site residues

EGFR had the highest edge count within the network and was implicated in MAPK, PI3K-Akt, Ras, and Jak-STAT signaling pathways. EGFR is recognized as a therapeutic target for HCC and in this study, used to virtually screen bioactive phytocompounds to infer intermolecular interactions with its active site. The wild-type EGFR kinase domain with dacomitinib was chosen from the Protein Data Bank (PDB) (https://www.rcsb.org/structure/4i23) and its missing residues were filled by Modeller[131] *ver* 9.10 using PDB ID 4I23 and UniProt accession no. P00533 as query. The PROCHECK web server was used to check the stereochemistry.

### 4.2.7. Least potential energy conformation by molecular dynamics (MD) simulation

MD simulation was performed for 50ns using Schrodinger Desmond v6.5 with OPLS force field to obtain EGFR lowest PE conformation. For MD simulation, a similar protocol was followed as mentioned in section Study 1 of 4.1.3.

### 4.2.8. Molecular Docking

#### 4.2.8.1. Preparation of ligand and protein target

Network analysis revealed that 11 phytocompounds from *Andrographis paniculata* and 3 from *Thespesia populnea* interact with EGFR. Thus, 14 phytocompound 3D structures were retrieved from PubChem and virtually screened against EGFR. The ligands were minimized by executing the "*prepare_ligand4.py*" script using the *mmff94* force field.[122]

#### 4.2.8.2. Ligand- Protein molecular docking

The AutoDock vina through the POAP pipeline was used to screen the compounds with EGFR with grid box center x = 4.00245, y = 10.9442, z = -4.3899; and size x,y,z = 26Å; spacing 1Å and key interactions were visualized by DSV v2019. The lead hit complexes were subjected to stability check by MD simulation.

### 4.2.9. Stability of protein-ligand complex

The above-mentioned “MD simulation section Study 1 of 4.1.3” procedure was followed and the trajectories generated were analyzed using in-build Desmond.

## 4.3. Study 3: Interaction of HBx with HBXIP and prioritized herbal drug candidates against HBx protein.

### 4.3.1. Retrieval of phytocompounds and target identification

In continuation of Study 2, we prioritized 11 and 3 phytocompounds from AP and TP which were virtually screened against HBx protein.

### 4.3.2. Homology modelling of HBx and HBXIP proteins

Presently, the x-ray crystallographic structure of HBx is not present, thus we employed homology modeling. HBx is called "X protein" since it has no sequence homology and we used RaptorX[132] server for modelling its structure. Likewise, HBXIP structure was obtained from RCSB with accession number 3MS6 and its missing residues were filled by template-based modelling of SWISS MODEL using UniProt accession number O43504. Ramachandran plots and the quality of both structures were obtained from the PROCHECK and ERRAT servers. CASTp was executed for their active site residue identification (CASTp; http://sts.bioe.uic.edu/castp/index.html?1bxw) server.

### 4.3.3. Protein-protein and protein-ligand docking

Molecular docking of HBx and HBXIP was performed by HADDOCK[133] 2.4. It is reported that residues 137CRHK140 within HBx are necessary for binding T36 of HBXIP. Further, 14 compounds docking with HBx was carried out by AutoDock vina through POAP pipeline[122] and interactions were inferred by DSV v2019.

### 4.3.4. Molecular dynamics

The apo form and lead hit protein-ligand complex structure MD simulation was performed for 100ns using Desmond v6.5 software with OPLS force field.[121] The above-mentioned “MD simulation section Study 1 of 4.1.3” procedure was followed and the trajectories generated were analyzed using in-build Desmond.

## 4.4. Study 4: Identification of a suitable chemical-induced hepatitis/HCC model that resembles HBV pathogenesis.

### 4.4.1. Identification of HBV-associated and chemically-induced hepatitis genes

A peer literature review and the GeneCards[134] database were used to obtain the list of modulated/regulated genes by HBV and chemicals (acetaminophen, isoniazid, alcohol, D-galactosamine, lipopolysaccharide, thioacetamide, and rifampicin) causing hepatitis. In the GeneCards, genes having a relevance score >20 were chosen for analysis to obtain the optimum number of genes for enrichment analysis and maintain cut-off consistency in all chemical-induced hepatitis, which helped to obtain the data on genes set pathway enrichment analysis. In addition, we used Venny 2.1 to find (1) common genes between GeneCards and literature, and (2) common genes between HBV and chemically-induced hepatitis.

### 4.4.2. Gene set molecular pathway enrichment and network analysis

A set of genes obtained for HBV and chemically induced hepatitis were submitted to STRING[130] and modulated biological pathways were obtained. After obtaining the list of pathways of HBV genes, they were compared to the HBV pathways of "KEGG ID: hsa05161" and as a result, 10 pathways were shortlisted. Further, pathways modulated by chemicals were matched with the above pathways of HBV. During evaluation, gene count and false discovery rate (FDR) analysis were considered. The network between HBV and chemicals with their targets (involved in hepatitis) and the regulated pathways were constructed using Cytoscape[125,126] (https://cytoscape.org/) ver 3.6.1 as mentioned in Study 1, section 4.1.8.

## 4.5. *In vitro* pharmacology

### 4.5.1. Collection of plant material, their authentication, and procurement of pure compound

Based on the *in silico* studies, the plants *Terminalia chebula, Bidens pilosa, Centella asiatica, Andrographis paniculata,* and *Thespesia populnea* were identified as lead anti-HBV medicinal plants (Figure 9) and were collected from local areas of Belagavi and certified by a qualified plant taxonomist at ICMR-NITM (RMRC), Belagavi and Shri B.M.K Ayurveda Mahavidyalaya (CFR), Belagavi .with voucher specimen number RMRC-1639, RMRC-1640, RMRC-1641, CFR/Auth/06/2023, and RMRC-1714, respectively. Standard drugs Tenofovir Disoproxil Fumarate (CAS No. 202138-50-9; SML1794) and 1,2,3,4,6-penta-O-galloyl--D-glucose (PGG, CAS No. 14937-32-7; G7548) have been purchased from Sigma, USA.

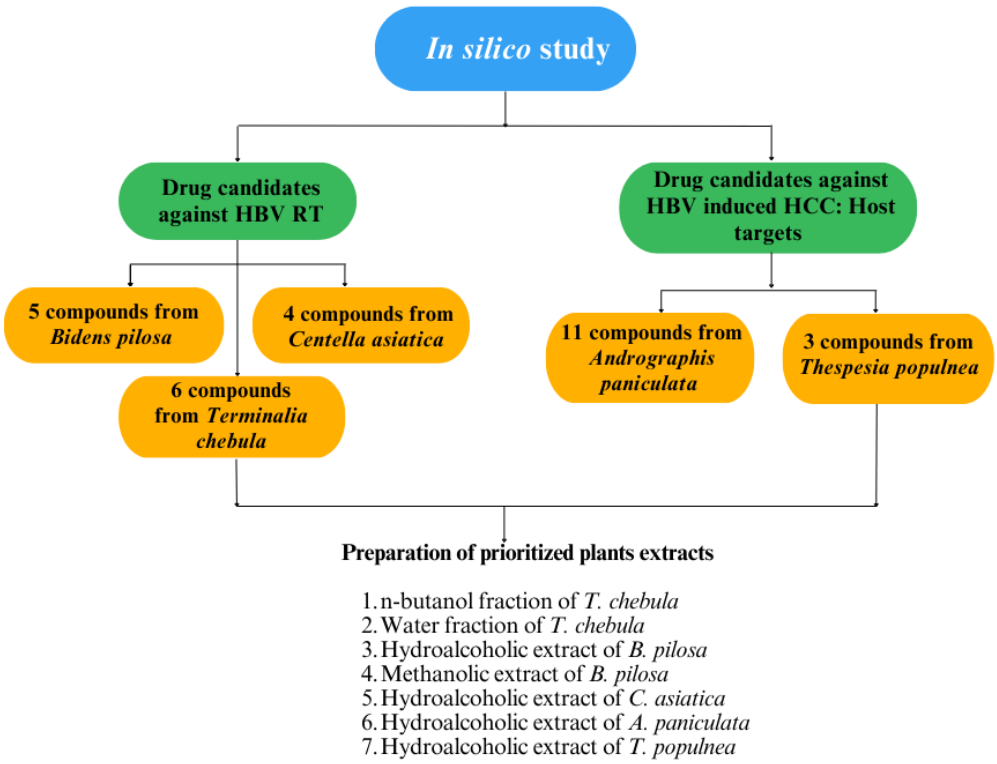


**Figure 9**: **Brief summary of the outcome of the *in silico* findings and preparation of extract.**

### 4.5.2. LC-MS analysis

*T. chebula* n-butanol (TCN) and water (TCW) fraction, *B. pilosa* hydroalcoholic (BPHA) and methanolic (BPM) extract, *C. asiatica* methanolic (CAM) extract, *A. paniculata* and *T. populnea* hydroalcoholic extract (APHA and TPHA) were subjected to LC-MS analysis (These extracts/fractions are reported to contain *in silico* identified compounds). The following conditions were maintained in running the sample on LC-MS ("(a) UPLC Make: Waters, USA, and Model: Acquity UPLC; (b) MS Make: Waters, USA and Model: Xevo G2-XS QTof); the C18 column (Accucore C18, 50 x 4.6, 2.6u) was used as a stationary phase; Mobile phase-A: 0.1% Formic acid in water and Mobile Phase- B: Acetonitrile was used; Capillary Voltage: 3.0KV, Collision Energy: 20V, Ramp Collision Energy: 30-90V, Source Temp: 150°C, Desolvation Temp: 450°C, Cone gas: 50L/Hr, Desolvation Gas Flow: 800L/Hr parameters were used". The extract was dissolved in the mobile phase and injected (volume 5 μL).[135]

### 4.5.3. *In vitro* cytotoxicity assay

#### 4.5.3.1. HepG2.2.15 cell line procurement and maintenance

HBV expressing HepG2.2.15 cell line "a subclone of HepG2 human hepatoblastoma that stably expresses the HBV" was kindly obtained from the International Centre for Genetic Engineering and Biotechnology (ICGEB) after approvals from the Institutional Biosafety Committee (IBSC) (IBKP TAI No. C100753). The cells were cultured DMEM with 10% FBS and antibiotics of choice (G418). The cells were cultured in T25 flasks and grown until they achieve 70% confluence in a humidified incubator at 37°C and 5% $CO_2$.

#### 4.5.3.2. Preparation of test samples

TCN, TCW, BPHA, BPM, CAHA, APHA, and TPHA were subjected to *in vitro* studies. The samples were first diluted to a stock concentration of 10mg/mL. From stock, different concentrations (15.65–2000µg/mL) for extracts and fractions and 15.62 to 250µM for PGG and TDF were prepared in DMEM and used for MTT assay.

#### 4.5.3.3. MTT assay

The cytotoxic activity of the above samples was tested on the HepG2.2.15 cell line and $CC_{50}$ was determined using MTT assay.[135] 20,000 cells/well were seeded onto a 96-well flat-bottom plate and were allowed to grow for 24h at 37°C in 5% $CO_2$. After incubation, the supernatant was discarded and treated with various concentrations of extract (250µL). After incubating for 24h, the supernatant was removed, and washed the wells thrice with PBS. MTT reagent (20µL, 5 mg/mL) was added and incubated for 4h. The MTT was removed and DMSO (100µL) was added to dissolve formazan crystals and read absorbance (Abs) at 570 nm. The $CC_{50}$ values were calculated using a linear regression curve.

$$\%\ Cell\ viability = \frac{Abs\ of\ control - Abs\ of\ sample}{Abs\ of\ control} \times 100$$

### 4.5.4. Reverse transcriptase inhibitory assay

The reverse transcriptase inhibitory assay of TCN, TCW, BPM, BPHA, CAHA, APHA, TPHA, PGG, and TDF was carried out using a manufacturer's protocol (Sigma Aldrich, USA; SKU No. 11468120910). In a separate tube, added 20µL of 4ng of RT and 20µL of the test drug diluted in lysis buffer. Lysis buffer was used as blank. Each tube was added with 20µL of the reaction mixture 3a and incubated for 1h at 37°C. The resultant mixture (60µL) was transferred to the kit's microplate modules and incubated

for 1h. The supernatant was discarded after incubation, and washed with 250µL of washing buffer five times. 200µL of Anti-DIG-POD (200 mU/ml, solution 5a) was added and incubated at 37°C for 1h. After incubation, washed the plates and added 200µL of ABTS substrate solution (solution 7) and incubated at 25°C for 10–30min. Finally, the Abs is read at 405nm.

$$\%\ RT\ Inhibition = \frac{Abs\ of\ control - Abs\ of\ sample}{Abs\ of\ control} \times 100$$

### 4.5.5. Relative quantification of intracellular HBV DNA and pgRNA by qRT-PCR

Based on the RT inhibitory activity, TCN, TCW, APHA, TPHA, PGG, and TDF were subjected to further studies. The genomic DNA free nucleic acid (Total RNA and viral DNA) was extracted from cells using RNeasy plus mini kit (Quiagen, Cat No. 74004) following the manufacturer's protocol. The extracted genomic free nucleic acid was quantified using Nanodrop (MAChine). cDNAs were synthesized using 200ng of genomic-free nucleic acid using PrimeScript RT Reagent Kit (DSS Takara Bio India, Cat No. RR037A) as per the manufacturer's protocol. The relative expression of pgRNA of HBV in each sample was quantified by real-time qPCR using SYBR green PCR Master Mix (DSS Takara Bio India; Cat No. RR820A) using primers HBVR-F: GAGTGTGGATTCGCACTCC, HBVR-R: GAGGCGAGGGAGTTCTTCT. Further, the HBV DNA from each sample was quantified using specific primers: HBVD-F: GTTGCCCGTTTGTCCTCTAATTC, HBVD-R: GGAGGGATACATAGAGGTTCCTTGA. RT PCR amplifications were performed on BIORAD CFX Maestro (Version 1.1). Cycle conditions were "95°C for 30s, followed by 40 cycles at 95°C for 5 s and 60°C for 30s". The relative mRNA expression was compared to that of beta-actin using the ΔΔCT technique. Specific transcript

amplification was confirmed through dissociation curve profiles with 1 cycle from 60 to 95°C at an increment of 0.5°C for 0.05s.

### 4.5.6. Time-course analysis of HBsAg and HBeAg secretion in HepG2.2.15 cell line

The cells were treated with different concentrations of test drugs (TCN, TCW, APHA, TPHA, PGG, and TDF) for 5 days. The level of HBsAg was measured on 24, 48, 72, 96, and 120h, and HBeAg was measured on 24, 72, and 120h in the culture medium (supernatant) using an ELISA kit according to the manufacturer's instructions [(HBsAg Hepalisa kit was purchased from J. Mitra & Co. Pvt. Ltd, Cat No. IR020096) and (HBeAg Kit was purchased from Bioneovan Co. Ltd, Cat No. BE103A)].

#### 4.5.6.1. Procedure for HBsAg

Briefly, 100µL of the positive and negative control and sample were added to the designated wells. To this, enzyme conjugate (50µL) was added and incubated for 60min at 37°C. After incubation, the plate was washed using a wash buffer for six times. Further, 100µL of the working substrate was added and incubated for 30 min at 27±2°C in the dark. Finally, 100µl stop solution was added to stop the reaction Abs was read at 450nm.

#### 4.5.6.2. Procedure for HBeAg

Briefly, 50µL of the positive and negative control and sample were added to the designated wells. To this, enzyme conjugate (50µL) was added and incubated for 60min at 37°C. After incubation, the plate was washed using a wash buffer for six times. Further, 100µL of the working substrate was added and incubated for 10min at 27±2°C in the dark. Finally, 50µl stop solution was added to stop the reaction Abs was read at 450nm.

The percentage HBsAg and HBeAg secretion inhibition is calculated as,

$$\%\ Inhibition = \frac{Abs\ of\ control - Abs\ of\ sample}{Abs\ of\ control} \times 100$$

### 4.5.7. HBx-HBXIP interaction inhibition assay

The level of HBx-HBxIP interaction inhibition was performed using a modified protocol of HBxAg (KinesisDX, Cat No. K12-1594) and HBXIP (KinesisDX, Cat No. K12-1577) ELISA kits. The percentage inhibition is calculated as,

$$\text{HBx} - \text{HBXIP interaction inhibition (\%)} = 100 - \frac{Abs\ of\ control - Abs\ of\ sample}{Abs\ of\ control} \times 100$$

## 4.6. *In vivo* pharmacology

### 4.6.1. *In vivo* pharmacology of TC and AP against alcohol-induced liver disease

The TC and AP effect on alcohol-induced liver disease was performed after receiving ethical approval from IAEC of ICMR-National Institute of Traditional Medicine, Belagavi (Reg. No. 1388/60/Re/S/10/CPCSEA Dated 03.02.2022 and Resolution No. IAEC/ICMR-NITM BGM/Apr2022/1); animals were maintained in pathogen-free conditions throughout the study; the complete study is detailed below.

### 4.6.2. Acute oral toxicity of TCN and AP

TCN and AP for *in vivo* study were selected based on all *in vitro* studies. The acute oral toxicity (OECD guideline No. 423) was performed to select the therapeutic doses. Since a single dose (2000 mg/kg) of TCN and AP administration did not cause any death of animals for the next 14 days, and hence, 3 doses in geometric series i.e. $1/20^{th}$ (100 mg/kg), $1/10^{th}$ (200 mg/kg), and $1/5^{th}$ (400 mg/kg) of 2000 mg/kg were considered for further study.

### 4.6.3. Induction of alcohol-induced liver disease and animal grouping

Animals were categorized into 12 groups, including a total of 72 male rats of which 6 served as healthy control. The study design is detailed as **(1) Normal**: vehicle

control; **(2) Alcoholic**: 5g/kg p.o. alcohol -treated[136–138]; **(3) Silymarin**: 100mg/kg p.o.[139,140]**; (4) TC100**: Alcoholic, TC (100 mg/kg)-treated, p.o.; (5) **TC200:** Alcoholic, TC (200 mg/kg)-treated, p.o.; **(6) TC400:** Alcoholic, TC (400 mg/kg)-treated, p.o.; (7) **AP100:** Alcoholic, TC (100 mg/kg)-treated, p.o.; (8) **AP200**: Alcoholic, TC (200 mg/kg)-treated, p.o.; (9) **AP400**: Alcoholic, TC (400 mg/kg)-treated, p.o.; **(10)** T+A100: Alcoholic, TC (50 mg/kg), AP (50 mg/kg)-treated, p.o.; **(11)** T+A200: Alcoholic, TC (100 mg/kg), AP (100 mg/kg)-treated, p.o.; (12) **T+A400**: Alcoholic, TC (200 mg/kg), AP (200 mg/kg)-treated, p.o.

### 4.6.4. Measurements and methods

#### 4.6.4.1. Measurement of body weight

The body weight of each rat was recorded every 3 consecutive days until 30 days and the percentage change in body weight was calculated.

#### 4.6.4.2. Euthanasia and organ collection

Following the separation of plasma and serum, the animals were euthanized using an overdose of anesthetic ether in order to obtain liver and kidney samples. Subsequently, the samples were washed with cooled phosphate buffer solution at a pH of 7.4. The liver was sectioned into 2 halves; one part liver was immersed in 10 % v/v formalin for histopathological examination. The 0.5 g of the second half of the liver was homogenized in chilled PBS (100mg/mL), centrifuged and the supernatant was deep-freezed for further use.

#### 4.6.4.3. Haematological and serum biochemical parameters

Blood was collected from the medial canthus of the eye on the last day of the experiment. Whole blood haematological parameters (RBC, WBC, Hb, MCV, etc.)

were determined. Serum lipid profiles viz., TG, TC, LDL, HDL, and the liver markers SGPT, SGOT, ALP, total bilirubin, total albumin, and creatinine level utilizing Erba kits.

#### 4.6.4.4. Estimation of anti-oxidant biomarkers

The enzymatic & non-enzymatic anti-oxidant profiles of TC and AP were quantified in liver homogenate (10% w/v, 0.5 mL) which are detailed below.

The **glutathione (GSH) level** was determined by incubating (30 min) the liver homogenate (250 µL) with DTNB (50µL) and sodium-phosphate buffer (2.5mL) and the absorbance was noted at 412 nm.[141] Further, to estimate **superoxide dismutase (SOD)**, the homogenate (25µL) was added to epinephrine (0.1mM in carbonate buffer, 50µL); change in absorbance was noted at 295 nm within 60 & 120 sec.[142] Also, **lipid peroxidation** was assessed by incubating (95℃, 1h) liver homogenate (200 µL) within the mixture of thiobarbituric acid (1.5mL, 0.8% w/v), $CH_3COOH$ (20% v/v), and SLS (200 µL, 8.1 w/v); cooled and centrifuged (10min, 4000rpm) to record the organic layer absorbance at 532nm; presented as TBARS nmol/mg of protein.[143]

#### 4.6.4.5 Estimation of serum TNF-α and IL6 level

Rat TNF-α (Catalog: ELR-TNFa) and IL-6 ELISA (Catalog: ELR-IL6) kits were procured from RayBio® and the manufacturer protocol was followed for estimation of TNF-α and IL6 concentration in serum. Briefly, added 100 µl standard TNF-α (2222, 740.7, 246.9, 82.3, 27.4pg/mL) and IL-6 (640, 256, 102.4, 40.96, 16.4pg/mL) and serum sample to each well (96 wells were provided separately for both kits) and incubated for 2.5h. Removed the supernatant and washed the wells four times. Added, 100 µl biotin antibody and again incubated 1h and again washed the wells. Further, added 100 µl Streptavidin and incubated for 45 min, and washed the wells. Finally, added 100 µl TMB Substrate, incubated for 30 min, added a stop solution and read the absorbance at 450

nm. The concentration of TNF-α and IL-6 in serum was determined using a standard calibration curve and expressed in pg/mL.

#### 4.6.4.6. Liver and kidney histopathology

Tissue samples were sectioned and were fixed with formalin (10% v/v); stained with hematoxylin-eosin to assess the effect of TC and AP over hepatic kupffer cell hyperplasia, venous congestion, portal triditis, ballooning degeneration, apoptosis, sinusoidal congestion, spotty necrosis, cholestasis, and inflammation at 10X and 40X magnification.

### 4.6.5. Statistics

#### 4.6.5.1. Statistical analysis

Gene set enrichment analysis was performed with a false discovery rate (FDR) cut-off of 0.05, and the network was analyzed using the "Edge count" topological parameter. Docking scores were expressed in kcal/mol, and the parameters describing structural stability were represented by C-α RMSF, backbone, and complex RMSD. MTT assay data were represented in % cell viability and $CC_{50}$ value. RT inhibition data were expressed as % inhibition and $IC_{50}$ value was determined. HBsAg and HBeAg levels are represented as % inhibition. The mRNA expression was analyzed using the relative fold change using ΔΔCT method. The *in vivo* experimental data were presented in Mean ± SEM wherever applicable. One-way and two-way analysis of variance (ANOVA) followed by post hoc Dunnett's test and Bonferroni multiple comparison test was applied to evaluate the quantitative data wherever applicable. Both quantitative and categorical data were evaluated using GraphPad Prism version 5.

# RESULTS

***In silico* pharmacology**

## 5.1. Study 1: Identification of herbal drug candidates against HBV reverse transcriptase by homology modelling, molecular docking, and dynamics studies.

### 5.1.1. Homology modelling

The Phyre2 server provided a structure of HBV-RT with a confidence score of >90% for 85% of the residues (out of a total of 343). Phyre2 modelled the structure of HBV-RT based on heuristics to optimize confidence, % identity, and alignment coverage using 6 HIV RT templates (5dmq, 3kk1, 1rth, 2zd1, 2opq, and 1mu2). The model structure was then refined using locPREFMD, yielding a final score of 1.302 (expected score<1.0). The model of HBV-RT was then refined until it reached an energetically favourable state using GalaxyRefine server. The Ramachandran plot showed ~97% of amino acids in the allowed and favoured region and ERRAT showed a quality score of 71.296 %.

### 5.1.2. Least potential energy conformation by MD simulation

All atom-explicit MD simulations were run for 100 ns to examine the structural stability of the improved HBV-RT model. At 89247ps, the lowest PE was found to be -150060.68 kcal/mol and that conformation was used further.

### 5.1.3. Stereochemical properties of refined HBV-RT model

The refined structure had ~98.7 % (including YMDD motif) amino acid in the favoured region and 0 % residues were found in the additionally allowed region and overall quality was 75.09%. Figure 10 represents the HBV RT modelled structure with its co-factor $Mg^{2+}$ and standard inhibitor.

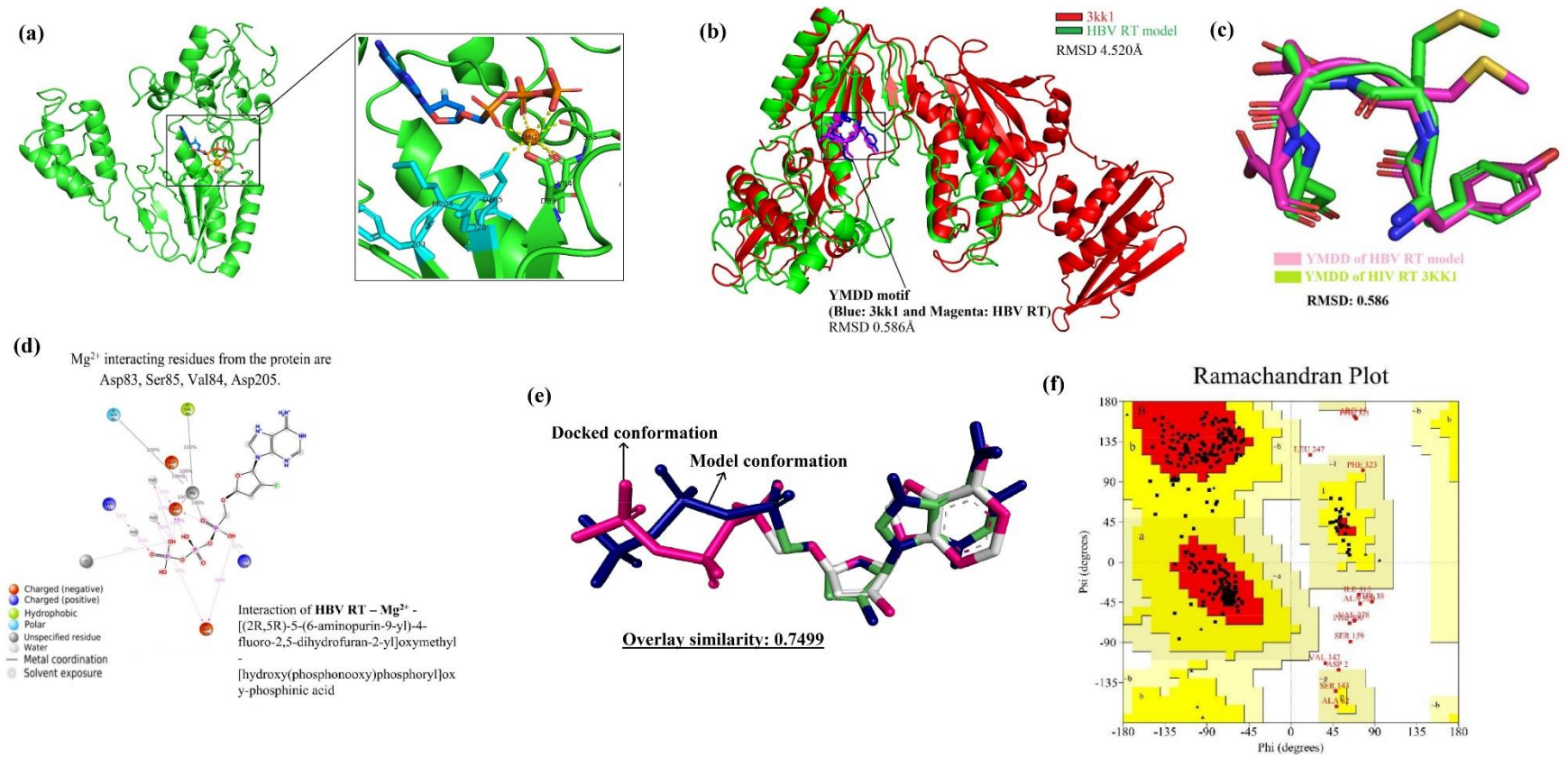


**Figure 10**: **Structural features of modelled HBV RT modelled structure.** (a) HBV with its co-factor $Mg^{2+}$ and standard inhibitor, (b) Overlay similarity of HBV RT model and HIV RT (PDB: 3kk1), (c) Overlay similarity of YMDD motif of HBV RT and HIV RT (PDB: 3kk1), (d) $Mg^{2+}$ ion interaction with standard drug, (e) Overlay similarity of standard drug before and after docking with HBV RT, and (f) Ramachandran plot of HBV RT model.

### 5.1.4. Structural similarity of HBV-RT

ModLoop was used to optimize the conformation similarity of the YMDD motif (active site) of the template and model. The overall structural similarity between the HBV-RT and 3kk1 was found to be RMSD of 4.520-Å and only for the YMDD motif was found to be RMSD of 0.586 Å. Furthermore, the structural study of HBV-RT (UniProt ID P03156) showed that the catalytic triads formed by the residues "Asp83, Asp205, and AspD206"—which are essential for the enzymatic activity—stabilize the two catalytic $Mg^{2+}$ ions. Only 3kk1 (one of the six templates utilized) was identified to have $Mg^{2+}$ and a known HIV RT inhibitor coupled to the active site. As a result, we used 3kk1 to remodel the HBV RT (i.e. HBV RT in complex with $Mg^{2+}$ and known inhibitor).

### 5.1.5. Metal ion and native ligand transfer

In the modelled "HBV-RT-$Mg^{+2}$ in complex with a known inhibitor, the $Mg^{2+}$ ion formed 5 co-ordination bonds with Asp83 (2.56 Å), Asp83 (2.75 Å), Val84 (2.23 Å), Ser85 (3.0 Å), Asp205 (2.26 Å), and known inhibitor formed one hydrophobic interaction i.e. Phe88 (2.94 Å), six hydrogen bonds i.e. Arg41 (2.18 Å), Asp83 (3.40 Å), Ala87 (1.97 Å), Asn236 (2.94 Å), Lys239 (2.97 Å), Lys239 (2.65 Å), one halogen bond Met171 (3.68 Å), and three salt bridges with Arg41 (4.41 Å), Arg41 (4.22 Å), and Lys239 (4.0 Å)".

### 5.1.6. Docking validation

The BE of a known inhibitor with HBV-RT was found to be -8.0kcal/mol. After docking, the $Mg^{2+}$ formed 5 co-ordination bonds with "Asp83 (2.56 Å), Asp83 (2.75 Å), Val84 (2.23 Å), Ser85 (3.0 Å), Asp205 (2.26 Å) and inhibitor formed five hydrogen bonds i.e. Arg41 (2.13 Å), Asp83 (3.13 Å), Arg41 (3.57 Å), Asp83 (3.71 Å), Lys239 (2.84 Å), one pi-cation interaction with Arg41 (3.78 Å), and three salt bridges with Arg41

(3.79 Å), Arg242 (5.24 Å), and Lys239 (5.36 Å)". Further, known inhibitor docked and model conformation structural superimposition showed a RMSD of 0.7499 Å.

### 5.1.7. Docking of phytocompound with HBV-RT

The virtual screening of 268 phytocompounds resulted in the top 15 molecules namely, Terflavin-C (BE -9.4kcal/mol), 1,3,6-Tri-O-galloyl-β-D-glucose (BE -9.3 kcal/mol), Tellimagrandin I (BE -9.1 kcal/mol), Chebulagic acid (BE -8.5 kcal/mol), 2,3,4,6 tetra-O-galloyl-β-D-glucose (BE -8.6 kcal/mol), and 1,2,3,4,6-penta-O-galloyl-e-D-glucose (BE -8.1 kcal/mol), from *Terminalia chebula*; Jacein (BE -8.5 kcal/mol), Centaurein (BE -7.9 kcal/mol), Okanin-4'-O-glucoside (Marein) (BE -7.8 kcal/mol), Okanin 4-methyl ether 3'-glucoside (BE -7.5 kcal/mol), and Okanin (BE -7.2 kcal/mol) from *Bidens pilosa*; Delphinidin 3-O-glucosyl-glucoside (BE -8.6 kcal/mol), Delphinidin 3,5-O-diglucoside (BE -8.2 kcal/mol), Castillicetin (BE -8.2 kcal/mol), and Isorhamnetin 3-O-rutinoside (BE -8.2 kcal/mol) from *Centella asiatica* were identified as potential inhibitors of HBV-RT via forming strong intermolecular interactions with YMDD and RT1 motif residues. Table 3 and Supplementary Table 2 represent the BE and interactions of prioritized and overall screened phytocompounds with HBV-RT, respectively.

**Table 3**: Binding energy and intermolecular interactions of phytocompounds with HBV-RT

| Plant name | Compound name | Class of compound | PubChem ID | Binding Energy (kcal/mol) | Hydrogen Bond interaction (No. of interactions) | Metal ion $Mg^{2+}$ interaction after MD simulation (Yes/No) | Van der waals, C-H, Pi-Cation, Pi-Anion, Amide-Pi stacked, Pi-Alkyl, Pi-Sigma |
|---|---|---|---|---|---|---|---|
| *Terminalia chebula* | 1,2,3,4,6-penta-O-galloyl-β-D-glucose | Tannin | 65238 | -8.1 | Val84, Ala87, Asp205 (2), Arg41, Lys239, Met171 (2) | Yes | Val43, Arg41, Ala87 |
| *Terminalia chebula* | Terflavin-C | Tannin | 101589227 | -9.4 | Lys239, Arg41 (2), Arg242, Asp206 (2), Asp205, Asn248 (2), Met250 | Yes | Lys239 (3), Asp83, Pro34, Arg41, Asp205, Arg242, Met250 |
| *Terminalia chebula* | Chebulagic acid | Tannin | 250397 | -8.5 | Arg41 (2), Asp205, Arg242, Asn248 (2), Gln262 | Yes | Met204 |
| *Terminalia chebula* | 2,3,4,6 tetra-O-galloyl-β-D-glucose | Tannin | 101011018 | -8.6 | Arg41, Ala87, Ser85, Asn236, Lys239, Asp206 (2) | Yes | Met204, Phe88, Met171, Val30, Val43, Ala86, Ser85, Asp205 (2), Asp206 |
| *Terminalia chebula* | 1,3,6-Tri-O-galloyl-β-D-glucose | Tannin | 452707 | -9.3 | Arg242, Asp206, Asp205 (2), Lys239, Val84, Ala87, Arg41 (2), Met171 | Yes | Met171, Lys239 |
| *Terminalia chebula* | Tellimagrandin I | Tannin | 442690 | -9.1 | Val44 (2), Arg41, Val84, Ala87 (2), Asp205 (3), Asp206, Arg242, Lys239 | Yes | Met204 (2), Ala87, Val43 |
| *Bidens pilosa* | Okanin | Flavonoid | 5281294 | -7.2 | Ser85, Arg41, Asp205 | Yes | Val48, Val30, Met171 |
| *Bidens pilosa* | Okanin-4'-O-glucoside (Marein) | Flavonoid | 6441269 | -7.8 | Met171, Phe88, Ala87, Ser85, Lys239, Asp206 (2) | Yes | Met171, Phe88 (2), Arg41, Asp205 |
| *Bidens pilosa* | Okanin 4-methyl ether 3'-glucoside | Flavonoid | 14162682 | -7.5 | Arg41 (2), Val44, Arg242, Asp206, Asp83 (2), Asp205 | No | Val43 |

| | | | | | | | |
|---|---|---|---|---|---|---|---|
| *Bidens pilosa* | Centaurein | Flavonoid | 5489090 | -7.9 | Asp205, Lys239, Arg242 | Yes | Arg41, Phe249, Phe88, Met171 |
| *Bidens pilosa* | Jacein | Flavonoid | 44259819 | -8.5 | Asp31, Lys239, Arg41 (2), Asp206, Asp205 | No | Ala86, Arg41 (2), Lys239, Asp31 |
| *Centella asiatica* | Castillicetin | Flavonoid | 102394640 | -8.2 | Asp206, Arg41, Asp83 | Yes | Arg41, Asp205, Val43, Val30, Met171 |
| *Centella asiatica* | Isorhamnetin 3-O-rutinoside | Flavonoid | 5481663 | -8.2 | Asp31, Asn248, Asp205, Ala87, Phe88 | Yes | Lys239, Asp206, Arg242 (3), Leu42, Met171 |
| *Centella asiatica* | Delphinidin 3-O-glucosyl-glucoside | Flavonoid | 5316496 | -8.6 | Arg41 (2), Met171, Arg242, Ser85, Val84, Ala87, Lys239, Asp205, Asn248, Asp206, | No | Arg41, Ala87, Asp206 |
| *Centella asiatica* | Delphinidin 3,5-O-diglucoside | Flavonoid | 10100906 | -8.2 | Val44, Ala87, Arg41, Asp205, Asp206 | No | Met171, Ser85, Val30 (2), Arg41 (2), Asp205, Met204 |
| **Standard inhibitor** | "[(2R,5R)-5-(6-aminopurin-9-yl)-4-fluoro-2,5-dihydrofuran-2-yl]oxymethyl-[hydroxy(phosphonooxy)phosphoryl]oxy-phosphinic acid | HIV RT Inhibitor from 3kk1 PDB | https://www.rcsb.org/ligand/914 | -8.0 | Phe88, Ala87, Arg41 (2), Lys239 | Yes | Arg242 (2), Asp83, Asp206, Asp205, Lys239, Arg41 |

### 5.1.8. Structural stability of docked complexes

The backbone and complex RMSD and C-α RMSF of MD simulation are the main measures of structural stability; in this study, we studied the RMSD of the backbone, the protein-ligand complex, and the RMSF (C-α) of a standard molecule, as well as 15 lead hit phytocompounds complexed with HBV-RT (refer Figure 11).

#### 5.1.8.1. Stability of HBV-RT – $Mg^{2+}$ – Std model

The backbone RMSD was between ~4.0 Å to 5.8 Å from 0 ns to ~35 ns and further showed more stability from 35 ns to 100 ns by sustaining within RMSD of 5.5Å to 6.4 Å. Likewise, RMSD of the protein-ligand complex fluctuated slightly and was steady between 0 and 35ns. The complex RMSD initially exhibited significant fluctuations (ranging from 7.5 to 11Å), but it eventually stabilized at a higher RMSD of 11.0Å till 100ns. The C-terminal loop region fluctuated the most due to the flexibility of the terminal residues. The C-terminal linker region that connects the helices Leu311 and Ala320 showed significant fluctuation >4Å. The active site residues Asp83, Val84, Ser85, Tyr203, Met204, Asp205, and Asp206 formed stable interactions with $Mg^{2+}$ and the ligand exhibited the least fluctuation up to ~1.5Å. The complex intermolecular interaction investigation revealed that Asp83, Val84, Ser85, and Asp205 form an extremely stable (100%) interaction fraction with $Mg^{2+}$. Tyr245 and Asn248 developed a persistent hydrophobic contact with the ligand for around 22% and 37%, respectively. Additionally, it was shown that Glu39, Arg41, Ala86, Tyr245, Asn245, and Gln262 were all involved in the formation of hydrogen-bonded contacts.

#### 5.1.8.2. Stability of HBV-RT-$Mg^{2+}$ -Std docked complex

The HBV-RT – $Mg^{2+}$ – Std docked complex showed an equilibration period of about 15ns, further which it showed stable RMSD value ranging from ~7.2 to 9 Å. A

similar trend of RMSD was also observed in the protein-ligand complex, but this complex got stabilized at a relatively higher RMSD of 9.5 to 14.5Å after the equilibration period of the first 15 ns. Similar to the control complex, this re-docked complex also showed higher fluctuations mainly at the C-terminal loop region. The linker joining the two helices at the C-terminal (Leu311 to Ala320) showed higher fluctuation >5 Å. The binding pocket residues Asp83, Val84, Ser85, Tyr203, Met204, Asp205, and Asp206 showed the least fluctuations up to ~2.0 Å, as these are actively engaged in forming stable interactions with $Mg^{2+}$ and ligand. Asp205 and Asp206 residues showed stable H-bonded interaction fractions for around 61% and 39%, respectively, and water bridge interaction fractions for about 15% and 10%, respectively. While Lys239 and Arg41 formed a water-bridge interaction fraction of around 11% (refer to Figure 12).

#### 5.1.8.3. Stability of HBV-RT-$Mg^{2+}$- Phytocompound complexes

The top-ranking 15 complexes were subjected to 100 ns MD simulation. In comparison to the reference molecule, the MD simulation showed 15 compounds from the plants *T. chebula* (6), *B. pilosa* (5), and *C. asiatica* (4) to exhibit stable ligand-protein interactions, stable RMSD, and least fluctuation of interaction with the active site. The HBV-RT - 1,2,3,4,6-penta-O-galloyl-D-glucose complex (from *T. chebula*) was shown to be the top ranking probable hit among these 15 complexes when taking into account the greatest binding affinity, stable contacts, stable RMSD, and RMSF values.

##### 5.1.8.3.1. Stability of HBV-RT and 1,2,3,4,6-penta-O-galloyl-β-D-glucose complex

In comparison to the other complexes, this complex demonstrated more stability in MD simulation, with RMSD values ranging from 4.0Å to 8.6Å. During the equilibration interval of 0–20 ns, a steady increase in RMSD value from 4.0Å to 7.5Å was seen, and it thereafter stabilized at higher RMSD values (8.0Å and 9.0Å). While the

RMSD for the whole protein-ligand complex remains relatively stable (4.8Å to 6.0Å) throughout the simulation period. The C-terminal linker region that connects the helices Leu311 and Ala320 showed significant fluctuation >4Å. The active site residues Asp83, Val84, Ser85, Tyr203, Met204, Asp205, and Asp206 formed stable interactions with $Mg^{2+}$ and the ligand and exhibited the least fluctuation up to ~1.4Å. Further, examined the intermolecular interactions, in which Asp205 forms a water bridge for 24% and hydrogen bond interactions for 53%, 34%, and 20%. Asp206 showed H-bonding interactions for 46%, 33%, and 21% of the interaction fraction as well as water-bridge formation (12%). Arg41 shows a water bridge for 34% and residues Ser40, Leu42, Ala87, Phe88, Gly172, Asn248, Phe249, Met250, Arg289, and Gly292 also showed water-bridge, hydrophobic, and hydrogen interactions with 1,2,3,4,6-penta-O-galloyl-D-glucose (refer to Figure 12).

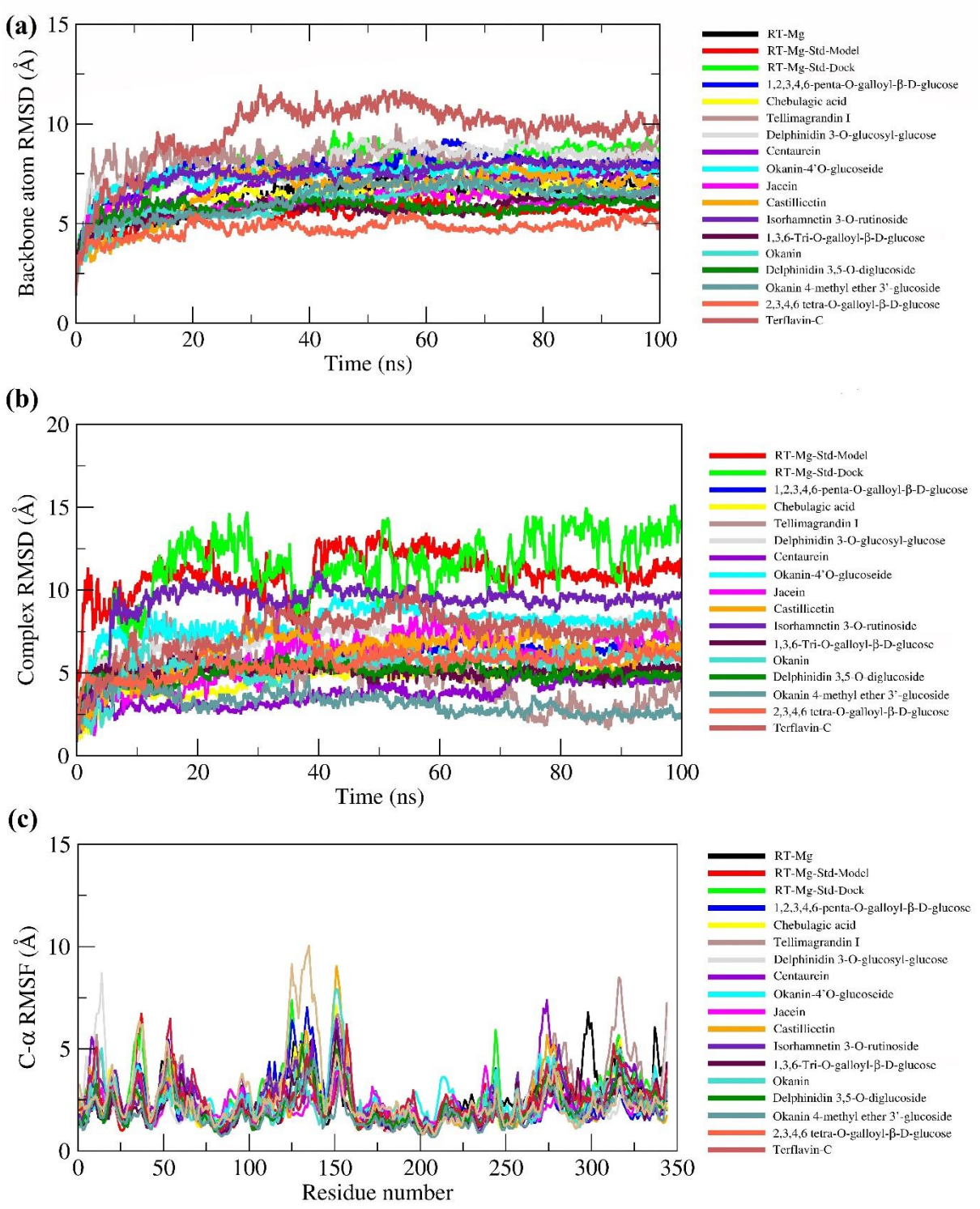


**Figure 11: Structural stability of standard molecule, as well as selected 15 phytocompounds complexed with HBV-RT.** (a) RMSD of the backbone atoms, (b) protein-ligand atoms (complex), and (c) RMSF of C-alpha atoms.

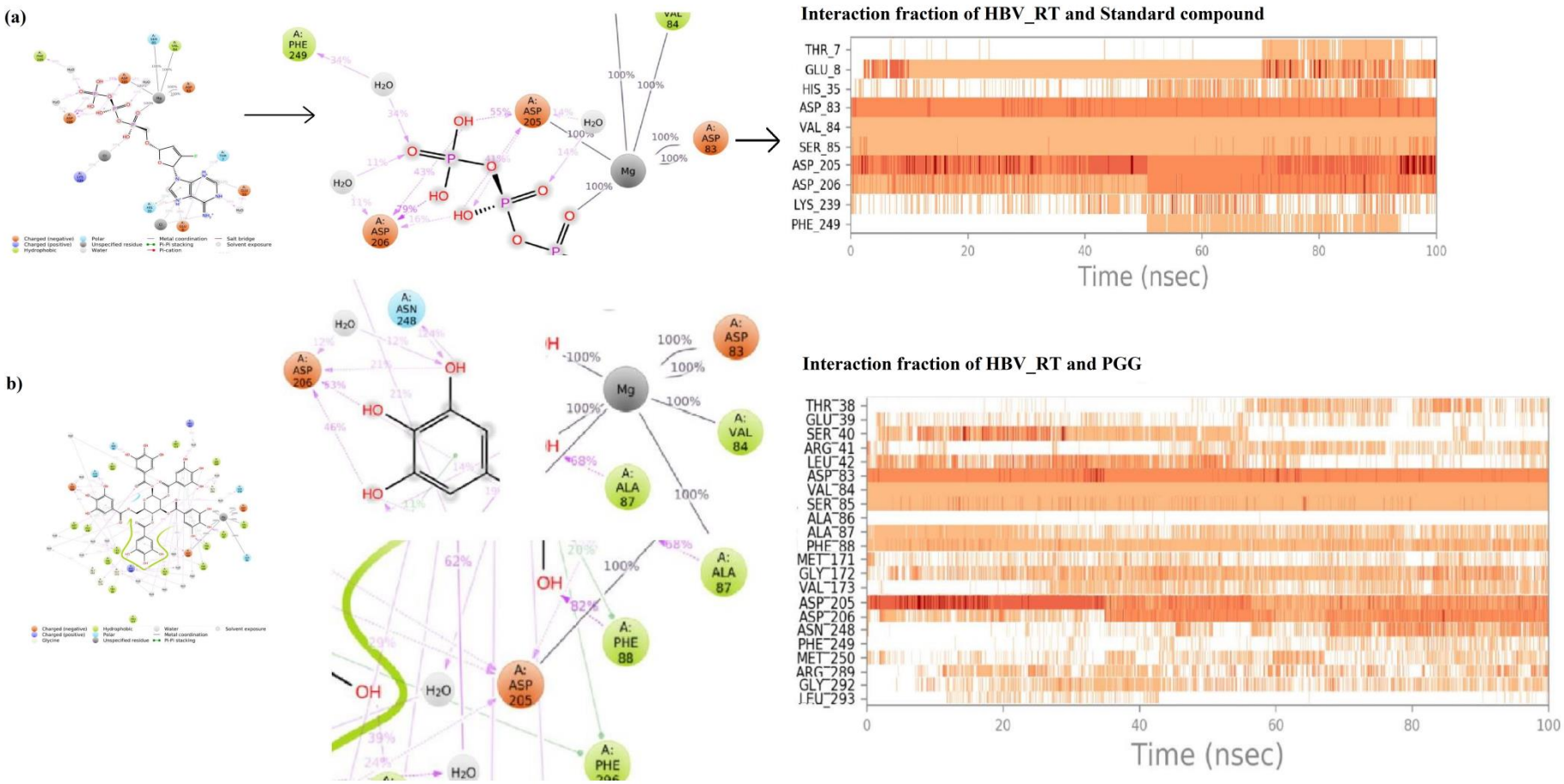


**Figure 12: Binding mode and interaction fraction of standard molecules and PGG with HBV RT.**

### 5.1.9. MM-GBSA calculation

The 1,2,3,4,6-penta-O-galloyl-e-D-glucose complex, which was one of the 15 complexes investigated, has the lowest free binding energy of -113.774 kcal/mol. On the other hand, the Okanin 4-methyl ether 3'-glucoside was shown to be the second-ranked complex with the least free binding energy of -87.165 kcal/mol. When compared to HBV-RT's known inhibitors, these complexes demonstrated much greater binding affinity (RT-$Mg^{2+}$-Std model complex = -25.075 kcal/mol and RT-$Mg^{2+}$-Std-Docked complex = -11.069 kcal/mol). Table 4 describes the energy components estimated with prime MM-GBSA calculation.

**Table 4**: **Prime MM-GBSA calculation of the HBV RT phytocompounds last frame complexes**

| Compound name | PubChem CID | ΔG Bind (kcal/mol) | ΔG Bind Coulomb | ΔG Bind Covalent | ΔG Bind Hbond | ΔG Bind Solv GB | ΔG Bind vdW |
|---|---|---|---|---|---|---|---|
| 1,2,3,4,6-penta-O-galloyl-e-D-glucose | 65238 | -113.774 | -55.649 | 2.943 | -2.913 | 78.094 | -85.004 |
| Chebulagic acid | 250397 | -41.325 | -273.990 | 9.770 | -1.492 | 301.630 | -52.452 |
| Tellimagrandin I | 442690 | -49.798 | -101.560 | 0.773 | -1.650 | 148.192 | -64.050 |
| 1,3,6-Tri-O-galloyl-β-D-glucose | 452707 | -28.760 | -20.085 | -2.028 | -1.613 | 53.421 | -41.834 |
| Okanin | 5281294 | -37.892 | -109.257 | 4.762 | -1.158 | 126.926 | -33.450 |
| Delphinidin 3-O-glucosyl-glucoside | 5316496 | -53.087 | -30.011 | 2.125 | -2.372 | 58.958 | -38.960 |
| Isorhamnetin 3-O-rutinoside | 5481663 | -45.786 | -22.371 | 7.223 | -1.244 | 46.273 | -47.676 |
| Centaurein | 5489090 | -48.112 | -51.000 | 8.306 | -1.676 | 71.999 | -49.091 |
| Okanin-4'-O-glucoside (Marein) | 6441269 | -32.156 | -16.680 | 6.381 | -0.981 | 53.801 | -42.894 |

| | | | | | | | |
|---|---|---|---|---|---|---|---|
| Delphinidin 3,5-O-diglucoside | 10100906 | -46.600 | -41.236 | 8.229 | -1.266 | 71.358 | -42.466 |
| Okanin 4-methyl ether 3'-glucoside | 14162682 | -87.165 | -49.590 | 7.105 | -2.323 | 50.091 | -55.394 |
| Jacein | 44259819 | -26.640 | -31.620 | 11.293 | -0.470 | 62.269 | -40.448 |
| 2,3,4,6 tetra-O-galloyl-β-D-glucose | 101011018 | -65.812 | -154.591 | 8.371 | -1.269 | 186.386 | -62.583 |
| Terflavin-C | 101589227 | -30.623 | -213.339 | 11.213 | -2.069 | 257.182 | -50.176 |
| Castillicetin | 102394640 | -34.733 | -28.701 | -1.388 | -2.345 | 48.782 | -26.827 |
| RT-Mg_Std-Model | -- | -25.075 | -401.053 | 0.793 | -0.542 | 403.698 | -22.107 |
| RT_Mg_Std_Dock | -- | -11.069 | -295.403 | 3.694 | -0.741 | 306.669 | -21.207 |

### 5.1.10. Gene set enrichment and network analysis

The gene set enrichment analysis of 15 phytocompounds modulated 74 targets (Supplementary Table 3) which were involved in 37 biological pathways (Supplementary Table 4). Out of 74 targets and 37 pathways, 39 targets were associated with 15 molecular pathways (Supplementary Table 5) in HBV associated HCC. Complement and coagulation cascades, Steroid hormone biosynthesis, Tryptophan metabolism, MicroRNAs in cancer, HIF-1 signalling pathway, Calcium signalling pathway, Proteoglycans in cancer, Bile secretion, Transcriptional misregulation in cancer, and Viral protein interaction with cytokines. TNF, PLAU, PTPN1, and MMP9 were shown to be hub genes within the network among these 39 protein targets as they scored edge counts of 11, 9, 9, and 9, respectively (Figure 13).

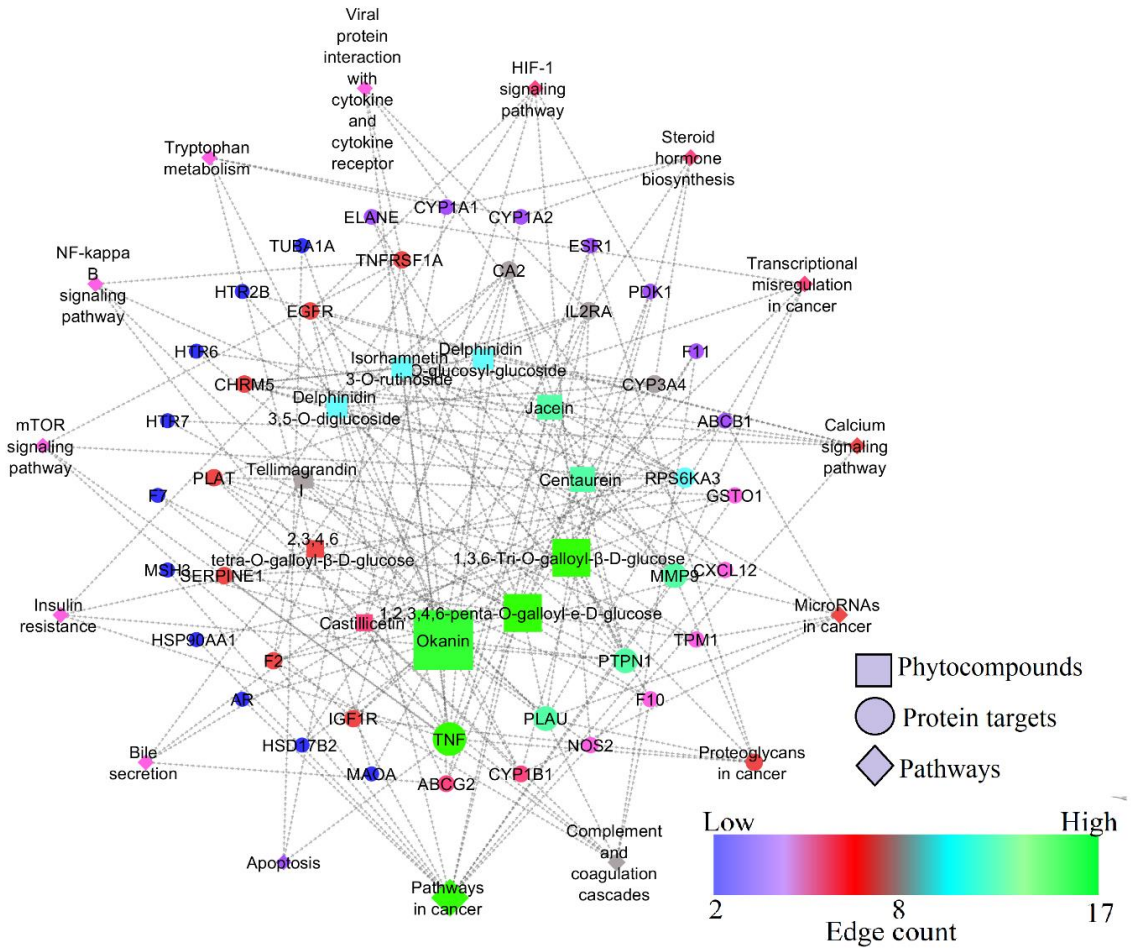


**Figure 13**: **Network representation of phytocompounds of *T. chebula, B. pilosa,* and *C. asiatica* and their modulated genes and pathways.**

### 5.1.11. Prediction of drug-likeness and biological spectrum

Terflavin-C scored the lowest DLS of 0.05, while 1,3,6-Tri-O-galloyl-D-glucose had the highest DLS of 0.92. Interestingly, all phytocompounds had positive DLS. Further, 15 compounds anti-viral biological spectra were retrieved from the PASS online service with Pa >0.3 including 13 compounds (2 of which were not predicted) that were found to have hepatoprotective and antiviral effects (Table 4).

Table 4: Antiviral biological spectrum of 15 phytocompounds

| **Plant name** | **Compound name** | **Druglikeness score** | **Activities confirmed (Pharmacological activity Pa>0.3)** |
|---|---|---|---|
| *Bidens pilosa* | Okanin | 0.23 | Antiviral (Influenza)(0.679), Hepatoprotectant(0.587), Hepatic disorders treatment(0.441), Antiviral (Herpes)(0.406), Antiviral(0.39), Antiviral (HIV)(0.322) |
| *Bidens pilosa* | Centaurein | 0.71 | Hepatoprotectant(0.972), Hepatic disorders treatment(0.672), Antiviral (Influenza)(0.56), Antiviral (Herpes)(0.495), Antiviral (Hepatitis B)(0.479) |
| *Bidens pilosa* | Okanin-4'-O-glucoside (Marein) | 0.61 | Hepatoprotectant(0.916), Antiviral (Influenza)(0.806), Hepatic disorders treatment(0.631), Antiviral (Herpes)(0.479), Antiviral(0.403), Antiviral (Hepatitis B)(0.402) |
| *Bidens pilosa* | Okanin 4-methyl ether 3'-glucoside | 0.64 | Hepatoprotectant(0.905), Antiviral (Influenza)(0.778), Hepatic disorders treatment(0.572), Antiviral (Herpes)(0.456), Antiviral (Hepatitis B)(0.356), Antiviral(0.338) |
| *Bidens pilosa* | Jacein | 0.65 | Hepatoprotectant(0.972), Antiviral (Influenza)(0.56), Antiviral (Herpes)(0.495), Antiviral (Hepatitis B)(0.479) |
| *Centella asiatica* | Delphinidin 3-O-glucosyl-glucoside | 0.24 | Not predicted: Molcharge: 1 |
| *Centella asiatica* | Isorhamnetin 3-O-rutinoside | 0.79 | Hepatoprotectant(0.976), Antiviral (Influenza)(0.728), Hepatic disorders treatment(0.668), Antiviral (Herpes)(0.506), Antiviral (Hepatitis B)(0.428) |
| *Centella asiatica* | Delphinidin 3,5-O-diglucoside | 0.67 | Not predicted: Molcharge: 1 |
| *Centella asiatica* | Castillicetin | 0.65 | Hepatoprotectant(0.8), Hepatic disorders treatment(0.545), Antiviral (Hepatitis B)(0.479), Antiviral (Herpes)(0.455), Antiviral (Influenza)(0.4) |
| *Terminalia chebula* | 1,2,3,4,6-penta-O-galloyl-e-D-glucose | 0.19 | Hepatoprotectant(0.752), Antiviral (Herpes)(0.53), Antiviral (Influenza)(0.505), Hepatic disorders treatment(0.479), Antiviral(0.384), Antiviral (Rhinovirus)(0.336) |
| *Terminalia chebula* | Chebulagic acid | 0.58 | Hepatoprotectant(0.798), Antiviral (Herpes)(0.559), Hepatic disorders treatment(0.422), Antiviral (Hepatitis B)(0.348) |
| *Terminalia chebula* | Tellimagrandin I | 0.3 | Hepatoprotectant(0.884), Antiviral (Herpes)(0.668), Hepatic disorders treatment(0.581), Antiviral (Hepatitis B)(0.377), Antiviral(0.343) |
| *Terminalia chebula* | 1,3,6-Tri-O-galloyl-β-D-glucose | 0.92 | Hepatoprotectant(0.783), Antiviral (Influenza)(0.676), Hepatic disorders treatment(0.557), Antiviral (Herpes)(0.513), Antiviral(0.411), Antiviral (Hepatitis B)(0.354), Antiviral (Rhinovirus)(0.348), Antiviral (Picornavirus)(0.305) |
| *Terminalia chebula* | 2,3,4,6 tetra-O-galloyl-β-D-glucose | 0.44 | Hepatoprotectant(0.608), Antiviral (Rhinovirus)(0.595), Antiviral (Influenza)(0.509), Hepatic disorders treatment(0.424), Antiviral(0.33), Antiviral (Adenovirus)(0.345), Antiviral (Herpes)(0.318), Antiviral (Picornavirus)(0.303) |
| *Terminalia chebula* | Terflavin-C | 0.05 | Hepatoprotectant(0.973), Hepatic disorders treatment(0.759), Antiviral (Herpes)(0.567), Antiviral (Hepatitis B)(0.513), Antiviral(0.365) |

## 5.2. Study 2: Identification of drug candidates against HBV-induced hepatocellular carcinoma based on network pharmacology analysis: compounds interaction with host targets.

### 5.2.1. Selection of plants, mining of phytocompounds, drug-likeness, and toxicity profile

Sixteen plants that remained in Study 1 were further processed for their interaction with host targets associated with HCC. Overall, 145 compounds showed positive drug-likeness properties (Supplementary Table 6). Among these 145 compounds, 36 compounds showed Pa≤0.5 and nontoxic properties (Supplementary Tables 7 and 8).

### 5.2.3 Target identification

Potential protein targets of 36 phytochemicals were predicted using BindingDB. All of these phytocompounds have been predicted to affect 206 different protein targets (refer to Supplementary Table 9). Out of 206 targets, 16 targets were found to be involved in the development of HBV infection-related HCC (Table 5).

**Table 5**: **Phytocompounds and their probable predicted protein targets involved in hepatitis B infection pathways and its associated hepatocellular carcinoma.**

| Plant name | Phytocompounds | Plant part | Compound type | Gene count | Protein targets involved in Hepatitis B infection and HCC pathways |
|---|---|---|---|---|---|
| *Aerva lanata* | Isorhamnetin | Aerial | Flavonoid | 7 | *CDK1, CDK2, CDK6, EGFR, HGF, IGF1R, TERT* |
| | Tiliroside | Aerial | Flavonoid | 1 | *TNF* |
| *Aloe vera* | 2-Methyl-2-Phytyl-6-Chromanol | Whole plant | Phylloquinone | 1 | *AKT1* |
| | Aloe-Emodin | Leaf, Juice | Anthraquinone | 1 | *BCL2* |
| | Aloenin | Whole plant | Glucoside | 1 | *TNF* |
| | Feralolide | Leaf | Coumarin | 2 | *MAP2K1, MAPK1* |
| *Andrographis paniculata* | 5-Hydroxy-7,8,2',3'-Tetramethoxyflavone | Whole plant, Root | Flavonoid | 6 | *CDK1, CDK6, EGFR, HGF, IGF1R, TERT* |

| | | | | | |
|---|---|---|---|---|---|
| | 5-Hydroxy-7,8,2'-Trimethoxyflavone | Whole plant, Root | Flavonoid | 6 | *CDK1, CDK6, EGFR, HGF, IGF1R, TERT* |
| | Neoandrographolide | Whole plant, Root | Diterpenoid | 1 | *STAT3* |
| | Paniculide-B | Whole plant, Stem | Diterpenoid | 3 | *PRKCA, PRKCB, PRKCG* |
| | Andrographiside | Whole plant, Stem | Flavonoid | 4 | *PRKCB, PRKCA, PRKCG, STAT3* |
| | Altisin | Whole plant, Stem | Flavonoid | 6 | *CDK1, CDK6, EGFR, HGF, IGF1R, TERT* |
| | 2'-hydroxy-5,7,8-trimethoxyflavone | Whole plant, Stem | Flavonoid | 6 | *CDK1, CDK6, EGFR, HGF, IGF1R, TERT* |
| | 5-hydroxy-7,8,2',3',4'-pentamethoxyflavone | Whole plant, Stem | Flavonoid | 6 | *CDK1, CDK6, EGFR, HGF, IGF1R, TERT* |
| | Wightin | Whole plant, Stem | Flavonoid | 6 | *CDK1, CDK6, EGFR, HGF, IGF1R, TERT* |
| | 5-hydroxy-7,8-dimethoxyflavanone | Whole plant, Stem | Flavonoid | 3 | *AKT1, HGF, TERT* |
| | 5-hydroxy-7,8-dimethoxyflavone | Whole plant, Stem | Flavonoid | 6 | *CDK1, CDK6, EGFR, HGF, IGF1R, TERT* |
| | Skullcapflavone I | Whole plant, Stem | Flavonoid | 6 | *CDK1, CDK6, EGFR, HGF, IGF1R, TERT* |
| | 5-hydroxy-7,8,2',5'-tetramethoxyflavone | Whole plant, Stem | Flavonoid | 6 | *CDK1, CDK6, EGFR, HGF, IGF1R, TERT* |
| | 5,4'-dihydroxy-7,8,2',3'-tetramethoxyflavone | Whole plant, Stem | Flavonoid | 6 | *CDK1, CDK6, EGFR, HGF, IGF1R, TERT* |
| | Andrographidine C | Whole plant, Stem | Flavonoid | 2 | *EGFR, TNF* |
| *Cassia auriculata* | Pelargonidin 5-galactoside | Leaves | Anthocyanidin | 2 | *EGFR, TNF* |
| *Centella asiatica* | 3-Glucosylkaempferol | Leaves | Flavonoid | 2 | *EGFR, TNF* |
| | 3-Glucosylquercetin | Leaves | Flavonoid | 2 | *EGFR, TNF* |
| *Mangifera indica* | Cyanidin 3-arabinoside | Peel | Anthocyanin | 1 | *TNF* |
| | Myrtillin | - | Phenolic compound | 1 | *TNF* |
| | Peonidin galactoside | Peel | Anthocyanin | 1 | *TNF* |
| | Petunidin 3-glucoside | Peel | Anthocyanin | 1 | *TNF* |
| *Phyllanthus virgatus* | Kaempferol 8-C-sulfate | Whole plant | Flavonoid | 1 | *EGFR* |
| *Pongamia pinnata* | Pinnatin | Seed | Flavonoid | 6 | *CDK1, CDK6, EGFR, HGF, IGF1R, TERT* |
| | Pongamone A | Stem | Flavonoid | 1 | *EGFR* |

| | | | | | |
|---|---|---|---|---|---|
| *Thespesia populnea* | Gossypetin | Flower, Stem, Root | Flavonoid | 7 | *CDK1, CDK2, CDK6, EGFR, HGF, IGF1R, TERT* |
| | Herbacetin | Flower | Flavonoid | 7 | *CDK1, CDK2, CDK6, EGFR, HGF, IGF1R, TERT* |
| | Kaempferol-7-Glucoside | Flowers | Flavonoid | 2 | *EGFR, TNF* |
| *Vernonia cinerea* | Luteolin-7-Mono-Beta-D-Glucoside | Seed | Flavonoid | 2 | *EGFR, TNF* |

### 5.2.4. Gene set enrichment analysis and network construction

The GO functional and process enrichment revealed that these 16 targets to affect 599 molecular processes and 46 molecular functions (Supplementary Tables 10 and 11, respectively). Furthermore, the KEGG pathway enrichment analysis showed that 36 phytocompounds affected 139 pathways *via* modulating 16 targets, in which 14 pathways were shown to be crucial in the development of HBV-induced HCC. The 36 phytocompounds with their 16 targets and 139 pathways were shown in Supplementary Table 12. Table 6 depicts the phytocompound-modified pathways that are only associated with HBV-induced HCC.

**Table 6**: **Pathways involved in the HBV infection and its associated hepatocellular carcinoma modulated by the phytocompounds**

| KEGG ID | Pathway name | Gene count | False Discovery Rate | Modulated gene within a pathway |
|---|---|---|---|---|
| hsa05161 | Hepatitis B | 11 | 1.07E-18 | *AKT1, BCL2, CDK2, CDK6, MAP2K1, MAPK1, PRKCA, PRKCB, PRKCG, STAT3, TNF* |
| hsa05225 | Hepatocellular carcinoma | 11 | 3.43E-18 | *AKT1, CDK6, EGFR, HGF, IGF1R, MAP2K1, MAPK1, PRKCA, PRKCB, PRKCG, TERT* |
| hsa01521 | EGFR tyrosine kinase inhibitor resistance | 11 | 6.37E-21 | *AKT1, BCL2, EGFR, HGF, IGF1R, MAP2K1, MAPK1, PRKCA, PRKCB, PRKCG, STAT3* |
| hsa05206 | MicroRNAs in cancer | 9 | 2.07E-14 | *BCL2, CDK6, EGFR, MAP2K1, MAPK1, PRKCA, PRKCB, PRKCG, STAT3* |
| hsa04010 | MAPK signaling pathway | 10 | 7.51E-14 | *AKT1, EGFR, HGF, IGF1R, MAP2K1, MAPK1, PRKCA, PRKCB, PRKCG, TNF* |
| hsa04151 | PI3K-Akt signaling pathway | 10 | 3.22E-13 | *AKT1, BCL2, CDK2, CDK6, EGFR, HGF, IGF1R, MAP2K1, MAPK1, PRKCA* |

| | | | | |
|---|---|---|---|---|
| hsa04014 | Ras signaling pathway | 9 | 5.60E-13 | *AKT1, EGFR, HGF, IGF1R, MAP2K1, MAPK1, PRKCA, PRKCB, PRKCG* |
| hsa04150 | mTOR signaling pathway | 8 | 1.52E-12 | *AKT1, IGF1R, MAP2K1, MAPK1, PRKCA, PRKCB, PRKCG, TNF* |
| hsa04210 | Apoptosis | 5 | 2.18E-07 | *AKT1, BCL2, MAP2K1, MAPK1, TNF* |
| hsa05203 | Viral carcinogenesis | 5 | 8.12E-07 | *CDK1, CDK2, CDK6, MAPK1, STAT3* |
| hsa04668 | TNF signaling pathway | 4 | 3.85E-06 | *AKT1, MAP2K1, MAPK1, TNF* |
| hsa04630 | Jak-STAT signaling pathway | 4 | 1.57E-05 | *AKT1, BCL2, EGFR, STAT3* |
| hsa04115 | p53 signaling pathway | 3 | 4.58E-05 | *CDK1, CDK2, CDK6* |
| hsa04110 | Cell cycle | 3 | 0.00021 | *CDK1, CDK2, CDK6* |

### 5.2.5. Network analysis

A network study found "Skullcapflavone I, Wightin, 2'-hydroxy-5,7,8-trimethoxyflavone, Altisin, Andrographiside, 5-Hydroxy-7,8,2'-Trimethoxyflavone,5-hydroxy-7,8,2',3',4'- pentamethoxyflavone, 5-hydroxy-7,8,2',5'- tetramethoxyflavone, 5,4'-dihydroxy-7,8,2',3'- tetramethoxyflavone, Andrographidine C, Wightin, 5-hydroxy-7,8-dimethoxyflavanone, 5-hydroxy-7,8-dimethoxyflavone, 5-Hydroxy-7,8,2',3'-Tetramethoxyflavone and Paniculide-B from *Andrographis paniculata* (whole plant); Herbacetin, Gossypetin, Kaempferol-7-Glucoside from *Thespesia populnea* (Flowers); had highest edge count via modulating AKT1, BCL2, HGF, IGF1R, MAP2K1, MAPK1, PRKCA, PRKCB, PRKCG, STAT3, CDK2, CDK6, STAT3, TNF, and TERT within the network and identified as enriched hub genes among the 14 pathways, which allowed for the identification of EGFR tyrosine kinase inhibitor resistance, hepatitis B, and hepatocellular carcinoma pathway" (Table 5 and Table 6). However, given to their likely affinity towards several targets and pathways, the aforementioned compounds were taken into consideration based on polypharmacology treatment. Figure 14 depicts the herb-compound-protein-pathway network. Based on the polypharmacology analysis, phytocompounds that are predicted to affect a variety of protein targets and pathways

were chosen for further docking studies. As a result, 11 phytocompounds from *Andrographis paniculata* were predicted to target 13 protein molecules, and 3 phytocompounds from *Thespesia populnea* were predicted to target 8 protein molecules involved in HBV-induced HCC. These predictions are shown in a Venn diagram (Supplementary Figure 1). Figure 15 illustrates the phytochemicals that potentially altered hepatitis B infection pathway checkpoints that were tracked from the KEGG pathway (hsa05161).

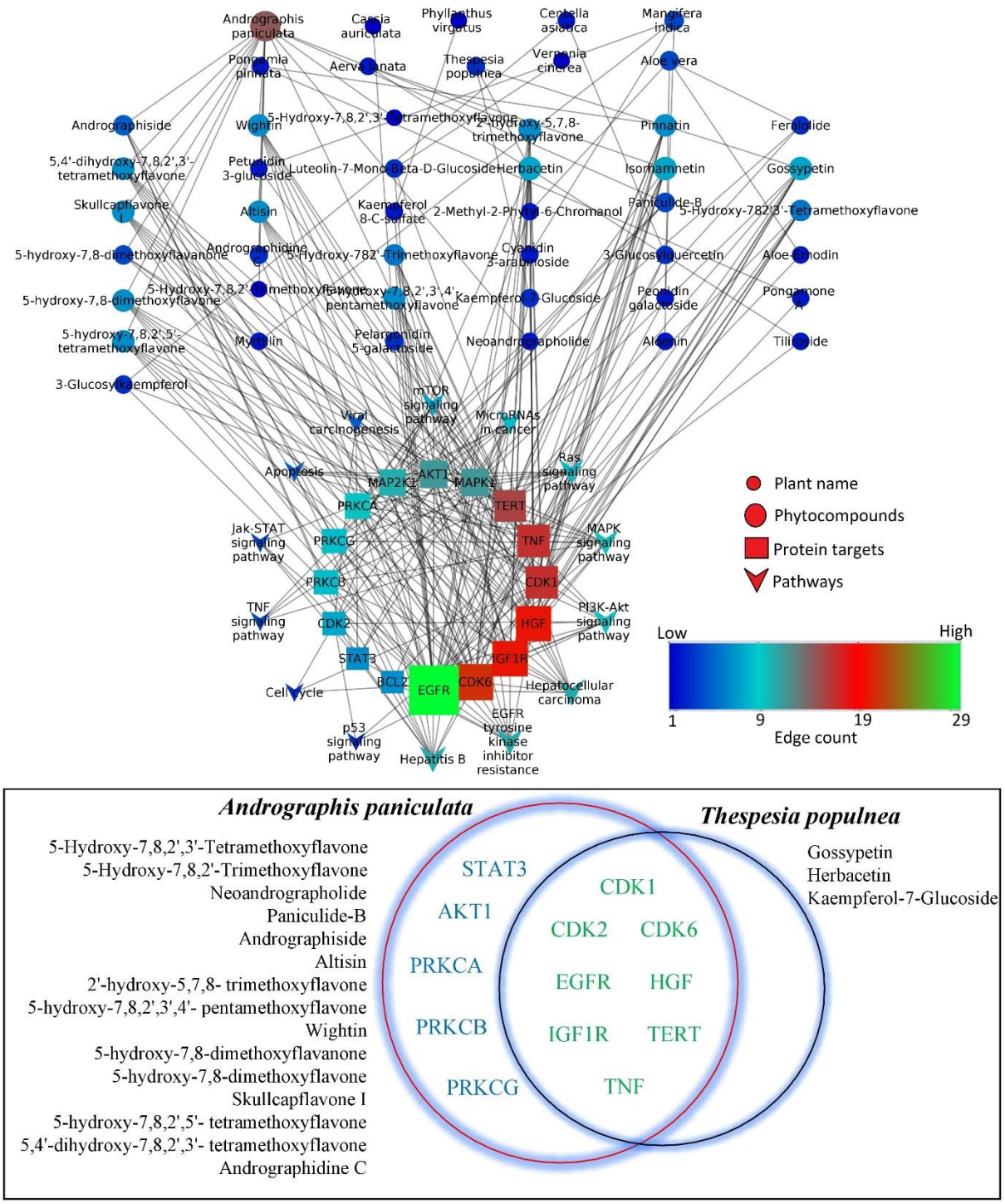





**Figure 14: Network diagram illustrating the herbs, their phytochemicals, proteins, and pathways involved in HBV-associated HCC.** A network interpretation was carried out by the "edge count" parameter with node size "Low to High" representing the degree of connection. It is clear that out of all the targets examined, the EGFR node had the greatest edge count of 29.

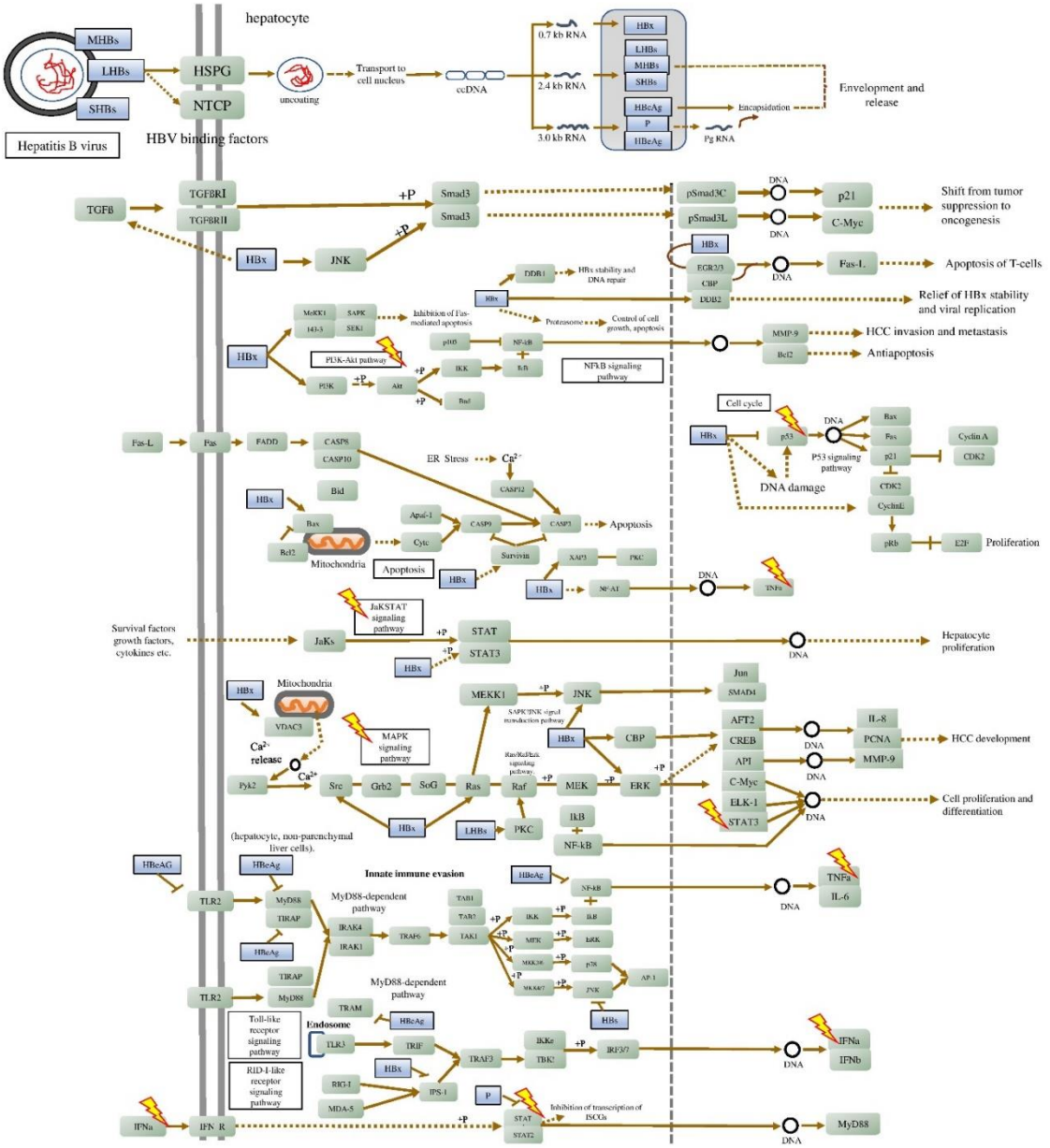


**Figure 15: Phytocompounds affected checkpoints of HBV infection. represents checkpoints affected.**

Further, the research is expanded to molecular docking and dynamics. EGFR was selected as the most promising target because it was found to be the network's most interconnected protein target and because it is a well-established therapeutic target for a wide variety of cancers, including lung cancer, glioma, breast carcinoma, HCC, and others[144]; also found to modulate hepatocellular carcinoma, mitogen-activated protein kinase (MAPK), phosphatidylinositol 3-kinase (PI3K), Janus kinase (Jak), and Ras

signalling pathways, as well as EGFR tyrosine kinase inhibitor resistance. The docking analysis revealed that 11 phytocompounds (8 from *A. paniculata* and eight from *T. populnea)* had the ability to inhibit EGFR protein.

### 5.2.6. Structure refinement, homology modeling, and active sites assessment

The WT-EGFR crystal structure (PDB id: 4I23) had missing residues and was filled using modeller v9.10. 100 homology structural models of WT-EGFR were constructed and model 30 was chosen as the best since it had the lowest DOPE score and the smallest root-mean-squared deviation (RMSD) from the template PDB id, 4I23. About 89.9% and 8.7% of residues were found to be in the most favoured and additionally allowed area of the Ramachandran plot (Supplementary Figure 2). The co-crystallized structure reveals that the active site of WT-EGFR consists of the amino acids Leu23, Ala48, Lys50, Glu67, Met71, Leu93, Thr95, Gln96, Met98, Pro99, and Gly101.[145]

### 5.2.7. EGFR model stability and lowest PE conformation

A 50 ns MD confirmed that the modelled structure of WT EGFR protein is very stable with minimal alterations. The lowest possible PE of the WT EGFR protein is -129809.51kcal/mol at the 45252.0$^{th}$ ps (45.2 ns) (refer to Supplementary Figure 3). Further, this conformation was chosen for docking analysis.

### 5.2.8. Molecular docking study

The BE and intermolecular interactions of 11 phytocompounds from *A. paniculata* and 3 from *T. populnea* docked with WT EGFR were summarized in Supplementary Table 13. Andrographin from *A. paniculata* has the lowest BE (-8.3kcal/mol) via forming two H-bonds (Met98...=O and Met98...OH) and ten hydrophobic contacts (Thr159, Lys50, Val31(2), Ala48(2), Leu149(2), and Leu23(2)). Among these interactions, seven interactions were with the active site. Figure 16A depicts the intermolecular interactions

between andrographin and wild-type EGFR. Likewise, Gossypetin from *T. populnea* has the lowest BE (-8.5kcal/mol) via forming the eight hydrophobic bonds and 3 H-bonds (Met98...OH, Thr95...OH (2). Among these interactions, six were with the active site. Figure 16B depicts Gossypetin's interactions with wild-type EGFR.

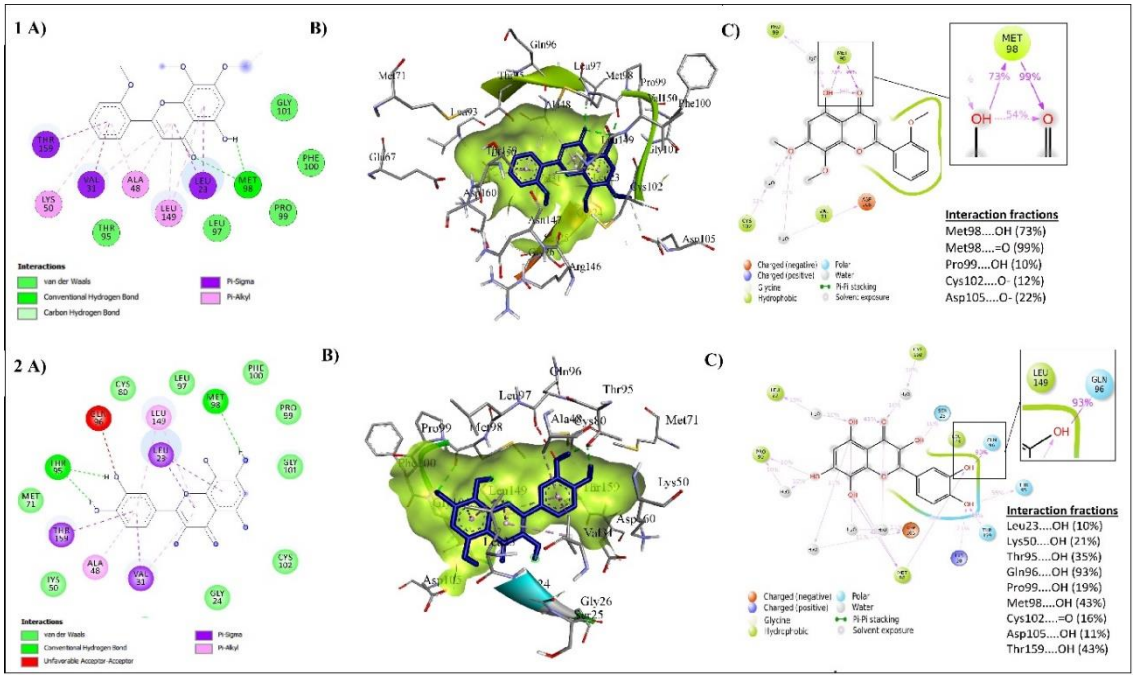


**Figure 16: Intermolecular interactions of (1) Andrographin and (2) Gossypetin with WT EGFR.** A) 2D B) 3D representation of compound within the binding pocket, and C) percentage interaction fraction.

### 5.2.9. Stability of protein-ligand complexes

Andrographin and Gossypetin were prioritized for MD simulation for 100ns because they had the lowest BE and the highest intermolecular interactions with active site residues. Andrographin and Gossypetin-EGFR complexes backbone and complex RMSD, and c-alpha RMSF are shown in Figure 17.

#### 5.2.9.1. Andrographin and WT EGFR complex

The avg RMSD of the backbone was 2.28Å, with a range of 0.70Å to 3.60Å. From 0 to 100ns, the complex RMSD was between 0.3Å and 3.5 Å with avg RMSD of 1.24Å.

In order to infer residue-wise fluctuations observed throughout 100 ns. The C-terminal residues showed higher flexibility leading to the highest fluctuations (2.5Å). While, the residues involved in ligand interactions (Gly24, Val31, Met98, and Leu149) had RMSF of <1.0Å. Further, the trajectory was analyzed for rGyr and was found to be 20 to 20.8Å indicating a higher compactness. In addition, the contact between Andrographin and EGFR revealed that Met98 established stable hydrogen-bonded contacts with the =O and OH group of Andrographin for about 98-99% and 73-77% of the fraction, respectively. Water-bridge interactions involving Pro99, Cys102, and Asp105 were observed, with interaction percentages of 10-15%, 12-20%, and 19-32%, respectively.

#### 5.2.9.2. Gossypetin and WT EGFR complex

Results showed that the complex RMSD fluctuation between 0.699-3.53Å, with an average of 2.6Å. In all three replicates, from 0 to 50 ns, the complex RMSD fluctuated slightly (0.7Å to 2.2Å) until reaching stability from 50 to 100 ns. In order to infer residue-wise variations (RMSF) seen throughout 100ns. The c-terminal loop region residues showed the largest fluctuations up to 2.5 Å. While, Ser25, Lys50, Cys80, Thr95, Gln96, Met98, Pro99, Leu149, and Thr159 are all active residues engaged in ligand interactions, and their RMSF was found to be ~1.3 Å. Similarly, the rGyr was also examined. Figure 17-2C shows that the Gossypetin-EGFR complex has higher compact since the rGyr ranges between 20 Å to 20.8 Å in all three replicas. Gossypetin-EGFR contact analysis revealed, Gln96 to establish stable H-bonded contacts with the OH group of Gossypetin for around 93% and 21% of the fraction, respectively. In all three replicates, the residues Met98, Thr95, and Asp105 were shown to participate in H-bonds, hydrophobic bonds, and water-bridge interactions.

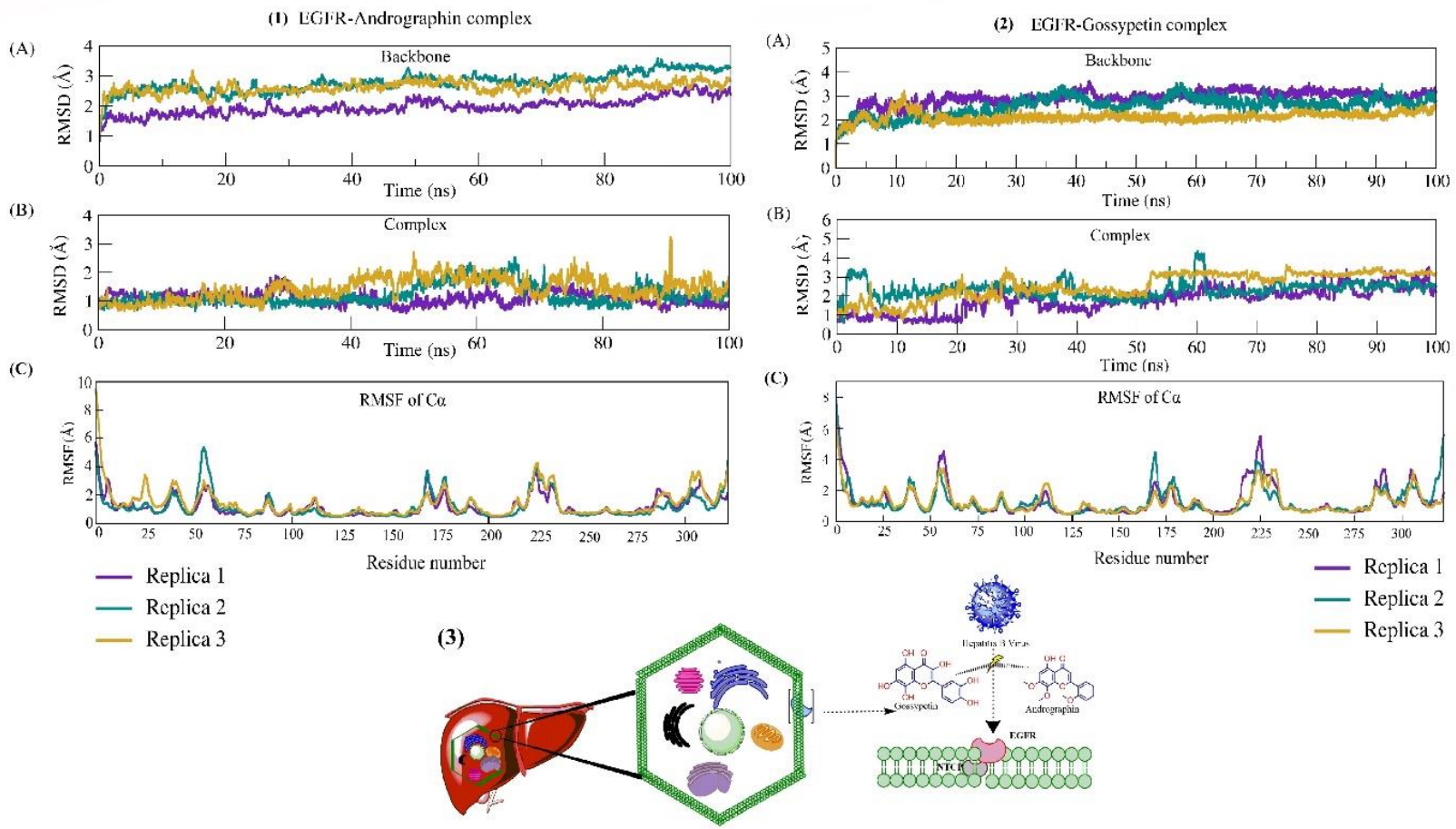


**Figure 17: 100ns MD simulation of EGFR with (1) Andrographin and Gossypetin.** (A) Protein Backbone RMSD, (B) Ligand-Protein complex RMSD, and C) RMSF of C-alpha atoms.

## 5.3. Study 3: Interaction of HBx with HBXIP and prioritized herbal drug candidates against HBx protein.

### 5.3.1. HBx and HBXIP proteins homology modelling

Both the HBx and HBXIP homology models were built with the help of the Raptorx and SWISS-MODEL servers, and their overall quality was verified by the ERRAT server and found to be 78.76% and 92.5%, respectively. The Ramachandran plot of HBx protein revealed about 72.4%, 19.7%, 4.7%, 3.1% of residues in most-favored, additionally, generously, and disallowed regions respectively. While, for the HBXIP protein, 84.8%, 15.2%, and 0% residues in the most favoured, additionally allowed, and disallowed regions, respectively. Leu9, Asp14, Val15, Leu16, Arg56, Leu71, Arg72, Tyr73, Thr74, Ser75, Ala76, Arg78, Glu80, and Lys95 were found to be the active site residues of HBx.

### 5.3.2. Protein-protein and protein-ligand docking

The HBx-HBXIP protein complex in haddock server had the lowest BE of -172.385kcal/mol. Thr36, Asp70, Glu40, and Asn71 of HBXIP and Lys140, Lys130, Arg4, and His139 of HBx had the interaction with distances of 2.76Å, 2.66Å, 2.69Å, 3.02Å respectively (Figure 18). 11 compounds of *A. paniculata* and 3 of *T. populnea* were docked to HBx protein. Kaempferol-7-Glucoside (*T. populnea*) formed 4 H-bonds with Lys130, Val133 (2), Trp120, and 2 hydrophobic bonds with Phe132 and Ile127, with BE of -6.6kcal/mol. However, andrographidine C (A. paniculata) formed 2 H-bonds with Val131 and Thr91 and 4 hydrophobic interactions with Ala85, Val133 (2), and His139. Here, it is identified as the best lead hit against HBx as it formed interaction with His139 which poses interaction with HBXIP.

Similarly, 5-Hydroxy-7,8-Dimethoxyflavone, 5-Hydroxy-2',3',4',7,8-Pentamethoxyflavone, 5,4'-Dihidroxy-7,8,2',3'-Tetramethoxyflavone, 5-Hydroxy-7,8,2'-Trimethoxyflavone, and 5-Hydroxy-7,8,2',3'-Tetramethoxyflavone were also the best lead molecules from A. paniculata with BE range of -6.0 to -5.7kcal/mol and formed interaction with Cys137 (interacts with HBXIP). However, Herbacetin, Gossypetin, and Kaempferol-7-Glucoside (compounds of *T. populnea)* didn't show interaction with 137CRHK140 of HBx. Table 7 represents the intermolecular interaction of compounds with HBx.

**Table 7: Binding energy and molecular interactions of phytocompounds from *A. paniculata* and *T. populnea* with HBx protein target.**

| Compound name | Ligand_Name | BE (kcal/mol) | HBI | NHBI |
|---|---|---|---|---|
| Kaempferol-7-Glucoside | 10095180 | -6.6 | Lys130, Val133 (2), Trp120 | Phe132, Ile127 (2), Glu121 |
| Andrographidine C | 5318484 | -6.4 | Val131, Thr91 | Ala85, Val133 (2), His139 |
| Gossypetin | 5280647 | -6.3 | Nil | Phe132,Val133 |
| Wightin | 12444943 | -6.1 | Nil | Val133, Phe132 |
| 2'-Hydroxy-5,7,8-Trimethoxyflavone | 21668878 | -6.1 | Val133, Lys130 | Phe132, Ile127, Val131, Glu121 |
| 5-Hydroxy-7,8,2',3'-Tetramethoxyflavone | 141423924 | -6 | Tyr111, Lys130 | Phe132, Lys130, Val133 (2), Cys137 |
| 5-Hydroxy-2',3',4',7,8-Pentamethoxyflavone | 12315479 | -6 | Tyr111, Lys130 (2) | Phe132, Val133, Cys137 |
| 5-Hydroxy-7,8-Dimethoxyflavone | 188316 | -6 | Val133 | Phe132, Val133 (2), Cys137 |
| Skullcapflavone I | 5320399 | -5.9 | Val131 | Phe132, Val133 |
| Herbacetin | 5280544 | -5.9 | Glu121, Lys140 | Phe132, Ile127 (2) |
| 5-Hydroxy-7,8,2'-Trimethoxyflavone | 44258542 | -5.8 | Val133 | Val133 (2), Cys137, Phe132 |
| 5-Hydroxy-7,8,2',5'Tetramethoxyflavone | 10948318 | -5.7 | Lys130, Trp120 | Ile127 (2), Phe132, Glu121, Glu126 |
| 5,4'-Dihidroxy-7,8,2',3'-Tetramethoxyflavone | 13963777 | -5.7 | Lys130 | Val133, Cys137 |
| Altisin | 15100719 | -5.3 | Val133, Lys130, Tyr111 | Phe132 (3), Ala85, Arg87 |

### 5.3.3. Molecular dynamics

#### 5.3.3.1 Stability of HBx-HBXIP protein complex

The HBx-HBXIP complex exhibited stable dynamics throughout 100 ns simulation. The average backbone RMSD was found to be ~6.5 Å. The RMSF plot revealed that Cys137, Arg138, His139, and Lys140 that are essential to interact with HBXIP showed lesser fluctuation (~3.0 Å). Whereas, loop region showed larger fluctuations up to 7 Å. Figure 18 represents the binding mode and stability interaction fraction of HBx with HBXIP with 20ns time interval upto 100ns.

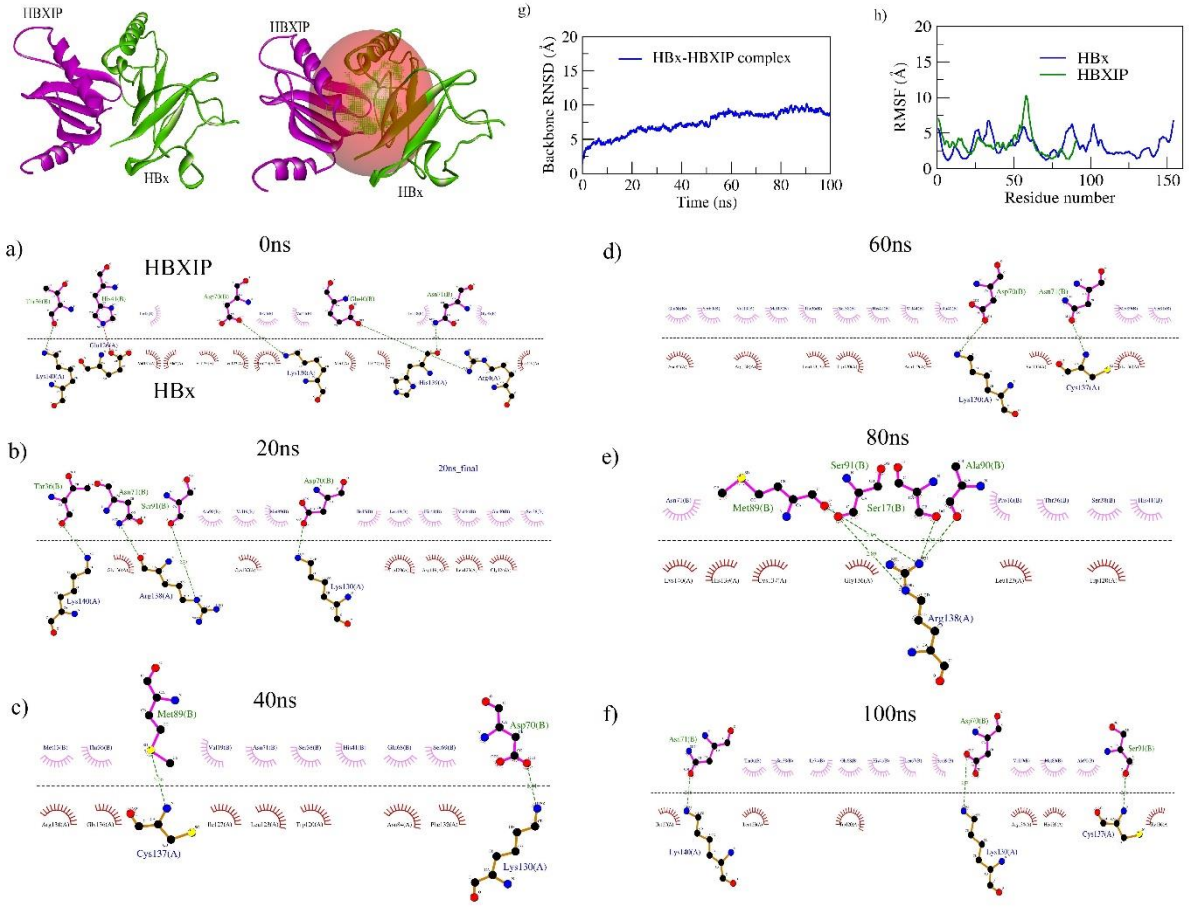


**Figure 18: Binding mode and stability interaction fraction of HBx with HBXIP.** a) HBx-HBXIP binding mode, b) RMSD of HBx-HBXIP complex during 100ns, c) RMSF of C-alpha atoms of HBx and HBXIP, and d) to i) stability interaction fraction from 0 to 100ns with 20ns interval frame.

### 5.3.3.2. Stability of Andrographidine C with HBx

The stability of Andrographidine C with HBx was inferred for 100ns (Figure 19). HBx showed an average RMSD of 6.58Å for its backbone and 6.24Å for complex with Andrographidine C. The complex RMSD decreased gradually from 0 and 25ns, then fluctuated between 25 and 63 ns, and finally stabilized till 100 ns. The Rg value increased from16.5Å to 19Å during 20ns to 63ns, and then steadily decreased from 63ns to 100 ns, demonstrating that the binding pocket opened and closed at 25 and 63 ns, respectively, and represents stable complex formation after 25 ns. The RMSF figure indicated that Arg138, His139, and Lys140, which are involved in stable and conserved non-bonded interactions, had little fluctuation (~3Å). However, residual fluctuation was shown to be greater in the loop region (12Å). Andrographidine C showed stronger contacts with Arg138 and His139 from 0 to 50ns and with Lys140, Trp141 from 50 to 82ns, as shown by the interaction map between HBx and Andrographidine C. Andrographidine C formed a 7% contact with Arg138, 5% with His139, and 12% with Lys140 during 100ns simulation, as shown by the interaction fraction plot.

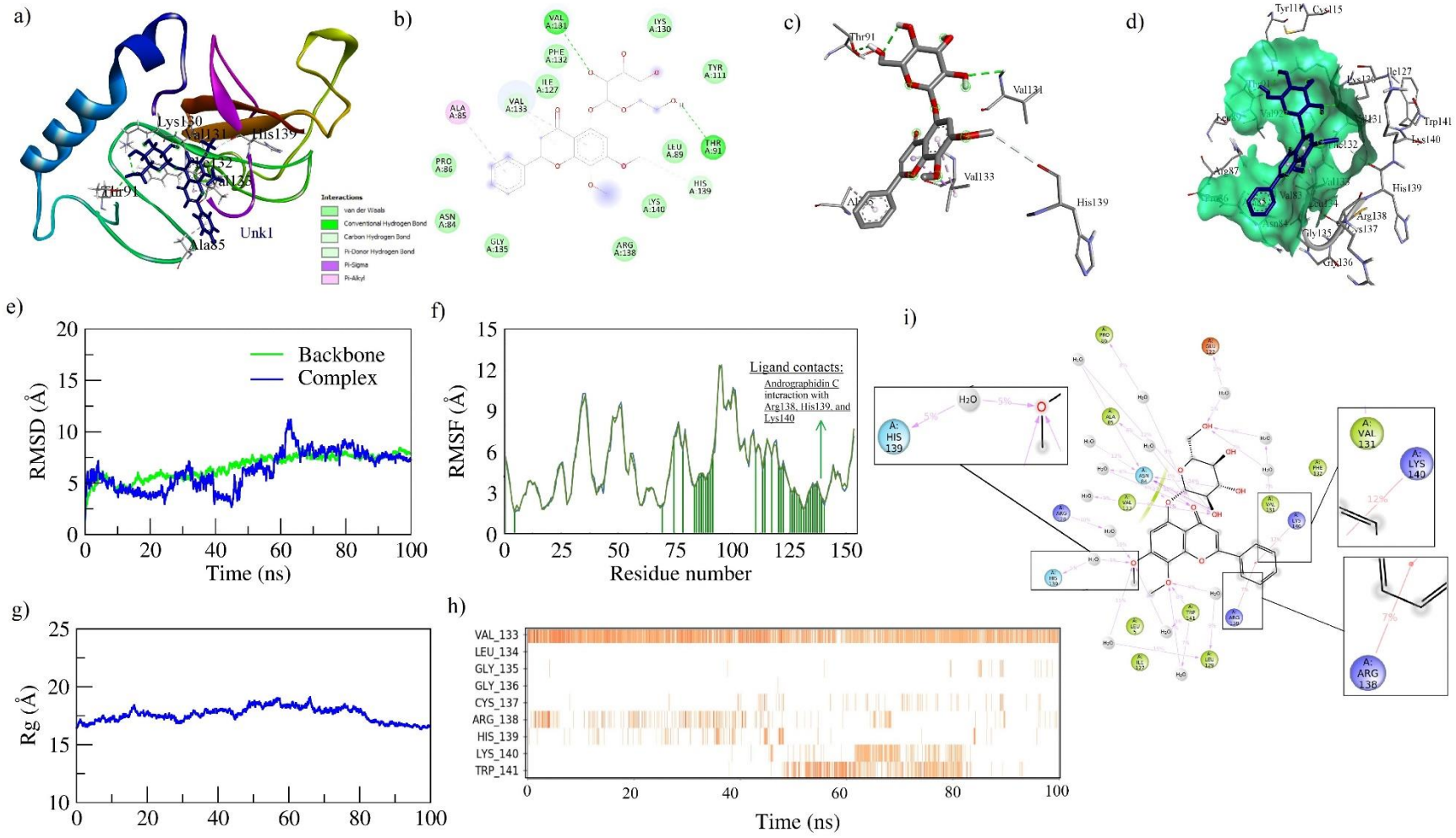


**Figure 19: Andrographidine C stability with HBx during 100ns.** (A) HBx backbone RMSD, (B) Ligand-Protein complex RMSD, C) RMSF of C-alpha atoms.

## 5.4. Study 4: Identification of a suitable chemical model that resembles to HBV pathogenesis.

### 5.4.1. Identification of HBV-associated and chemically-induced hepatitis genes

The literature search resulted in 42 genes (from 36 papers) that were shown to be altered in HBV-induced hepatitis. Similarly, 1538 genes were retrieved from the GeneCards database that had a relevance score of at least 20. IFN had the greatest relevance score of 166.85. Likewise, for alcohol (66 genes from 25 articles), acetaminophen (38 genes from 11 articles), isoniazid (30 genes from 10 articles), D-galactosamine (31 genes from 14 articles), lipopolysaccharide (44 genes from 39 articles), rifampicin (33 genes from 26 articles), and thioacetamide (33 genes from 23 articles) were also collated from the literature. For acetaminophen-, isoniazid-, D-galactosamine-, lipopolysaccharide-, and rifampicin-induced hepatitis, TNF had a high relevance value of 75.06, 77.71, 69.39, 95.44, and 51.13, respectively, but for thioacetamide, IL6 had the highest relevance value of 55.21. Supplementary Tables 14 to 21 provide a summary of the genes/protein molecules that are regulated by HBV and each chemical-induced hepatitis, as determined by a systematic literature study and GeneCards (a list of references was provided).

### 5.4.2. Analysis of genes involved in hepatic toxicity

Only 2% (31) of genes were shared between the literature review and the GeneCard database for HBV-induced hepatitis; for “acetaminophen, isoniazid, alcohol, D-galactosamine, lipopolysaccharide, thioacetamide, and rifampicin, the common genes between literature review and GeneCard database were 9.2% (14), 5.6% (4), 8.8% (33), 15.3% (11), 9% (25), 10.5% (6), and 5.6% (3) respectively; further, the shared genes between HBV- with acetaminophen, isoniazid, alcohol, D-galactosamine, lipopolysaccharide, thioacetamide, and rifampicin-induced hepatitis were 9.1% (140),

3.7% (57), 25.2% (399), 3.8% (59), 17.6% (273) and 3.4% (52), and 3.2% (50) respectively". Among these, the similarity between HBV and alcohol genes was greatest at 25.2%, followed by lipopolysaccharide genes at 17.6%. Figure 20 illustrates (a) genes shared by the literature review and GeneCards and (b) HBV and chemical-induced hepatitis.

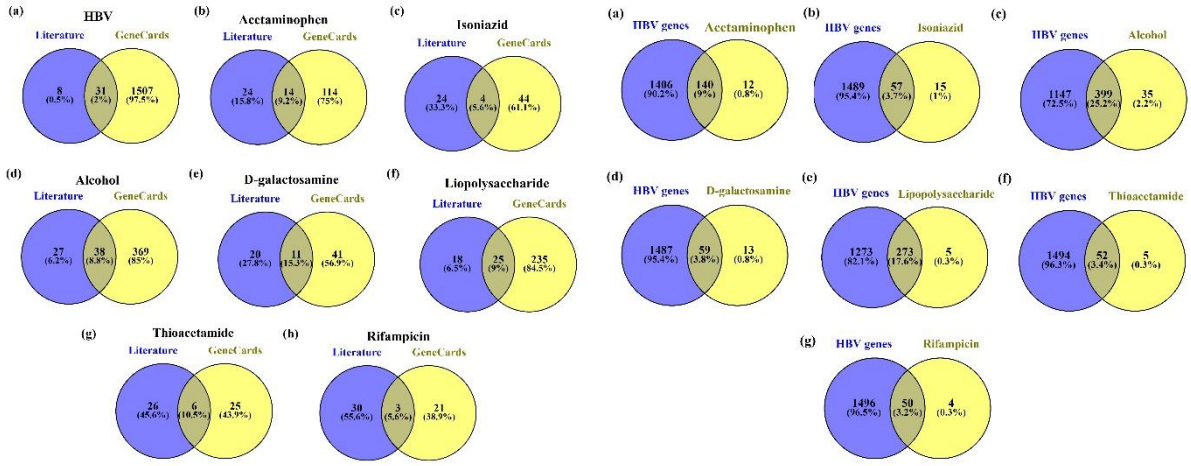


**Figure 20: The common genes between (a) literature review and GeneCards and (b) HBV and chemical-induced hepatitis.**

### 5.4.3. Functional enrichment analysis to assess the hepatotoxicity

Initially, "HBV, acetaminophen, isoniazid, alcohol, D-galactosamine, lipopolysaccharide, thioacetamide, and rifampicin were identified to modulate 1546, 152, 72, 434, 72, 278, 57, and 54 genes respectively and these gene sets were found to modulate 217, 185, 184, 200, 185, 202, 167, and 172 biological pathways respectively". Biological/molecular pathways modulated by HBV and chemicals were shown in Supplementary Tables 22 to 29.

In the HBV-induced hepatitis model, "out of 217 pathways modulated, 9 pathways viz., PI3K-Akt, TNF, JAK-STAT, MAPK, Chemokine, NF-kappa B, TGF-beta signaling pathways, Apoptosis, and Cell cycle were prioritized to compare with chemically-induced hepatitis as these pathways were significantly associated with progression of

HCC by HBV (refer KEGG ID: hsa05161); in which, the PI3K-Akt signaling pathway scored the lowest FDR of 1.39E-33 and the highest gene count of 57; whereas, TNF, JAK-STAT, MAPK, Chemokine, NF-kappa B, TGF-beta signaling pathways, Apoptosis, and Cell cycle scored the lowest FDR of 1.56E-27, 1.38E-22, 5.4E-20, 7.77E-13, 6.49E-12, 7.26E-27, 4.34E-09 respectively and gene count of 34, 33, 38, 24, 18, 11, 35, and 16 respectively".

Lipopolysaccharide-induced hepatitis exhibited the greatest resemblance to HBV-induced HCC among chemically-induced HCC, while alcohol-induced hepatitis had the second-highest similarity. Pathways modulated by HBV and chemicals are represented in Table 8. Here, "lipopolysaccharide was found to modulate 202 molecular pathways, in which the PI3K-Akt signaling pathway scored the lowest FDR of 2.46E-41 and the highest gene count of 58; whereas, TNF, JAK-STAT, MAPK, Chemokine, NF-kappa B, TGF-β signaling pathways, apoptosis, and cell cycle scored the lowest FDR of 4.49E-46, 1.48E-35, 5.8E-30, 3.71E-21, 4.11E-38, 0.000000036, 2.35E-38, 7.55E-08 and gene count of 45, 41, 44, 30, 38, 12, 41, and 13 respectively".

Likewise, "alcohol was found to modulate 200 molecular pathways, in which the PI3K-Akt signaling pathway scored the lowest FDR of 2.87E-21 and the highest gene count of 31. Whereas, TNF, JAK-STAT, MAPK, Chemokine, NF-kB, TGF-beta signaling pathways, Apoptosis, and Cell cycle scored the lowest FDR of 5.92E-23, 2.93E-14, 4.07E-16, 3.25E-10, 3.10E-11, 3.36E-05, 3.77E-24, 0.0063 and gene count of 23, 18, 24, 15, 13, 7, 25, 5 respectively". The network of genes and pathways that are regulated by (a) HBV, (b) lipopolysaccharide, and (c) alcohol is shown in Figure 21.

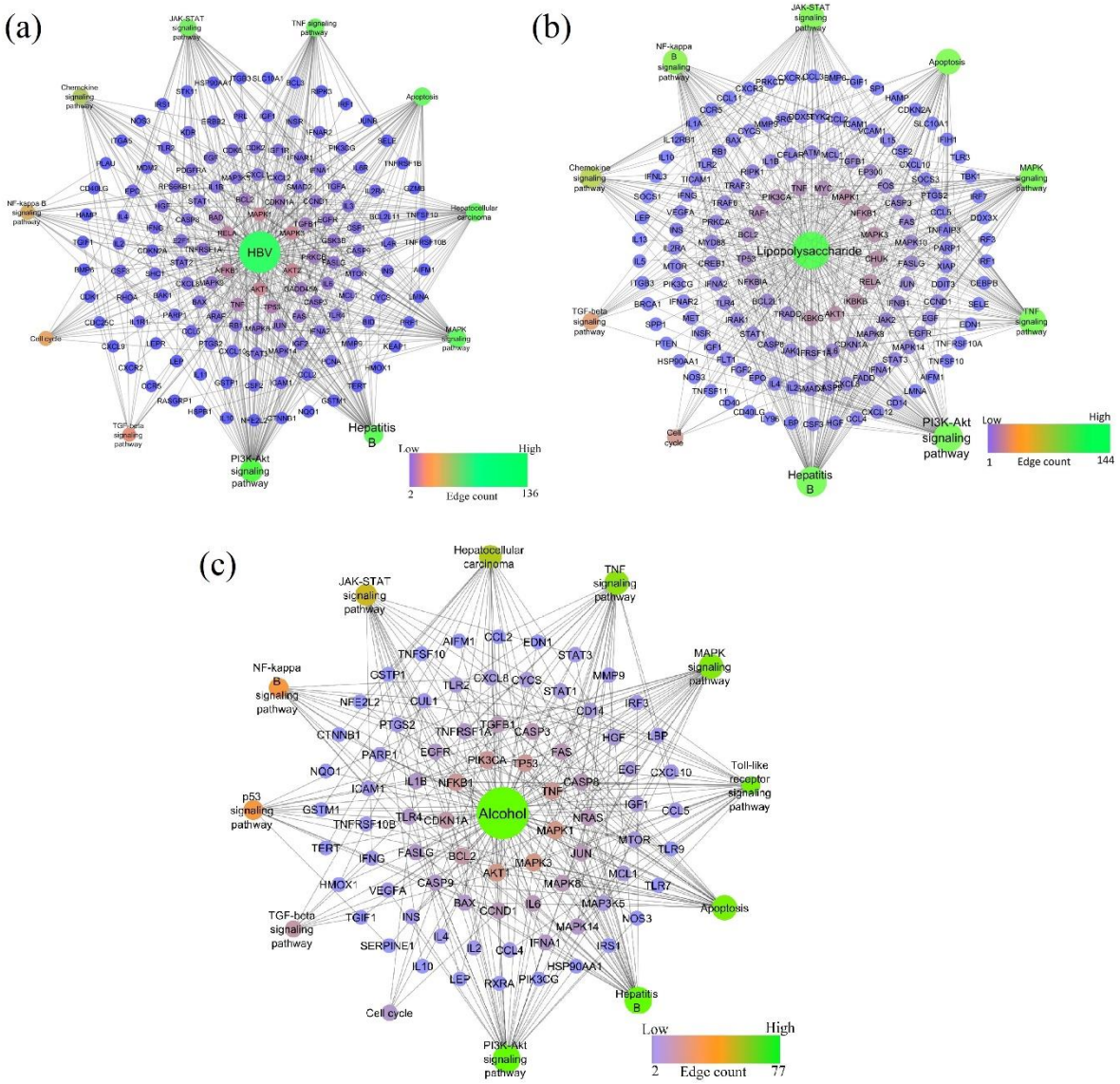


**Figure 21: Network of genes and pathways that are regulated by (a) HBV, (b) lipopolysaccharide, and (c) alcohol.**

**Table 8**: **Pathways modulated by HBV and chemicals**

| Hepatitis Model | | HBV | | Acetaminophen | | Isoniazid | | Alcohol | | D-galactosamine | | Lipopolysaccharide | | Thioacetamide | | Rifampicin | |
|---|---|---|---|---|---|---|---|---|---|---|---|---|---|---|---|---|---|
| **KEGG ID** | **Pathway Description** | **GC** | **FDR** | **GC** | **FDR** | **GC** | **FDR** | **GC** | **FDR** | **GC** | **FDR** | **GC** | **FDR** | **GC** | **FDR** | **GC** | **FDR** |
| hsa05161 | Hepatitis B | 42 | 6.6E−32 | 21 | 3.46E−19 | 19 | 7.91E−22 | 30 | 8.48E−29 | 28 | 8.90E−36 | 66 | 1.14E−68 | 18 | 1.17E−21 | 18 | 3.57E−22 |
| hsa04151 | PI3K-Akt signaling pathway | 57 | 1.39E−33 | 23 | 2.02E−15 | 14 | 1.02E−10 | 31 | 2.87E−21 | 20 | 3.35E−17 | 58 | 2.46E−41 | 16 | 5.34E−14 | 16 | 1.78E−14 |
| hsa04668 | TNF signaling pathway | 34 | 1.56E−27 | 9 | 2.56E−07 | 7 | 5.89E−07 | 23 | 5.92E−23 | 14 | 2.21E−16 | 45 | 4.49E−46 | 9 | 3.49E−10 | 11 | 2.34E−13 |
| hsa04210 | Apoptosis | 35 | 7.26E−27 | 10 | 8.51E−08 | 9 | 5.93E−09 | 25 | 3.77E−24 | 15 | 6.20E−17 | 41 | 2.35E−38 | 9 | 1.16E−09 | 13 | 1.89E−15 |
| hsa05225 | Hepatocellular carcinoma | 36 | 1.35E−25 | 16 | 2.12E−13 | 14 | 8.53E−15 | 20 | 1.56E−16 | 18 | 4.48E−20 | 30 | 8.42E−23 | 12 | 6.46E−13 | 12 | 2.65E−13 |
| hsa04630 | JAK-STAT signaling pathway | 33 | 1.38E−22 | 12 | 4.22E−09 | 8 | 3.73E−07 | 18 | 2.93E−14 | 12 | 8.40E−12 | 41 | 1.48E−35 | 12 | 6.46E−13 | 9 | 3.01E−09 |
| hsa04010 | MAPK signaling pathway | 38 | 5.4E−20 | 16 | 4.47E−10 | 12 | 1.80E−09 | 24 | 4.07E−16 | 19 | 2.32E−17 | 44 | 5.8E−30 | 12 | 2.56E−10 | 16 | 1.74E−15 |
| hsa04062 | Chemokine signaling pathway | 24 | 7.77E−13 | 8 | 7.08E−05 | 4 | 0.0072 | 15 | 3.3E−10 | 11 | 7.06E−10 | 30 | 3.71E−21 | 8 | 2.68E−07 | 6 | 3.44E−05 |
| hsa04064 | NF-kappa B signaling pathway | 18 | 6.49E−12 | 7 | 1.39E−05 | 4 | 0.00094 | 13 | 3.10E−11 | 8 | 2.50E−08 | 38 | 4.11E−38 | 3 | 0.0075 | 6 | 1.54E−06 |
| hsa04110 | Cell cycle | 16 | 4.34E−09 | 5 | 0.0023 | | | 5 | 0.0063 | 6 | 2.06E−05 | 13 | 7.55E−08 | 3 | 0.0115 | 5 | 5.74E−05 |
| hsa04350 | TGF-beta signaling pathway | 11 | 0.00000324 | ND | | 3 | 0.0075 | 7 | 3.36E−05 | ND | | 12 | 0.000000036 | 3 | 0.00041 | 4 | 0.0045 |

GC: Gene count; FDR, False discovery rate.

### 5.5. *In vitro* pharmacology

Based on *in silico* study (Study I, II, and III), **5 plants** were prioritized for *in vitro* study and these include (1) *Terminalia chebula*, (2) *Bidens pilosa*, (3) *Centella asiatica*, (4) *Andrographis paniculata*, and (5) *Thespesia populnea*. PGG was used as a pure compound (from *T. chebula*) and TDF as a standard antiviral drug.

#### 5.5.1. LC-MS profile of fraction and extracts

LC-MS profiles of TCW, TCN, BPM, BPHA, CAM, APHA, and TPHA were examined for active principles which were identified through *in silico* studies. The identified compound's retention time with molecular weight is provided in Supplementary Table 30.

#### 5.5.2. Cytotoxicity assay

The MTT assay experiment showed that after 24h of treatment, TCW (1048.43µg/mL) had a $CC_{50}$ higher than TCN (853.354µg/mL). Similarly, the BPM $CC_{50}$ (1187.94 µg/mL) was greater than BPHA (615.558µg/mL). The $CC_{50}$ of CAHA was found to be 881.828µg/mL. AP showed a greater $CC_{50}$ (832.915 µg/mL) than TP (593.122 µg/mL). AP showed about 3.6 and 2.6% cell viability at 2000 and 1000 µg/mL, respectively. Whereas TP had cell viability at around 24, and 28%, respectively. This indicates that AP at greater concentrations causes significant cytotoxicity. Further, the $CC_{50}$ of PGG and TDF was found to be >250µM, indicating a non-toxic concentration. Based on the MTT assay, test concentrations of 500µg/mL were used for TCN, TCW, BPHA, BPM, and CAHA, while 250µM was used for PGG and TDF for further studies. The concentration-dependent percentage of viable cells and $CC_{50}$ value for each test drug are shown in Figure 22 and Supplementary Table 31.

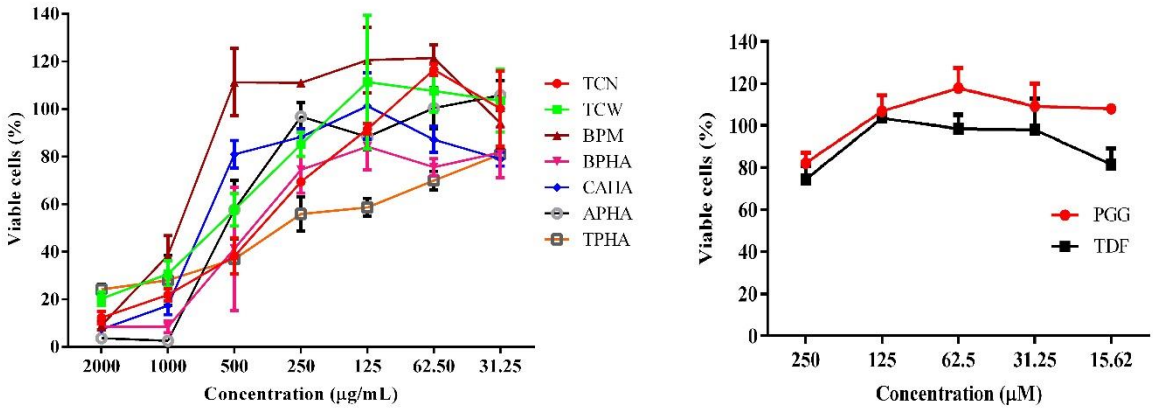


**Figure 22**: **Cytotoxicity of extracts/fraction, PGG, and TDF in HepG2.2.15 cell line after 24h treatment.** The results are expressed as the mean±SEM of three independent biological replicates.

### 5.5.3. RT inhibitory assay

The *in vitro* RT inhibitory activity of the test drugs was evaluated using the RT colorimetric assay kit (Figure 23). TCW had an $IC_{50}$ of 149.214 µg/mL and TCN had an $IC_{50}$ of 147.077µg/mL, both of which strongly inhibited the RT enzyme. While TPHA $IC_{50}$ was found to be 553.88µg/m and APHA showed RT inhibitory action with an $IC_{50}$ of 304.52µg/mL. BPM, BPHA, and CAHA did not exhibit RT inhibitory action, and their $IC_{50}$ values have been determined to be 2056.25, 2000.955, and 1928.313µg/mL, respectively. Similarly, PGG, TDF, a standard molecule, did not exhibit RT inhibitory action at a concentration of 250µM. However, PGG showed RT inhibitory activity with an $IC_{50}$ of 149.075µM. Supplementary Table 32 provides each test drug's concentration-dependent percentage RT inhibition. Based on these results, the following were prioritized: TCN, TCW, APHA, TPHA, PGG, and TDF for further studies.

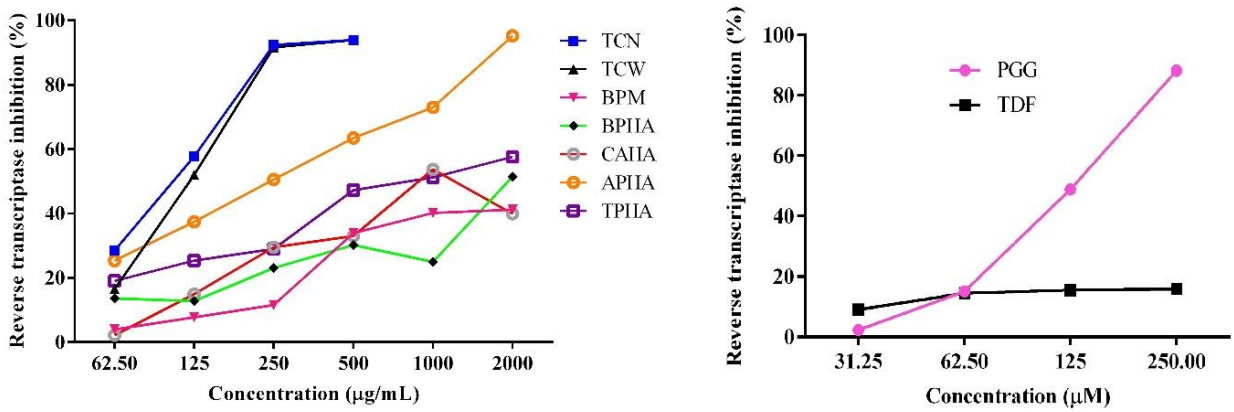


**Figure 23**: RT enzyme inhibitory effect of extracts/fraction, PGG, and TDF.

### 5.5.4. Effect of TCN, TCW, APHA, TPHA, PGG, and TDF on intracellular HBV DNA and pgRNA in HepG2.2.15 cell line by qRT-PCR

As Figure 24 shows, treatment of HepG2.2.15 cells with TCN 125, 250, and 500 µg/mL for 24h decreased the intracellular HBV DNA by $2^6$ fold. Whereas, TCN 62.5 and 31.25 µg/mL decreased by $2^5$ fold. Similarly, TCW 500 µg/mL showed $2^7$ fold decrease in HBV DNA. TCW 250, 125, 62.5, and 31.25 µg/mL also showed $2^6$, $2^6$, $2^6$, and $2^5$ fold decrease in intracellular HBV DNA. Treatment of HepG2.2.15 cells with AP 125, 250, and 500 µg/mL for 24h decreased the intracellular HBV DNA by $2^5$ fold. Whereas, AP 62.5 and 31.25 µg/mL decreased by $2^4$ and $2^3$ fold respectively. Similarly, AP 125, 250, and 500 µg/mL showed $2^1$ fold decrease in pgRNA level. TP 500 µg/mL showed $2^6$ fold decreases in intracellular HBV DNA and TP 250, 125, 62.5 µg/mL showed $2^4$ fold decreases in intracellular HBV DNA. TP didn't show any significant effect on pgRNA level. PGG 100µM showed about $2^5$ fold decrease and PGG 50, 25, 12.5, and 6.25µM showed about $2^3$ fold decrease in HBV DNA. Whereas, TDF concentration range between 6.25 to 100 µM showed about $2^1$ - $2^2$ fold decrease in intracellular HBV DNA.

On looking into the pgRNA level, only TCN and TCW 500 µg/mL, and PGG 100 µM showed about $2^2$ fold decrease in the pgRNA. This indicates TCN, TCW, APHA, TPHA, and PGG to have a significant effect on intracellular HBV DNA but not on pgRNA.

### 5.5.5. Time-course analysis of HBsAg for TCN, TCW, APHA, TPHA, PGG, and TDF

The % inhibition of HBsAg secretion in the cell supernatant was analyzed at different time intervals (24, 48, 72, 96, and 120h). All the test drugs exhibited strong HBsAg inhibitory activity. At 24 and 48h, only TCN500 showed about 80% inhibitory effect and at 72, 96, and 120h TCN500 (~85%), TCN250 (~80%) and TCN125 (~75%) exhibited an inhibitory effect. Interestingly, a similar effect was observed for TCW. AP500 showed about 75% inhibitory effect at 24, 48, and 72h, and about ~95% inhibition was seen at 92 and 120h. TP500 showed about 70 to 75% inhibition at 24, 48, and 72h and showed >80% at 92 and <80% at 120h. Whereas, PGG100 showed ~80% inhibitory effect at 96h and ~70% at 120h. A standard compound TDF100 also showed ~80% inhibitory effect at 96 and 120h. Figure 25 and Supplementary Table 33 represent the HBsAg inhibitory effect of TCN, TCW, PGG, and TDF.

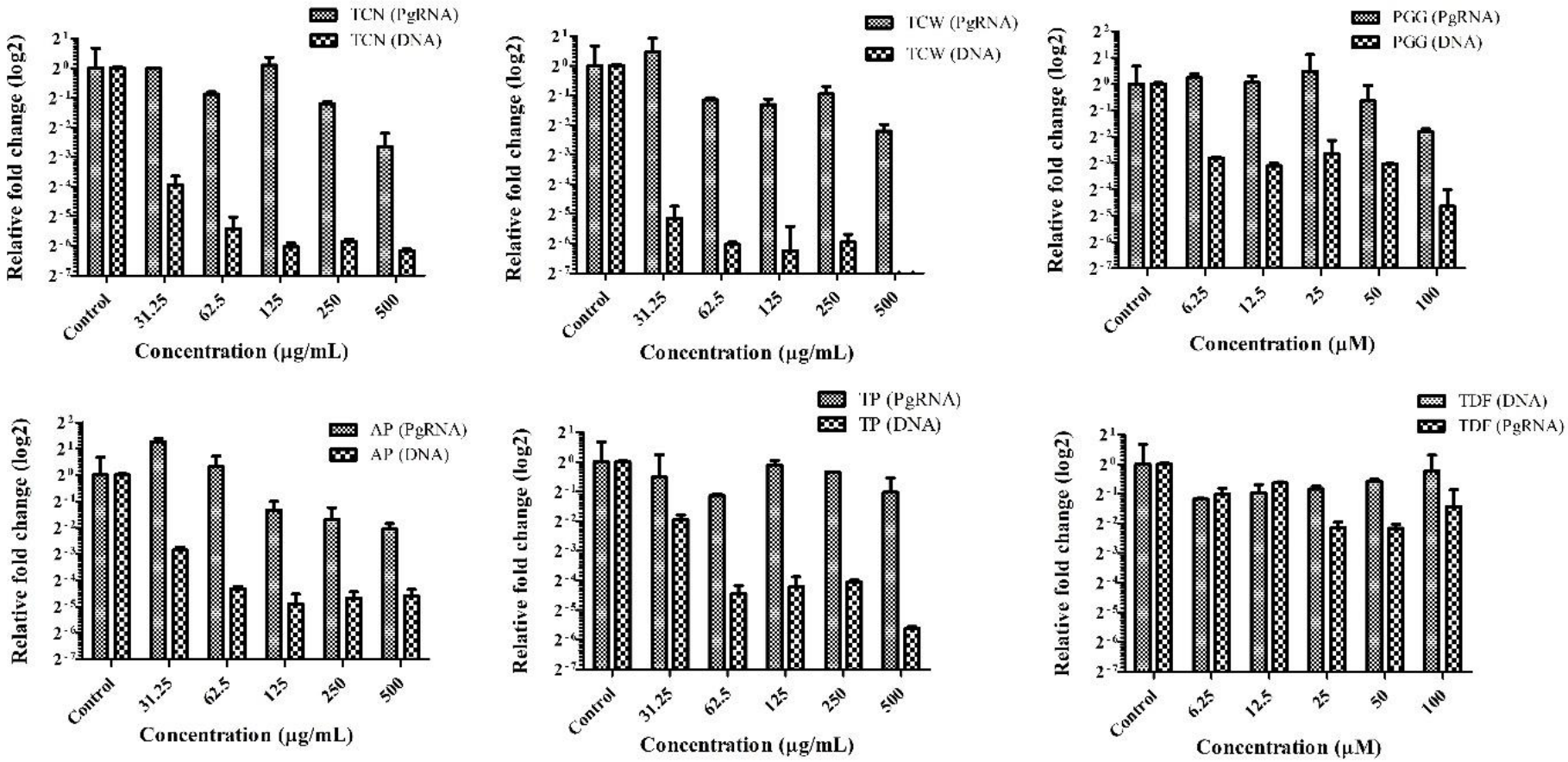


**Figure 24: Effect of TCN, TCW, APHA, TPHA, PGG, and TDF treatment on intracellular HBV DNA and pgRNA. HepG2.2.15 cells were treated with or without drugs at the indicated concentrations for 24h.** Total intracellular HBV pgRNA and DNA were quantified using qRT-PCR. The results are expressed as the mean±SEM of two independent biological replicates and two dependent technical replicates.

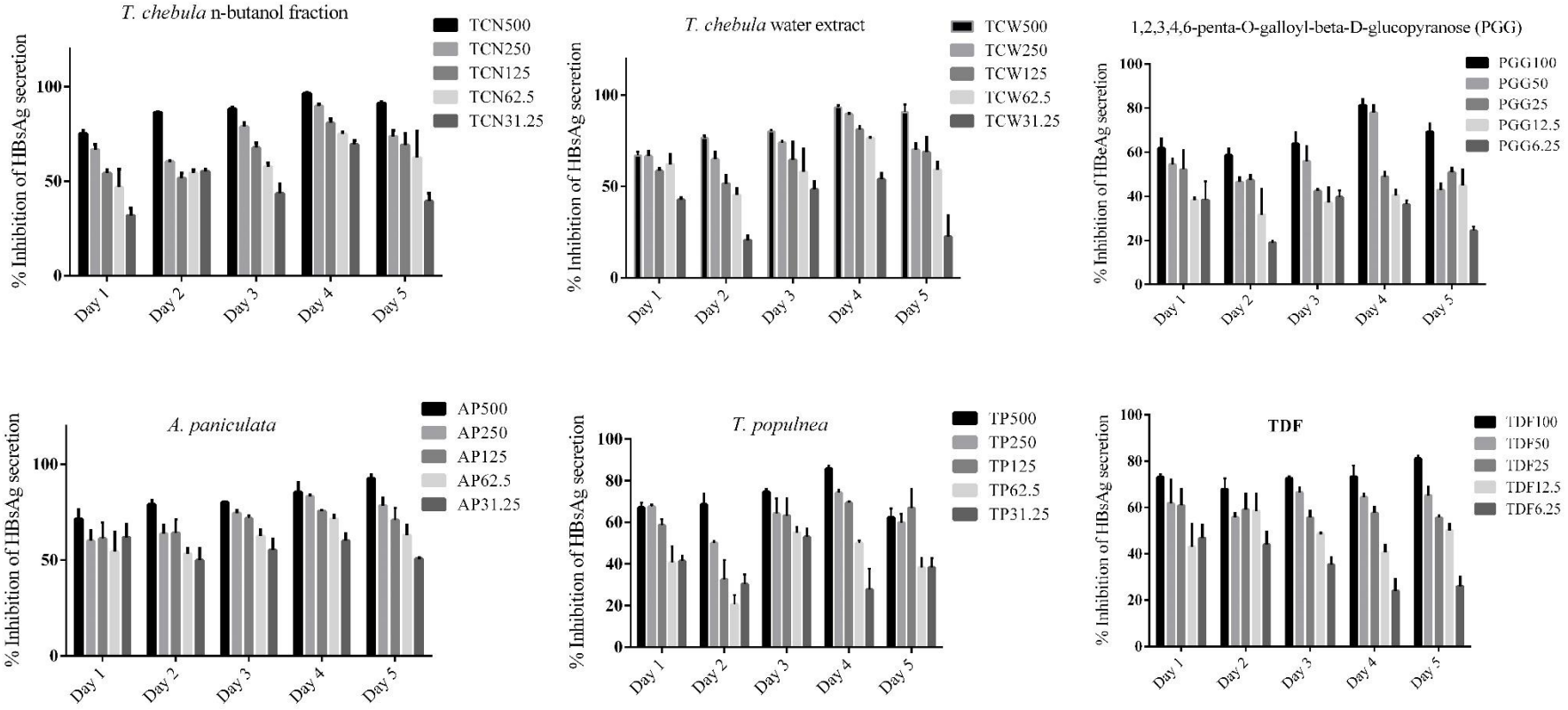


**Figure 25**: **Effect of TCN, TCW, APHA, TPHA, PGG, and TDF on HBsAg level in HepG2.2.15 cell line.** The results are expressed as the mean±SEM of two independent biological replicates.

### 5.5.6. Time-course analysis of HBeAg for TCN, TCW, APHA, TPHA, PGG, and TDF

The % inhibition of HBeAg secretion in the cell supernatant was analyzed at different time intervals (24, 72, and 120h). Among the selected test drugs, TCN and TCW exhibited strong HBeAg inhibitory activity. At 24h TCN500 showed about 80% inhibitory effect and at 72 and 120h showed about ~72% and 60%. A similar effect was also observed for TCW. AP500 showed about 75 to 82% inhibitory effect at 24, 72, and 120h. TP500, TP250, and TP125 showed about 90% inhibition at 24h and decreased to >80% at 72h and 120h. Whereas, PGG100 and TDF100 exhibited ~43% and ~20% inhibition, respectively. At 72 and 120h, a decrease in the inhibitory effect of HBeAg secretion was observed for all the test drugs. Figure 26 and Supplementary Table 34 represent the HBeAg inhibitory effect of TCN, TCW, PGG, and TDF.

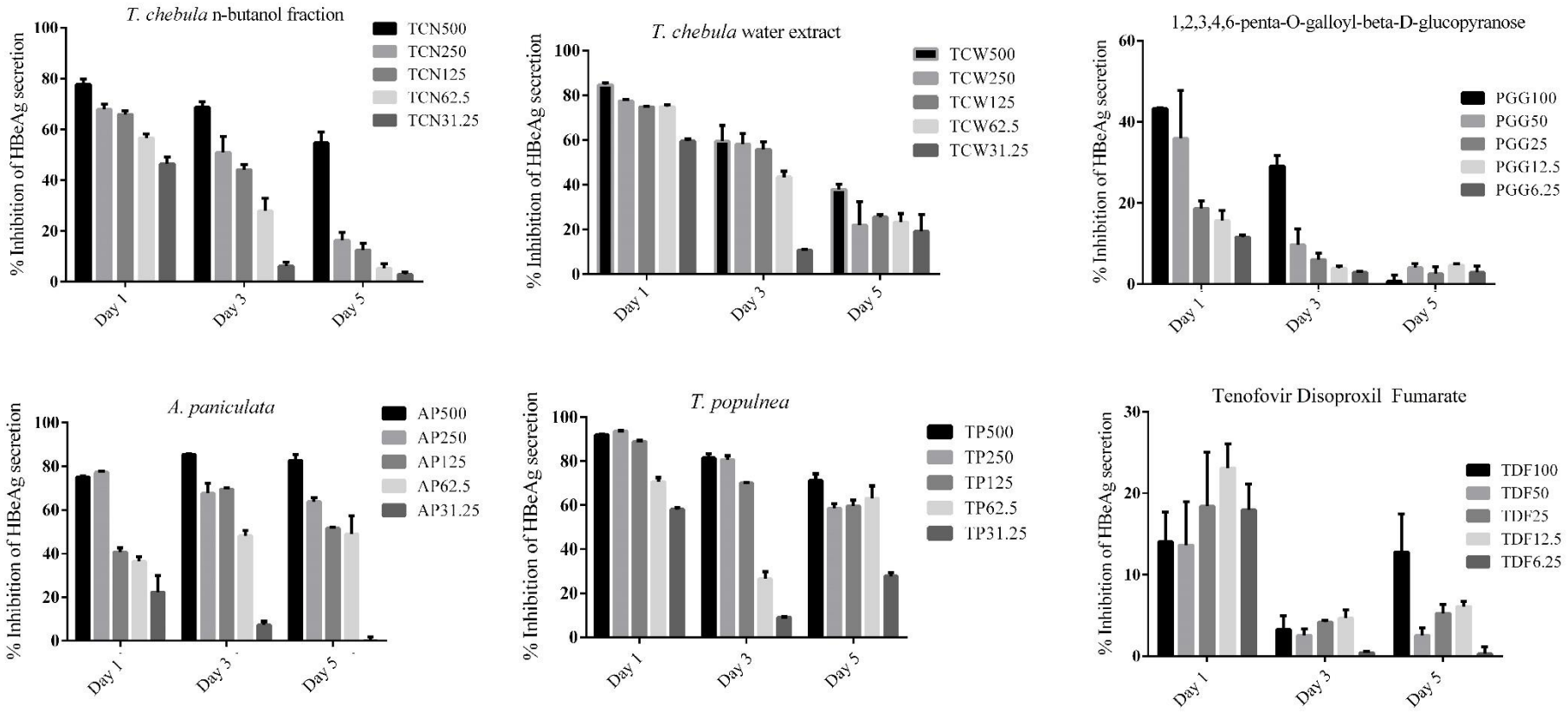


**Figure 26**: **Effect of TCN, TCW, APHA, TPHA, PGG, and TDF on HBeAg level in HepG2.2.15 cell line.** The results are expressed as the mean±SEM of two independent biological replicates.

### 5.5.7. HBx-HBXIP interaction inhibition assay

Based on Study 3 *in silico* study, only APHA and TPHA were subjected to this assay as these were found to modulate host targets triggered by HBx of HBV. AP showed about 72% inhibition at 500 µg/mL and about 57% inhibition at 62.5 µg/mL (Figure 27). The $IC_{50}$ of AP was found to be <62.5 µg/mL for HBx-HBXIP interaction inhibition. TP showed about 31.48% inhibition at 500 µg/mL and its $IC_{50}$ was found to be 806.69 µg/mL.

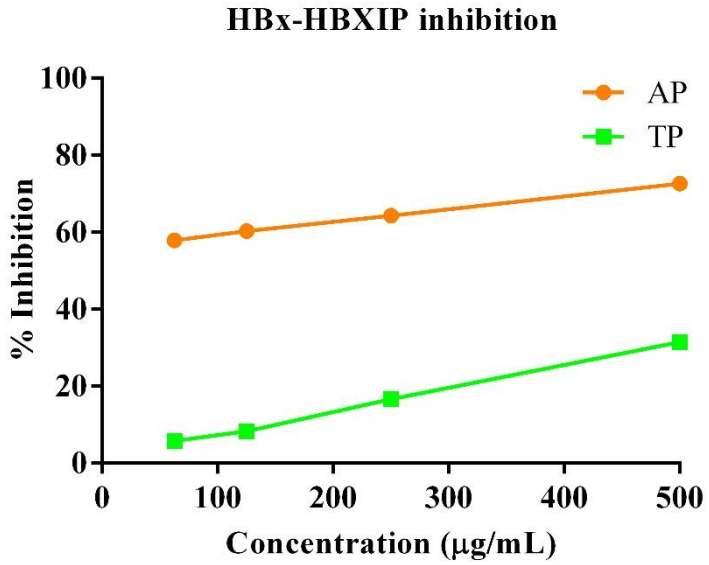


**Figure 27: Effect of APHA, TPHA on HBX-HBXIP interaction in HepG2.2.15 cell line.**

### 5.6. *In vivo* studies

Based on the *in vitro* analysis, TCN and APHA (hereafter abbreviated as TC and AP) were subjected to hepatoprotective potential in alcohol-induced rat model (this model was identified to resemble the HBV pathogenesis)**.**

#### 5.6.1. Effect of TC and AP on body weight

From day 21, a significant increase ($p<0.01$) in body weight was observed in Alc group compared to normal which was significantly reversed ($p<0.01$ from day 18 to 21 and $p<0.001$ from day 21 to 30) with all the treatment group except TC100 compared to Alc group (Figure 28).

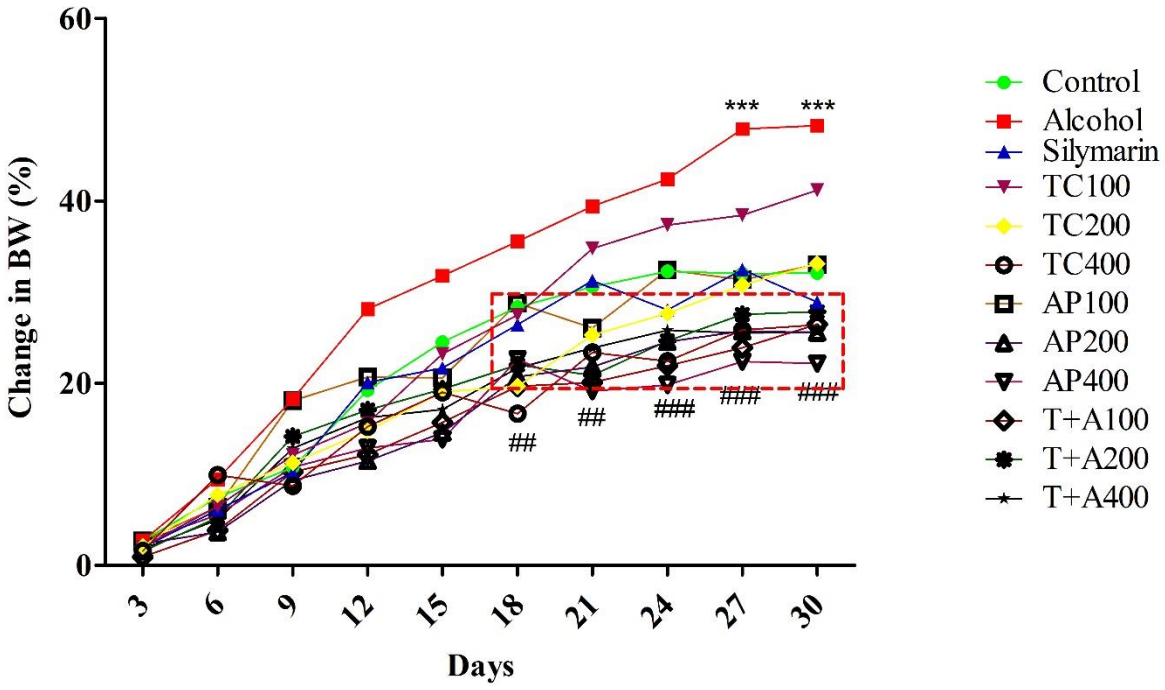


**Figure 28**: **Effect of TC and AP on BW.** All the data are presented in Mean±SEM (n=6). **p< 0.01, ***p< 0.001 compared to normal, ##p<0.01, ###p< 0.001 compared to alcoholic.

### 5.6.2. Effect of TC and AP on lipid profile and kidney markers

TC and TG levels were significantly increased ($p<0.05$ and $p<0.01$, respectively) in the Alc group compared to normal which was significantly decreased ($p<0.001$) with Silymarin ($p<0.05$), TC100 ($p<0.001$), AP100 ($p<0.001$), T+A100 and T+A200 ($p<0.01$). In contrast, the HDL level was significantly reduced ($p<0.001$) in the Alc group which was reversed with TC400 ($p<0.01$) and T+A200 ($p<0.05$). A slight increase (non-significant) in the LDL level was observed in the Alc group and was decreased in the Silymarin, TC100, TC200, TC400, AP100, and T+A100 groups. Similarly, BUN was significantly increased ($p<0.05$) in the Alc group and was reversed in all groups except the combination group. Whereas, Creatinine was increased ($p<0.05$) in the Alc group and was reversed significantly in the TC400 and AP200 group ($p<0.001$) (Figure 29 and Table 9).

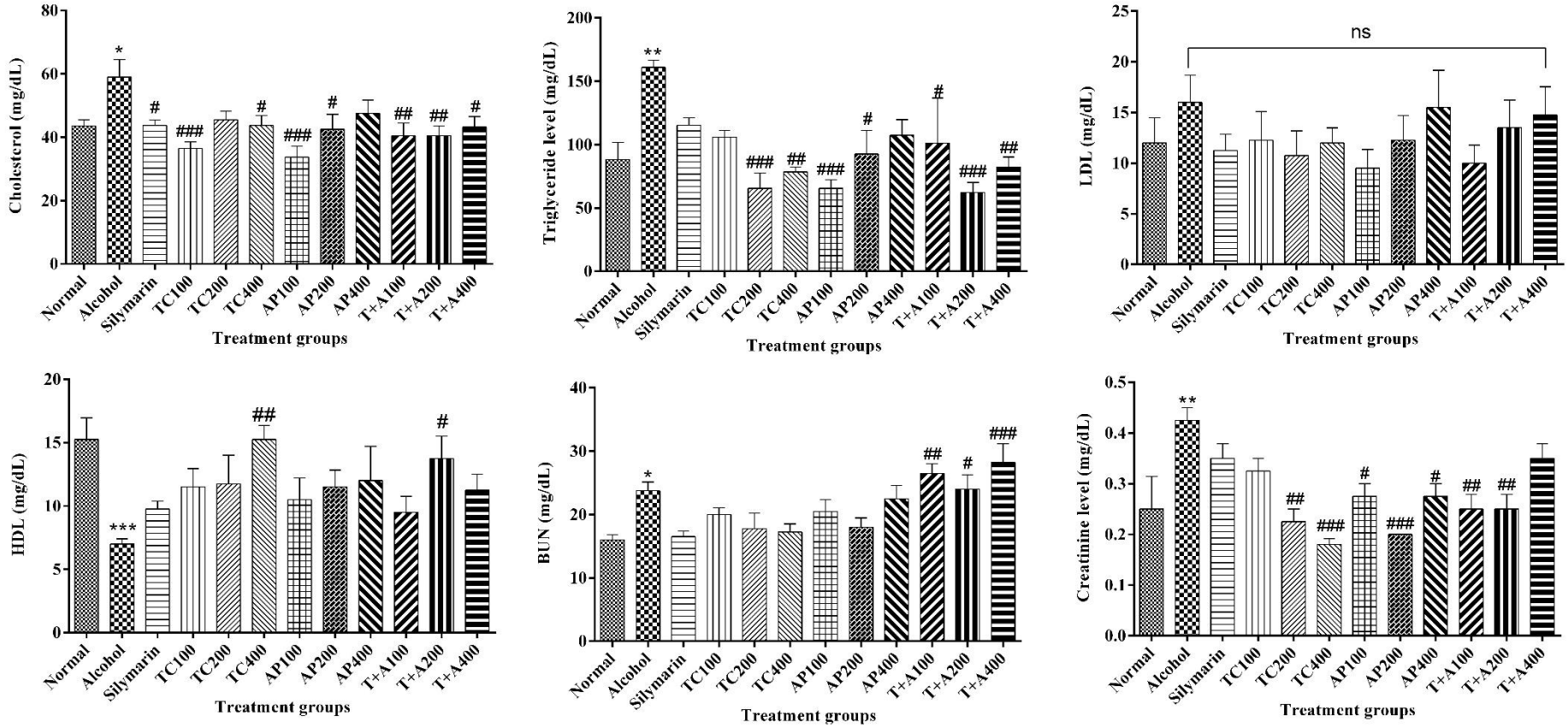


**Figure 29: Effect of TC and AP on lipid profile and kidney markers.** All the data are presented in Mean±SEM (n=6). *p< 0.05, **p< 0.01, ***p< 0.001 compared to normal, #p<0.05 ##p<0.01, ###p< 0.001 compared to alcoholic.

**Table 9:** Effect of TC and AP on lipid profile and kidney markers**.**

| Group Name | Cholesterol (mg/dL) | Triglycerides (mg/dL) | LDL (mg/dL) | HDL (mg/dL) | BUN (mg/dL) | Creatinine (mg/dL) |
|---|---|---|---|---|---|---|
| Normal | 43.5 ± 2.02 | 88.25 ± 13.52 | 12 ± 2.48 | 15.25 ± 1.7 | 16 ± 0.82 | 0.25 ± 0.06 |
| Alcohol | 59 ± 5.48* | 161 ± 5.52** | 16 ± 2.68 | 7 ± 0.41*** | 23.75 ± 1.38 | 0.43 ± 0.02** |
| Silymarin | 43.75 ± 1.65# | 115.25 ± 6.05 | 11.25 ± 1.6 | 9.75 ± 0.63 | 16.5 ± 0.87 | 0.35 ± 0.03 |
| TC100 | 36.5 ± 2.02### | 105.75 ± 5.53 | 12.25 ± 2.84 | 11.5 ± 1.44 | 20 ± 1.08 | 0.33 ± 0.03 |
| TC200 | 45.5 ± 2.72 | 65.5 ± 12.02### | 10.75 ± 2.43 | 11.75 ± 2.25 | 17.75 ± 2.5 | 0.23 ± 0.02## |
| TC400 | 43.75 ± 3.15# | 78.5 ± 3.75## | 12 ± 1.47 | 15.25 ± 1.11### | 17.25 ± 1.25 | 0.18 ± 0.01### |
| AP100 | 33.75 ± 3.47### | 65.5 ± 6.79### | 9.5 ± 1.85 | 10.5 ± 1.71 | 20.5 ± 1.85 | 0.28 ± 0.02# |
| AP200 | 42.5 ± 4.73# | 92.5 ± 18.59# | 12.25 ± 2.43 | 11.5 ± 1.32 | 18 ± 1.47 | 0.2 ± 0### |
| AP400 | 47.5 ± 4.21 | 107.5 ± 12.22 | 15.5 ± 3.66 | 12 ± 2.71 | 22.5 ± 2.06 | 0.28 ± 0.02# |
| T+A100 | 40.5 ± 4.05## | 101.25 ± 35.48# | 10 ± 1.78 | 9.5 ± 1.26 | 26.5 ± 1.5## | 0.25 ± 0.03## |
| T+A200 | 40.5 ± 3.07## | 62.25 ± 7.92### | 13.5 ± 2.72 | 13.75 ± 1.75# | 24 ± 2.27# | 0.25 ± 0.03## |
| T+A400 | 43.25 ± 3.3# | 82.25 ± 8.01## | 14.75 ± 2.78 | 11.25 ± 1.25 | 28.25 ± 2.93### | 0.35 ± 0.03 |

All the data are presented in Mean±SEM (n=6). *p< 0.05, **p< 0.01, ***p< 0.001 compared to normal, #p<0.05 ##p<0.01, ###p< 0.001 compared to alcoholic.

### 5.6.3. Effect of TC and AP on liver enzymes

SGPT and ALP were significantly increased (non-significant) in the Alc group compared to normal which was significantly reversed by all the treated groups. SGOT was increased (non-significant) in the Alc group compared to normal which was significantly reversed by all the treated groups, especially T+A100 ($p<0.001$). Whereas, a slight increase (non-significant) of TP, TB, and albumin in the Alc group was seen compared to normal and was reversed with TC100, AP100, and AP200. There was no significant effect of Alc on SGPT, whereas, TC100 and TC400 showed an increase in the level of SGPT compared to the normal group (Figure 30 and Table 10).

### 5.6.4. Effect of TC and AP on Antioxidant markers

GSH level was significantly decreased in Alc group ($p<0.001$) compared to normal, which was significantly reversed by TC400 ($p<0.01$), AP400 ($p<0.05$), and T+A400 ($p<0.001$). The LPO level was significantly increased in the Alc group ($p<0.001$) compared to normal and was reversed by all the treatment groups ($p<0.0001$). Similarly, in the Alc group, SOD activity was significantly inhibited ($p<0.01$) compared to normal and was significantly reversed in the Silymarin ($p<0.01$), TC400 ($p<0.01$), and AP400 ($p<0.05$) groups (Figure 31).

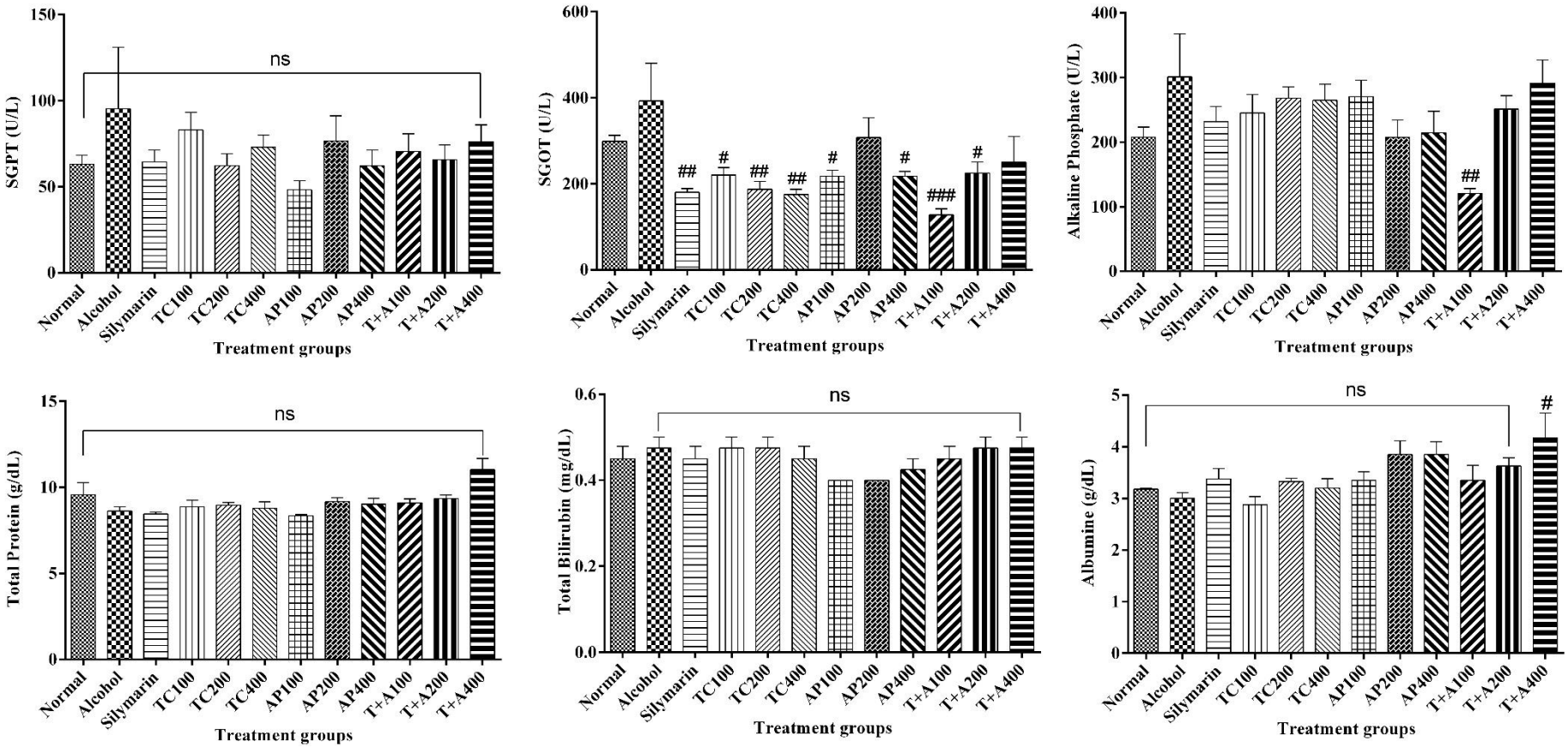


**Figure 30: Effect of TC and AP on liver enzymes.** All the data are presented in Mean±SEM (n=6). *p< 0.05, ***p< 0.001 compared to normal, #p<0.05 ##p<0.01, ###p< 0.001 compared to alcoholic.

**Table 10**: Effect of TC and AP on liver enzymes.

| Group Name | SGOT (U/L) | SGPT (U/L) | Alkaline Phosphatase (U/L) | Total Protein (g/dL) | Albumin (g/dL) | Total Bilirubin (mg/dL) |
|---|---|---|---|---|---|---|
| Normal | 298.75 ± 13.9 | 63 ± 5.28 | 207.75 ± 15.64 | 9.58 ± 0.71 | 3.18 ± 0.03 | 0.45 ± 0.03 |
| Alcohol | 392.5 ± 87.79 | 95.25 ± 35.69 | 301.25 ± 66.35 | 8.63 ± 0.25 | 3 ± 0.11 | 0.48 ± 0.03 |
| Silymarin | 180.25 ± 8.73## | 64.5 ± 6.81 | 231.75 ± 23.55 | 8.45 ± 0.13 | 3.38 ± 0.2 | 0.45 ± 0.03 |
| TC100 | 220.25 ± 17.39# | 83 ± 10.26 | 245.25 ± 28.46 | 8.88 ± 0.38 | 2.88 ± 0.16 | 0.48 ± 0.03 |
| TC200 | 187.25 ± 18.03## | 62.25 ± 6.86 | 268.25 ± 17.4 | 8.98 ± 0.14 | 3.33 ± 0.06 | 0.48 ± 0.03 |
| TC400 | 175 ± 12.42## | 73 ± 6.98 | 265 ± 24.77 | 8.78 ± 0.39 | 3.2 ± 0.18 | 0.45 ± 0.03 |
| AP100 | 217.5 ± 13.77# | 48.25 ± 5.27 | 270.5 ± 25.57 | 8.35 ± 0.06 | 3.35 ± 0.17 | 0.4 ± 0 |
| AP200 | 307.5 ± 45.89 | 76.5 ± 14.75 | 207.25 ± 27.14 | 9.18 ± 0.23 | 3.85 ± 0.26 | 0.4 ± 0 |
| AP400 | 217.5 ± 11.09# | 62.25 ± 9.1 | 214.5 ± 33.31 | 9.03 ± 0.34 | 3.85 ± 0.25 | 0.43 ± 0.02 |
| T+A100 | 127.5 ± 14.36### | 70.5 ± 10.3 | 120.5 ± 7.54### | 9.1 ± 0.24 | 3.35 ± 0.29 | 0.45 ± 0.03 |
| T+A200 | 225 ± 25.33# | 65.75 ± 8.5 | 251 ± 20.96 | 9.35 ± 0.21 | 3.63 ± 0.16 | 0.48 ± 0.03 |
| T+A400 | 250 ± 59.58 | 76.25 ± 9.66 | 291.5 ± 35.61 | 11.03 ± 0.65 | 4.18 ± 0.48# | 0.48 ± 0.03 |

All the data are presented in Mean±SEM (n=6). *p< 0.05, ***p< 0.001 compared to normal, #p<0.05 ##p<0.01, ###p< 0.001 compared to alcoholic.

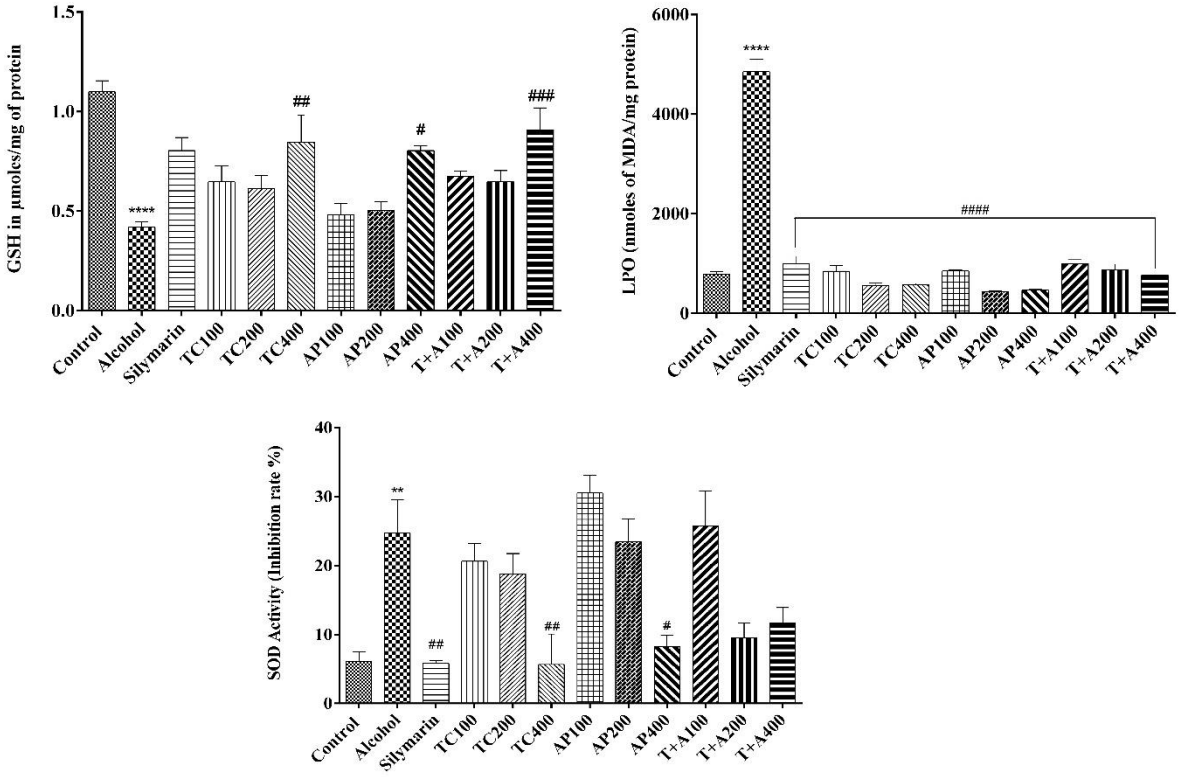


**Figure 31: Effect of TC and AP on antioxidant markers**. All the data are presented in Mean±SEM (n=6). **p< 0.01, ****p< 0.0001 compared to normal, #p<0.05 ##p<0.01, ###p< 0.001, ####p< 0.0001 compared to alcoholic.

**Table 11**: Effect of TC and AP on antioxidant markers

| Group Name | GSH (µmoles/mg of protein) | LPO (nmoles of MDA/mg protein) | SOD (Inhibition rate %) |
|---|---|---|---|
| Normal | 1.0989 ± 0.2241 | 786.859 ± 50.972 | 6.063 ± 1.43 |
| Alcohol | 0.4192 ± 0.0865*** | 4854.167 ± 249.058*** | 24.71 ± 4.79** |
| Silymarin | 0.8039 ± 0.1687 | 1001.603 ± 146.419### | 5.82 ± 0.439## |
| TC100 | 0.6472 ± 0.1433 | 844.551 ± 120.619### | 20.629 ± 2.612 |
| TC200 | 0.6139 ± 0.1327 | 552.885 ± 54.605### | 18.814 ± 2.945 |
| TC400 | 0.8471 ± 0.1992## | 580.128 ± 24.339### | 5.649 ± 4.428## |

| | | | |
|---|---|---|---|
| AP100 | 0.4808 ± 0.0511 | 849.359 ± 28.246### | 30.526 ± 2.583 |
| AP200 | 0.5052 ± 0.0372 | 439.103 ± 15.371### | 23.427 ± 3.389 |
| AP400 | 0.8042 ± 0.0224# | 464.744 ± 20.689### | 8.232 ± 1.625# |
| T+A100 | 0.6763 ± 0.0233 | 995.192 ± 86.296### | 25.784 ± 4.994 |
| T+A200 | 0.6475 ± 0.0501 | 873.397 ± 114.92### | 9.49 ± 2.148 |
| T+A400 | 0.908 ± 0.0994### | 766.026 ± 5.551### | 11.644 ± 2.257 |

All the data are presented in Mean±SEM (n=6). **p< 0.01, ****p< 0.0001 compared to normal, #p<0.05 ##p<0.01, ###p< 0.001, ####p< 0.0001 compared to alcoholic.

### 5.6.5. Effect of TC and AP on TNF-α and IL6

Serum TNF-α significantly higher in Alc group (p<0.01) compared to normal and was significantly reversed by all the treatment groups in dose dose-dependent manner (p<0.05 to p<0.001) except TC100. Similarly, in the Alc group, serum IL6 level was significantly higher (p<0.001) compared to normal and was significantly reversed by all the treatment groups in dose-dependent manner (p<0.05 to p<0.001) except AP100 and T+A100 (Figure 32).

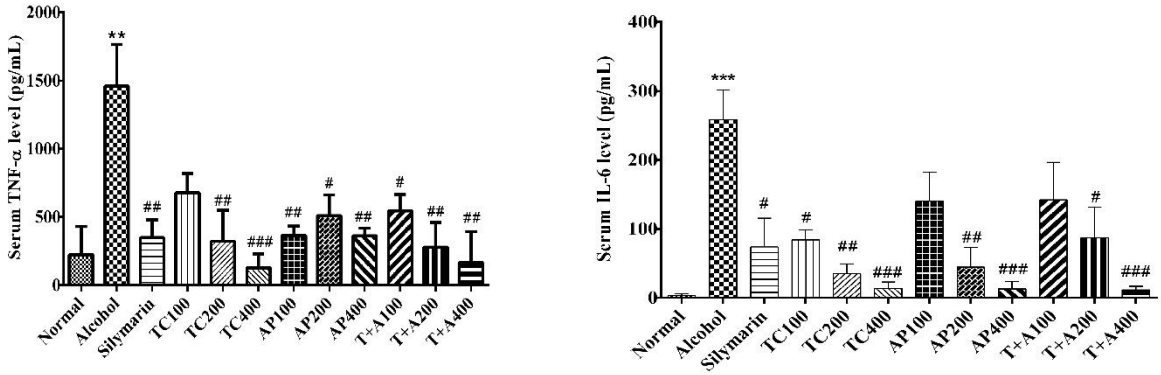


**Figure 32**: **Effect of TC and AP on TNF-α and IL6**. All the data are presented in Mean±SEM (n=6). **p< 0.01, ***p< 0.001, compared to normal, #p<0.05 ##p<0.01, ###p< 0.001 compared to alcoholic.

### 5.6.6. Effect of TC and AP on Haematology

The normal range of rat haematology parameters was obtained from the CPCSEA compendium. All the groups showed normal haematology and the readings were found within the range (Table 12).

### 5.6.7. Histopathology of liver

As shown in Figure 33A and 33B, Alc group showed observable ballooning degeneration (red) and was reversed by TC200, TC400, and T+A200. Alc group showed observable centrilobular, piecemeal, and spotty necrosis (green) and was found to be absent in all the groups except T+A400 for centrilobular necrosis and TC100 for spotty necrosis. Alc group showed observable inflammation (square box) and was reduced in TC200, AP100, AP200, AP400, T+A100, and T+A400. Alc group showed Portal triditis and was found to be absent in all groups except TC400 and T+A400. Alcohol group showed Sinusoidal and venous congestion (circle) and was found to be absent in all the groups except TC100, AP400, and T+A400.

**Table 12**: **Effect of TC, AP, and their combination on haematology.**

| Parameters | Hb (g/dL) | Total WBC (X10³/mm³) | Neutrophils (%) | Lymphocytes (%) | Eosinophils (%) | Monocytes (%) |
|---|---|---|---|---|---|---|
| Normal Range (Compendium of CPCSEA) | 11-18 g/dL | 6-17 X10³/mm³ | 9-34 (%) | 65 – 85 (%) | 0-6 (%) | 0-5 (%) |
| Normal | 10.65±3.1 | 24302.5±930.35 | 17.25±2.06 | 88.75±2.02 | 1.25±0.25 | 1.75±0.75 |
| Alcohol | 9.75±0.1 | 12057.5±2139.68 | 14±1.47 | 81.5±1.44 | 0.75±0.25 | 3.75±1.55 |
| Silymarin | 12±1.26 | 20217.5±2058.34 | 16.75±4.03 | 89.75±0.63 | 1.25±0.25 | 1.5±0.29 |
| TC100 | 11.9±0.62 | 10210±937.12 | 17.25±4.03 | 77.75±4.61 | 1±0 | 4±1.08 |
| TC200 | 11.13±0.67 | 12690±1933.26 | 17±2.52 | 78±2.48 | 1.5±0.29 | 3.5±0.96 |
| TC400 | 11.05±0.67 | 14797.5±1308.6 | 16.25±0.85 | 82.75±1.11 | 0.5±0.29 | 3±0.71 |
| AP100 | 11.68±0.23 | 7305±1074.12 | 17.25±1.25 | 77.75±1.25 | 0.75±0.25 | 4.25±1.03 |
| AP200 | 12.53±0.56 | 14777.5±2579.91 | 18.75±3.09 | 76.25±2.93 | 0.5±0.29 | 4.5±0.87 |
| AP400 | 10.68±0.23 | 15970±2816.94 | 16.25±1.25 | 79.75±2.46 | 0.75±0.25 | 3.25±1.03 |
| T+A100 | 12.45±0.47 | 12242.5±809.87 | 18.5±4.5 | 76±5.16 | 0.75±0.25 | 4.5±1.32 |
| T+A200 | 11.53±0.55 | 12520±1680.97 | 20.5±1.71 | 75.5±2.02 | 0.5±0.29 | 3.5±1.04 |
| T+A400 | 11.95±0.43 | 16687.5±2581.87 | 22.25±7.28 | 84.75±2.17 | 0.5±0.29 | 2.5±0.29 |

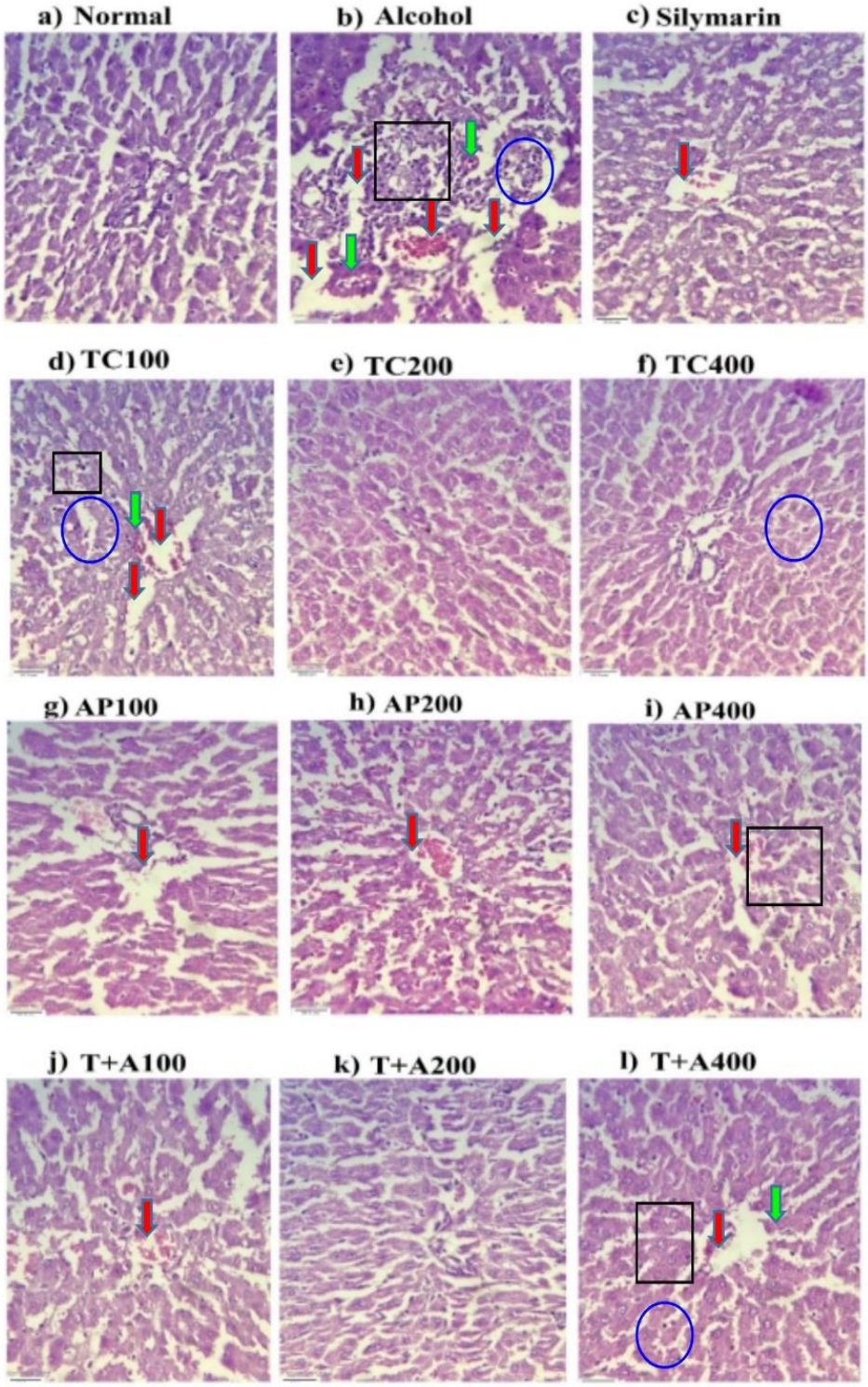


**Figure 33A: Effect of TC, AP, and their combination on hepatocytes (40X) in alcohol induced liver injury.**

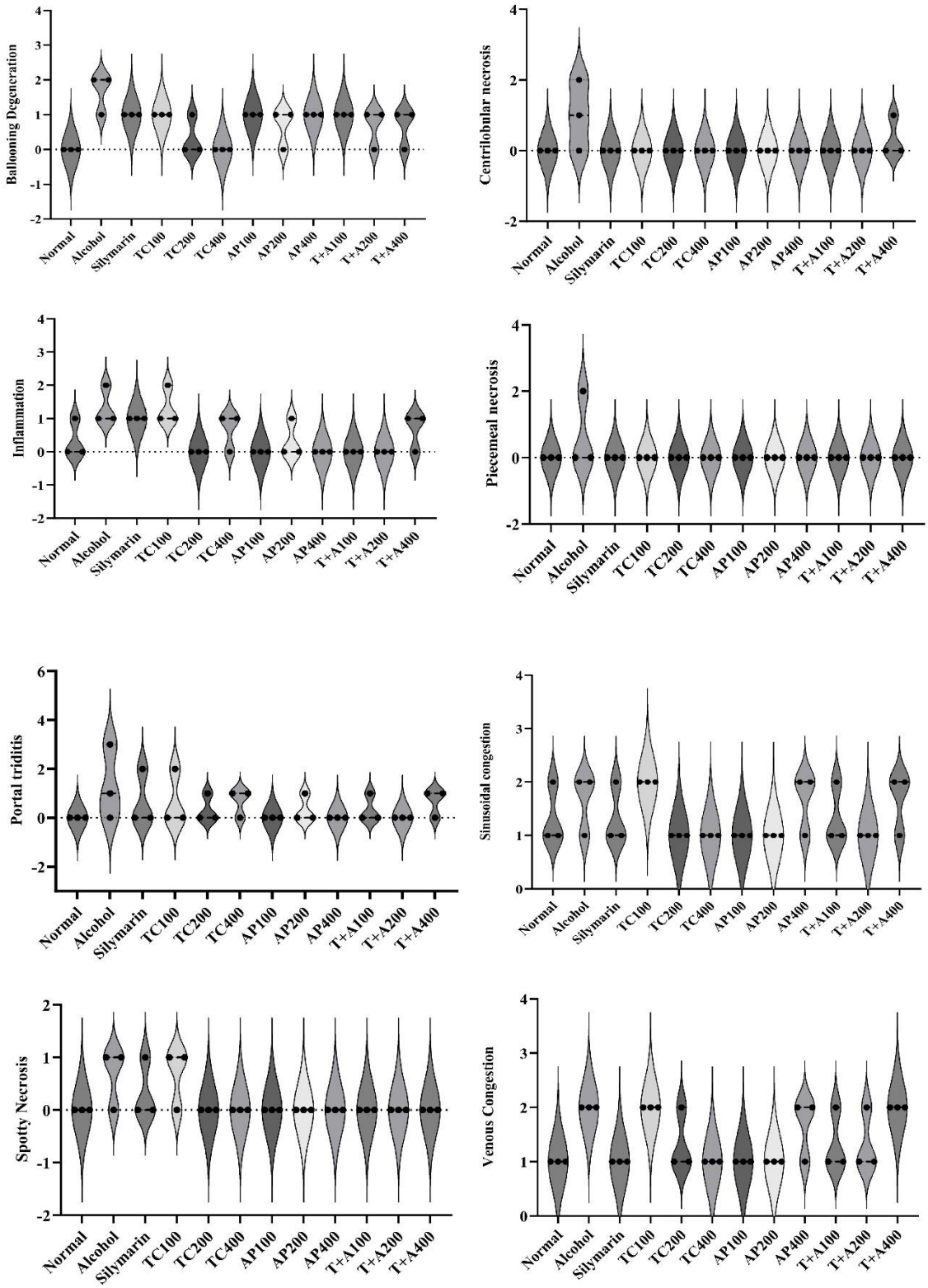


**Figure 34B: Effect of TC, AP, and their combination on hepatocytes (40X) in alcohol induced liver injury.**

# DISCUSSION

The present study employed multiple bioinformatics approaches combined with *in vitro* and *in vivo* studies to identify the bioactive constituents from traditional medicinal plants against HBV and its associated complications like HCC. First, the lead compounds possessing anti-HBV (RT and HBx protein inhibition) and hepatoprotective potential (modulation of host protein involved in HCC) were prioritized through the computational studies including homology modelling, molecular docking, and dynamics, gene set enrichment, and network pharmacology studies. Secondly, these phytocompounds containing extracts/fraction(s) were tested through *in vitro* methods for anti-HBV activities namely HBV RT inhibition, HBsAg and HBeAg secretion inhibition, quantification of HBV DNA and pgRNA, and HBx-HBXIP inhibition. Finally, the *in vitro* study prioritized extracts/fraction(s) were further tested for hepatoprotective potential in chemical-induced hepatitis animal model that resembles HBV pathogenesis.

## 6.1. *In silico* studies

### 6.1.1. Phytocompounds affinity towards HBV RT

Since the discovery of HBV, numerous studies have reported the construction of the full-length DNA polymerase or its functional domains crystal structures, however, these structures failed to get its three-dimensional structure.[146,147] Thus, in this study, we modelled and validated a plausible structure of HBV-RT with its cofactor $Mg^{2+}$ and HIV-RT inhibitor. The "HBV-RT domain is known as a catalytic center of polymerase, and it has a high degree of homology with HIV1-RT enzyme and both possess conserved multiple catalytic activities".[147] The HBV-RT model was constructed utilizing the Phyre2 server because of its ability to efficiently construct 3D models, predict ligand binding sites and assess the effect of amino acid variations on a particular protein sequence.[116] Further, LocPREDMD server was utilized to energy minimize the modelled protein, as

it uses "molecular dynamics (MD) simulations via employing force field-based minimization, refines the structure, and calculates (a) clash score, rotamer outliers (%), Ramachandran outliers from MolProbity, (b) VERIFY3D, (c) G-factor, mainchain bonds (%), mainchain angles (%), sidechain planarity (%) from PROCHECK w.r.t. initial structure; since LocPREDMD first reconstructs side chains and executes side-chain repacking, followed by overall structural relaxing using MD simulation". The resulting structure from LocPREDMD was submitted to GalaxyREFINE[118] and further all-atom explicit MD simulation was performed to determine the lowest PE conformation (-150060.689 kcal/mol). The active site "YMDD motif" amino acid residues "Y203 and D206" position having RMSD >1 was constrained in ModLoop for loop refinement and as a result, the YMDD motif RMSD was found to be 1. This improved the structural similarity and accuracy of the modelled protein with respect to a template structure. About 98.7% of the residues, including YMDD, were discovered to fall within the preferred region after post-refinement. In addition, a Modeller software was used to construct the HBV-RT in complex catalytic $Mg^{2+}$ and known inhibitor at its active site.

Medical plants possess a wide range of bioactive compounds, deal with polygenic diseases, and may have inhibitory effects on viral protein targets.[148,149] In the current study, 19 medicinal plants were chosen for this investigation based on their effectiveness in treating conditions resembling hepatitis and traditional claims. The phytocompounds were virtually screened against modelled HBV-RT. As a result, 15 phytocompounds (out of 268) were found to target the YMDD motif and RT1 motif of HBV-RT. These 15 compounds include: 6 compounds from *T. chebula,* 5 from *B. pilosa,* and 4 from *C. asiatica* were found to interact with the residues of the RT1 motif (aa21–aa51) and the YMDD motif (aa203–aa206). The G box (aa-24-aa36) and F box (aa37-aa47) which together make up the RT1 motif are crucial for H-binding because they interact with the

T3 motif in TP to facilitate the packaging of a particular pgRNA into viral nucleocapsids and the start of reverse transcription.[150,151] In addition, the YMDD motif is highly conserved in RNA-dependent DNA polymerase and is implicated in nucleotide binding to the polymerase's catalytic site in both HIV and HBV.[152] Terflavin-C and 1,3,6-Tri-O-galloyl-D-glucose from T. chebula had the lowest BE -9.4 kcal/mol and -9.3 kcal/mol, respectively among the 15 compounds. Molecular dynamics was employed to assess the structural stability of 15 phytocompounds with HBV-RT for 100 ns. All 15 of the complexes have been found to have stable backbones and complex RMSD with the least residual fluctuation (RMSF) at the ligand-binding site. The compounds also displayed stable interactions with the RT1 and YMDD motif residues throughout the course of a 100-ns production run. The binding free energies of complexes were also computed using the Prime MMGBSA module to confirm the binding affinity. 1,2,3,4,6-penta-O-galloyl-e-D-glucose had the lowest binding free energy of -113.774 kcal/mol, whereas the known inhibitor had a score of -11.069 kcal/mol. It's interesting to note that other compounds likewise have binding free energies between -87.165 to -26.640 kcal/mol. The findings suggested that phytocompounds were more effective against HBV-RT than standard inhibitor.

Additionally, the investigation is expanded to gene set enrichment and network pharmacology to know the phytocompound interaction with host protein targets and pathways. This approach helps to identify the function of these phytocompounds on host targets that are essential for hepatoprotection. As a result, 11 phytocompounds (out of 15) were targeted at 75 host proteins and 37 pathways. 40.54% Out of 37, 15 pathways were identified as likely to be involved in HBV infection and its related complications via majorly targeting TNF, PLAU, PTPN1, and MMP9 protein targets.

Drug-likeness characteristics are used in computer-aided drug design that evaluates a small molecule's absorption, biodistribution, bioavailability, and excretion features based on knowledge of the structure and properties of its atoms. To speed up wet-lab research, this prediction is often generated before the chemicals are separated from medicinal plants or produced in the lab.[153] These 15 compounds were predicted to exhibit positive DLS based on the rule of five. 1,3,6-Tri-O-galloyl-D-glucose had the highest DLS of 0.92. Furthermore, the PASS server was used to predict the biological spectra of 15 phytocompounds (Pa 0.3). Except for 2 compounds, all the compounds were predicted to have biological activity for hepatoprotective (Pa=0.608 to 0.972), hepatic disorders treatment (Pa= 0.422 to 0.759), and antiviral (Pa=0.33 to 0.403) properties. Interestingly, out of 13 compounds, 10 compounds showed antiviral effects against hepatitis B with Pa=0.348 to 0.513.

### 6.1.2. Phytocompounds mode of action towards HBV pathogenesis

The development of safe and effective novel treatments for HBV-induced HCC focuses primarily on the discovery of potential therapies from herbal medicines. Therefore, it must be considered that the benefits of using herbs outweigh their potential risks.[154] One of the most serious factors during treatment is hepatotoxicity triggered by herbs. Post-marketing warnings and product withdrawals have frequently been caused by this problem.[155] Researchers have shown that herbs can trigger both common and severe side effects involving the liver. To date, *Teucrium chamaedrys, Larrea tridentate, Cimicifuga racemosa, Scutellaria lateriflora,* and *Scutellaria baicalensis* have been identified as the most hepatotoxic plants.[156] In this study, we screened 16 herbs for their druggability and significant adverse drug reactions/side effects (such as hepatotoxicity, cardiac toxicity, nephrotoxicity, and the potential to induce myocardial infarction). As a result, 36 compounds were found to have druggability with lesser side effects (probable

toxic activity (Pa) <0.5 in ADVERPred). Furthermore, the compounds possible pharmacological targets were predicted using BindingDB (p-value>0.7), and the target corresponding to HBV infection and HCC were identified with the help of the available literature, the KEGG pathway, and the Therapeutic Target Database (TTD). The predicted target's role in the regulation of molecular functions, processes, and pathways with higher significance (p 0.05) and, those that are only associated with HBV-induced HCC was retrieved using the STRING and KEGG database and the connection between compounds, their targets, and the pathways were built by Cytoscape. The network pharmacology theory explain that "one pathway containing many protein molecules modulated by one compound is more essential than the function of one protein that involves many pathways modulated by one drug molecule; that is the impact of one target in numerous pathways may be less, and the impact of one pathway with multiple protein targets modulated by one compound could be large".[157] Based on this theory, we chose 11 phytocompounds, viz., "Andrographidine C, 5-Hydroxy-7,8,2′-Trimethoxyflavone (Andrographin), Skullcapflavone I, 2′-hydroxy-5,7,8-trimethoxyflavone, 5,4′-dihydroxy-7,8,2′,3′-tetramethoxyflavone, 5-hydroxy-7,8-dimethoxyflavone, 5-hydroxy-7,8,2′,5′-tetramethoxyflavone, 5-hydroxy-7,8,2′,3′,4′-pentamethoxyflavone, Wightin, 5-Hydroxy-7,8,2′,3′-Tetramethoxyflavone, and Altisin from *A. paniculata* (are of Andrographolide derivatives) contained in *A. paniculata* whole plant and Gossypetin, Herbacetin, and Kaempferol-7-Glucoside contained in *T. populnea* flowers".[158] These phytocompounds have been identified to be flavonoids and diterpenoids, had been found to alter the activity of thirteen protein molecules (CDK1, CDK2, CDK6, EGFR, HGF, IGF1R, TERT, STAT3, PRKCA, PRKCB, PRKCG, AKT1, and TNF) essential for the progression of HBV infection to HCC. In addition, these protein targets were found to regulate 14 major molecular pathways, including the Hepatitis B pathway, the PI3K-

Akt, Ras, mTOR, apoptosis, TNF, Jak-STAT, and p53 signalling pathways, and the cell cycle.

The aforementioned compounds were predicted to target EGFR, the highest-scoring node in the network. Secondly, the literature revealed EGFR as a potential therapeutic target for cancer treatment (it was found to be involved in the MAPK, PI3-Akt, Ras, and Jak-STAT signalling pathways). Overexpression of EGFR is common in HCC, as was shown in previous research; this suggests that it contributes to the pathophysiology and management of the disease. As a result, EGFR was selected as the most probable target. "It is well known that NTCP host receptors are essential for HBV entry; however, NTCP expression alone is not enough for the entry of HBV, because EGFR is a host cofactor that regulates the host cell's ability to support HBV internalization and is essential for NTCP's viral receptor activity".[159] The EGFR endocytosis mechanism is activated once HBV attaches to NTCP on the cell surface, resulting in EGFR phosphorylation and the subsequent recruitment of adaptor molecules such "AP2A1 and EPS15".[160–162] HBV transport in the endosomal network (early and late endosomes, and lysosomes) is coordinated by the EGFR-sorting machinery, which includes EGFR ubiquitination, STAM, and LAPTM4B.[160] In addition, via siRNA-mediated suppression of endogenous EGFR in HepG2-NTCP cells, HepaRG cells, and primary human hepatocytes, researchers evaluated the EGF-related host factor(s) in HBV infection and saw a substantial decline in HBV infection. The quantity of HBV DNA internalized into cells was dramatically lowered by EGFR knockdown, even if HBV viral attachment was not diminished in EGFR-knockdown cells.[161] The EGFR signalling pathways have been identified as a key role in all phases of the liver response to injury, from early inflammation and hepatocellular proliferation to fibrogenesis and neoplastic transformation.[163,164] 11 compounds from A. paniculata and 3 from T. populnea that were

docked to the EGFR to study their intermolecular interactions with active site residues. As a result, 5-Hydroxy-7,8,2′-Trimethoxyflavone (Andrographin) from *A. paniculata* and Gossypetin (*T. populnea*) were identified as lead hits against EGFR based on the BE and highest interaction with active site residues. All the compounds were predicted to pose interaction with the active site residues. The MD simulation was utilized to post-docking investigations to determine the effect of protein structural stability on ligand binding (for Andrographin and Gossypetin with WT-EGFR in triplicate) and as a result the protein-ligand interactions RMSD were shown to be stable and maintained stable connections throughout 100 ns simulation run.

### 6.2. *In vitro* anti-HBV activity studies

To validate the *in silico* findings, *T. chebula* n butanol fraction (TCN) and water extract (TCW), *B. pilosa* methanol (BPM), hydroalcoholic (BPHA) extract, *C. asiatica* hydroalcoholic (CAHA), *A. paniculata* hydroalcoholic (APHA), *T. populnea* hydroalcoholic (TPHA), PGG (pure compound from *T. chebula*), and a standard drug TDF were further evaluated by *in vitro* methods. The *in silico* prioritized compounds within the prepared extracts were first identified using LC-MS profiles of extracts/fractions. Furthermore, HepG2.2.15 cells that express HBV were used to evaluate each test drug for cytotoxicity. Then, we prioritized TCN, TCW, AP, TP, PGG, and TDF for further investigations based on the results of a colorimetric RT inhibitory assay (test drug's RT inhibitory action). Further research looked at the effects of TCN, TCW, PGG, AP, TP, and TDF on intracellular HBV DNA and pgRNA in HepG2.2.15 cells. Finally, TCN, TCW, AP, TP, PGG, and TDF were tested in HepG2.2.15 cells to study time- and concentration-dependent HBsAg (24, 48, 72, 96, and 120h) and HBeAg (24, 72, and 120h) secretion. Additionally, to confirm the Study 3 findings, the HBx and

HBXIP assay kit was used to assess the suppression of HBx-HBXIP interaction for AP and TP.

### 6.2.1. *In vitro* RT inhibitory assay

TCN, TCW, BPM, BPHA, CAHA, APHA, TPHA, PGG, and TDF were tested for their RT inhibitory activity. TCN ($IC_{50}$ = 147.077 µg/mL), TCW ($IC_{50}$ = 149.214 µg/mL), APHA ($IC_{50}$ = 304.52 µg/mL), TPHA ($IC_{50}$ = 553.88 µg/mL), and PGG ($IC_{50}$ = 149.075 µM) were identified as potent RT enzyme inhibitors and were identified as dose-dependent. While, BPM, BPHA, and CAHA did not showed RT inhibition. While, standard compound TDF also failed to exhibit RT inhibition action at a dose of 250µM. This is due to the fact that TDF is a prodrug that undergoes conversion to tenofovir monophosphate (nucleoside/tide) analogue and then to tenofovir diphosphate, which is the active metabolite. Tenofovir diphosphate inhibits RT/POL by direct binding competition with the deoxyadenosine 5'-triphosphate and causes viral DNA chain termination.[165] Similarly, we investigated effect of TCN, TCW, AP, TP, PGG, and TDF effect on intracellular HBV DNA and pgRNA in HepG2.2.15 cell line. Here, the intracellular HBV DNA was lowered by $2^6$ and $2^7$ fold by TCN, TCW, AP, TP, 125, 250, and 500 g/mL on 24h, and by about $2^5$ fold by PGG at 100µM. This shows that TDF and all of the studied medications efficiently prevented the synthesis of viral rcDNA from pgRNA by blocking the RT enzyme, which also prevented the development and release of HBV virion. Additionally, only the pgRNA levels in TCN, TCW, AP, TP 500µg/mL, and PGG100µM decreased by $2^2$ folds. This is due to the fact that the HepG2.2.15 cells are already contain the HBV genome incorporated into the HepG2 chromosome, unlike in a normal HBV infection; which is expressing HBV pgRNA on a constitutive basis. As a result, all the tested extracts nor TDF had a significant effect on the amount of pgRNA. A previous study by Kim et al showed inhibition of HBV DNA POL by *T. chebula* extract

at a concentration ranging from 64 to 128µg/mL.[166] Interestingly, a study by Lee et al (2006) showed PGG to decrease the level of extracellular HBV in a dose-dependent manner ($IC_{50}$=1.0µg/mL).[167] Likewise, Dehydroandrographolide and andrographolide (diterpenoids) isolated from *A. paniculata* showed HBV DNA replication inhibition with $IC_{50}$ of 22.58 and 54.07µM, respectively.[168] Hence, previous investigations as well as the present study (*in silico* and *in vitro*) studies on *T. chebula* and *A. paniculata* indicate considerable anti-HBV (*via* RT inhibition) efficacies due to the presence of Pentagalloylglucose moieties in *T. chebula* and flavonoids and diterpenoids in *A. paniculata* and *T. populnea*

### 6.2.2. Effect on HBsAg and HBeAg

Furthermore, the effect of TCN, TCW, AP, TP, PGG, and TDF were tested HBsAg and HBeAg secretion in HepG2.2.15 cells at various hours. TCN, TCW, AP, and TP showed significant HBsAg and HBeAg secretion inhibition (~80%) compared to PGG and TDF. As time progresses, the inhibition of HBeAg expression/secretion decreased may be due to the time-dependent reduced effect of test drugs on 3.5 kb RNA expression. However, uniform inhibitory effect was seen for all test drugs from 24 to 120hrs, which is may be because of strong inhibition of 2.4/2.1kb RNA expression. Taken together, the *in vitro* data suggests that TCN, TCW, AP, TP, and PGG are effective against HBV infection because they strongly inhibit RT enzyme, reduce the synthesis of HBsAg and HBeAg, and prevent the formation of active HBV particles, as evidenced by lower levels of viral DNA.

### 6.3. *In vivo* studies

#### 6.3.1. Alcohol induced liver injury resembled HBV pathogenesis

Animal models are often used to investigate the biology of chronic hepatitis B and to develop novel medications or treatments.[169] However, only humans and chimpanzees are susceptible to HBV and chimpanzees are not often used in HBV research, nevertheless, owing to ethical and practical considerations.[170] There have also been initiatives to transfer HBV to smaller non-human primates. The tree shrew is the only rodent shown to be susceptible to HBV infection, however the *in vivo* system still requires significant development.[68,171] Mice having the HBV genome transfected, transduced, or transgenic can only sustain HBV replication, leaving the HBV life cycle incomplete due to the lack of viral entry, cccDNA synthesis, and viral spread. When human liver cells that maintain HBV infection are transplanted into immuno-deficient mice, the animals show apparent immunodeficiency, and their maintenance systems are very sophisticated.[76,171,172]

The previous studies showed that some of the chemical induced liver injury model are reported to induce hepatitis in rats are known to result in pathophysiology that is similar to the pathogenesis of HBV in humans.[173–175] Therefore, the objective of the present research was to identify a chemically induced hepatitis model that is identical to HBV pathogenesis utilizing gene set enrichment and network pharmacology analysis. The research found that the pathogenesis of HBV in the alcohol- and LPS-induced hepatitis models is identical. The enrichment analysis revealed that, nine pathways—namely, “PI3K-Akt, TNF, JAK-STAT, MAPK, Chemokine, NF-kappa B, TGF-beta signaling pathways, Apoptosis, and Cell cycle” were majorly associated with HBV infection (KEGG ID: hsa05161) and these were also triggered significantly (with lowest FDR score and highest gene count) by both LPS and alcohol. Based on the literature it is

identified that, chronic hepatitis may be studied using alcohol, while an acute inflammatory response to hepatitis may be studied using lipopolysaccharide. Therefore, HBV induced hepatitis is chronic and we used alcohol-induced hepatitis model for *in vivo* study.

### 6.3.2. *In vivo* hepatoprotective effect of TP and AP

*T. chebula and A. paniculata* have been utilized widely in herbal formulation and a long been regarded as Ethnomedicine/ folk medicine due to their various therapeutic properties (https://nitmmedplantsdb.in/). *T. chebula* plant is also known as the "King of Medicine" in Tibetan medicine. It is known as "Arura" which means it cures all diseases caused by Vayu, Pitta, Kapha, and clears the diseases of all 7 dhatus (blood, plasma, fat, muscle, nerve/ bone marrow, and reproductive tissue) and it is considered to be a great panace and it is listed top of the list of "Ayurvedic Materia Medica".[176–178] *T. chebula* has been shown to have exerted restorative efficacies against malignancy,[179,180] liver toxicity/infection,[181] inflammation,[182] etc. Water extract of *T. chebula* is reported to possess anti-apoptotic and anti-necroptotic activity *by* inhibiting tumor necrosis factor-induced necroptosis through the suppression of TNF-induced ROS.[183] Similarly, *A. paniculata* Nees., a member of the Acanthaceae family, is regarded as the "king of bitters" and is natively from India and Sri Lanka. The roots and leaves are utilised as medicine in Ayurveda.[184] It is a key ingradient of multiple herbal formulation to treat liver illness, hepatitis, diabetes, cancer, and other diseases.

### 6.3.3. TC and AP promotes cholesterol utilization

During 30days of treatment, from day 12 an increase in the body weight (BW) was observed in Alc treated rats and was found to be significant on day 24 compared to normal. Treatment with the minimum, moderate, and maximum dose of TC, AP alone,

and their combination showed significant decrease in the BW from day 18 compared to Alc. The results indicated that treatment with TC, AP, and their combination to have significant effect on the reduction of Alc induced gain in body weight. This effect is may be due to reduction of Alc induced adipogenecity as evidented by the significant decrease in the cholesterol and TG level in all the treatment groups. In the Alc treated group, slight increase in the LDL level was observed compared to normal, however, it is decreased in the all the treated group except AP400 and T+A400, this indicates higher dose of AP to cause liver injury. A previous studies also demonstrated TC and AP constituents (pentagallyol moieties of TC and andrographolides and flavonoids of AP) as a potent anti-obese molecules which suppress the lipogenesis via reduction in FAS expression, higher fatty acid oxidation and thereby reducing the cholesterol and TG level.

### 6.3.4. TC and AP effect on liver function

The membrane damage and cellular necrosis causes the enzyme to be released into circulation; can be detected in the blood serum. An abnormal (increased/decreased) level of serum enzymes suggests cell membrane damage and cellular leakage of liver.[185] SGPT catalyze the conversion of alanine to pyruvate and glutamate. SGPT is more specific to the liver damage and hence a better parameter for determining the liver injury.[186] SGOT catalyzes the conversion of aspartate to oxaloacetate and glutamate. Increases in SGOT levels are associated with hepatic damage, myocardial infarction, and muscular injury. Serum ALP is associated with the liver and the bones, whereas bilirubin is associated with the liver and the blood.[187]

In the present study, after 30 days of treatment with Alc, SGPT, SGOT and ALP were significantly increased and treatment with lower and moderate dose of TC, AP, and combination significantly decreased the SGPT, SGOT and ALP. The higher dose of AP

and combination again increased the SGPT, SGOT and ALP level which indicates the toxic effect of higher dose of AP on liver function.

The synthesis of serum protein relies on a well-functioning liver, which is responsible for a significant portion of protein metabolism. When the liver becomes injured/infected, protein synthesis slows dramatically, leading to low blood protein levels. Albumin contributes in limiting intravascular fluid loss and our immune system relies heavily on globulins. Patients with liver disease tend to have elevated blood total protein levels.[188] When red blood cells perish, they produce a substance called bilirubin, which is then transported to the liver. Bilirubin is secreted by the liver in a fluid known as bile. If the liver fails to perform its task properly, bilirubin won't be cleared out of the body. One of the most sensitive tests used for hepatic illness detection is serum bilirubin. The biliary system was blocked, leading to hyperbilirubinemia caused by an excess of heme breakdown. When the biliary duct is blocked, the conjugation process is drastically slowed, and unconjugated bilirubin is released from injured and dead hepatocytes.[189,190] In the present study, a slight increase in the bilirubin and no effect on total protein and albumin level was seen in the Alc group, and treatment with TC, AP, and combination of all doses revealed normal range of total protein, bilirubin, and albumin level except T+A400 group for total protein and albumin.

### 6.3.5. Effect of TC and AP on oxidative enzymes

During alcohol metabolic process, free radicals and ROS are formed, leading to oxidative stress. Degenerative alterations in the cell's pathophysiology are mostly attributable to oxidative stress; as a result, numerous biomolecules and chemicals inside cells become unstable.[191] The metabolic byproducts of alcoholism cause oxidative stress, which is characterised by its involvement in the mitochondrial energy-producing machinery. Both ROS and reactive nitrogen species (RNS) are produced during alcohol

metabolism.[192] To respond to oxidative stress under physiological conditions, cells rely on both enzymatic and non-enzymatic antioxidant systems. Oxidative stress is measured by measuring the activity of antioxidant enzymes including CAT, SOD, and GSH-Px and non-enzymatic electron receptors such as GSH. The antioxidant defence system helps to keep the levels of free radicals, which are produced in excess during periods of oxidative stress. Antioxidant enzymes like SOD and CAT play crucial roles in the body's immune response. Reduced expression of SOD and CAT in liver cells was seen with consumption of alcohol, indicating an alteration in the equilibrium between stress management mechanisms. SOD scavenges the free radical superoxide anion ($O_2$.) and transforms it to the less harmful hydrogen peroxide. Alcohol poisoning may lead to an increase in $O_2^-$, $H_2O_2$, or the products generated by their breakdown due to the lower activity of SOD. Similarly, alcohol increases lipid peroxidation, decreases glutathione levels and activation of peroxisomal acyl CoA oxidase, which facilitates xanthine dehydrogenase's conversion to xanthine oxidase, could be responsible for this oxidative stress.[193] In this study, SOD activity was significantly inhibited in Alc treated group and was significantly reversed in the Silymarin, TC400, and AP400 groups. GSH level was significantly decreased in Alc group and was significantly reversed by TC400, AP400, and T+A400 and the LPO activity was significantly increased in the Alc group and was reversed by all the treatment group. The results suggests a strong inhibition of alcohol-induced oxidative stress.

### 6.3.6. Effect of TC and AP on TNF-α and IL-6

Many animal and human studies revealed that alcohol induced liver injury initiates the expression of pro-inflammatory cytokines viz., TNF-α and IL6.[194] The report was supported by the study that anti-TNF-α antibody administration to the alcohol induced rats showed protective effect by reduced expression of TNF-α in mice lacking

TNF type I receptor do not develop alcoholic liver injury.[195] Furthermore, alcohol-fed rats livers have been shown to over-expression of TNF-α and to show elevated production of Th1-type cytokines such as IL-6, IL-12, and IFN, all of which contribute to alcohol-induced steatosis.[196] In the present study, serum TNF-α and IL-6 levels were significantly high ($p<0.01$) in Alc group compared to normal and were significantly reversed by all the treatment groups in dose-dependent manner ($p<0.05$ to $p<0.001$) except TC100 for TNF-α and AP100 and T+A100 for IL-6. In previous studies, TC and AP showed anti-inflammatory properties through the inhibition of TNF-α and IL6 and interestingly, the *in silico* study showed both TC and AP constituents to target TNF and IL-6. Hence, the gene set enrichment and network pharmacology analysis clearly inferred the pathways that corroborate with previous reports on selected medicinal plants to combat HBV induced HCC *via* RT inhibition and host immunomodulation. Thus, *T. chebula* and *A. paniculata* extracts and their herbal formulations can be utilized as a potential chemopreventive agent to combat HBV infection and associated complications like HCC.

### 6.3.7. TC and AP effect on kidney

Previous studies and reports have observed that the chronic HBV infection is associated with various chronic kidney diseases[197] and also consumption of alcohol alters the kidneys' structure and function and impairs their capacity to control the amount and make-up of fluid and electrolytes in the body. Hepatorenal syndrome is associated with severe liver disease in which BUN) levels and serum concentrations of the waste product creatinine are elevated.[198] In the present study, both BUN and creatinine levels were significantly elevated and were reversed by the lower and moderated dose of TC, AP and combination. However, higher dose of AP and in combination with TC didn't showed change in the BUN and creatinine level compared to Alc group.

# CONCLUSION

The current study employed bioinformatics approaches combined with multiple *in vitro* anti-HBV studies and *in vivo* hepatoprotective activity to identify the potent medicinal plant bioactives from the Western Ghats region of Karnataka to possess anti-HBV and hepatoprotective effects. Herein, we first modelled and validated HBV-RT structure in complex with $Mg^{2+}$ ion and known inhibitor. Virtual screening and MD simulation studies revealed 15 hit moieties (out of 268 phytocompounds from 18 plants) to have greater binding affinity and very stable interaction with the catalytic residues mainly tannins from *Terminalia chebula* (6) and flavonoids from *Bidens pilosa* (5) and *Centella asiatica* (4). These molecules also possess interactions with the host targets associated with HBV infection and associated complications like HCC. Secondly, from the remaining 16 plants, identified flavonoids and diterpenoids of AP and flavonoids of TP as a group of druggable and nontoxic phytocompounds to modulate the therapeutic proteins involved in HBV infection and HCC without expecting adverse drug reactions.

Further, the *in vitro* study identified *T. chebula* n-butanol and water fraction and hydroalcoholic extract of *A. paniculata* and *T. populnea* to potentially inhibit RT, decrease the intracellular DNA and pgRNA, and time-dependent decrease in HBsAg and HBeAg levels in HepG2.2.15 cell line.

Since HBV only infects humans and chimpanzees, despite the fact that researchers have developed multiple *in vivo* models for HBV, and there are currently no specific laboratory animal models available to study HBV pathogenesis or immune response due to their limitations. The present study identified alcohol- and LPS-induced hepatitis (out of seven chemically induced hepatitis) were found to resemble the molecular mechanisms involved in HBV-induced hepatitis The key pathways altered by HBV, alcohol, and LPS with significant gene counts and FDR scores, include “apoptosis,

cell cycle, PI3K-Akt, TNF, JAK-STAT, MAPK, chemokine, NF-kappa B, and TGFB". As an outcome, chronic hepatitis can be studied using alcohol, whereas acute hepatitis can be studied with lipopolysaccharide.

The effect of TC, AP, and their combination were further tested for their hepatoprotective activity in alcohol-induced liver injury (the model is used for chronic hepatitis and resembles HBV pathogenesis). In the hepatoprotective animal study, we observed a significant amelioration of the liver and kidney function by all doses of TC, a moderate dose of AP, and a moderate dose of combination which was evidented by decreased levels of SGPT, SGOT, ALP, BUN, and creatinine levels; regulating the inflammation by inhibiting TNF-α and IL6 secretions; and regulation of anti-oxidant biomarkers in the liver tissue viz., GSH, SOD, and LPO; which was followed by histological restoration of the liver. Theoretical knowledge combined with predicted and validated results of this study confirms TCN, TCW, AP, TP, and PGG as valuable resources for the management of HBV infection and associated complications like HCC.

# SUMMARY

The study modelled the plausible structure of **HBV-RT in complex with cofactor $Mg^{2+}$** and **known inhibitor** and identified **Pentagalloyl glucose moieties from *Terminalia chebula*** as potent HBV-RT inhibitors as these molecules were found to interact with the **YMDD and RT1 motif**. The network pharmacology revealed that flavonoids and diterpenoids from ***Andrographis paniculata* and *Thespesia populnea*** as potential modulators of HBV-induced HCC with negligible side effects and these compounds were predicted to act majorly via the MAPK and PI3K-Akt signaling pathways. Further, flavonoids of ***A. paniculata*** were identified to interact with the HBx active site and may potentially inhibit its interaction with HBXIP. The *in vitro* studies revealed that n-butanol and water fractions of ***T. chebula*** and hydroalcoholic extract of *A. paniculata* as promising antiviral against HBV as these decreased the intracellular HBV DNA and pgRNA level in HepG2.2.15 cell line, inhibited HBV RT and reduced HBsAg and HBeAg secretions in a dose-dependent manner. Also, hydroalcoholic extract of *A. paniculata* was identified as a potent inhibitor of HBx-HBXIP interaction inhibitor.

Currently, there are no specific laboratory animal models are available to study HBV infection because HBV can only infect humans and chimpanzees and this study identified **Lipopolysaccharide and Alcohol-induced** live injury models to resemble HBV immunobiology and pathogenesis through the target identification and gene set enrichment analysis. Finally, all the selected doses ***T. chebula*** and lower and medium doses ***A. paniculata*** and their **combinations** were shown promising **hepatoprotective activity**. Hence, the combination of higher doses of *T. chebula* and lower doses of *A. paniculata* could be a promising therapy for HBV infection and associated complications like HCC.

# LIMITATION & PROSPECTIVE

The current study identified and validated anti-HBV and hepatoprotective bioactives through *in silico, in vitro* studies, and in the animal model predicted to mimic the HBV infection. Further, the identified leads need to be tested in HBV-infected chimpanzees and/or in clinical settings. Also, the study was conducted only as an alternative therapy, however, these leads need to be tested in combination with conventional anti-HBV drugs like Lamivudine, Tenofovir, Tenofovir Disoproxil Fumarate, etc., and for their herb-drug interaction, PK-PD profile for developing adjuvant therapy for HBV patients.

# REFERENCES

1. Tu T, Patel K, Shackel NA. Viral Hepatitis. Genomic Precis Med Prim Care Third Ed. 2017;317–40.
2. Louten J. Hepatitis Viruses. Essent Hum Virol. 2016;213–33. Available from: https://linkinghub.elsevier.com/retrieve/pii/B9780128009475000120
3. Nelson NP, Easterbrook PJ, McMahon BJ. Epidemiology of Hepatitis B Virus Infection and Impact of Vaccination on Disease. Clin Liver Dis. 2016;20(4):607–28.
4. Rajbhandari R, Chung RT. Treatment of Hepatitis B: A Concise Review. Clin Transl Gastroenterol. 2016;7(9):e190.
5. Stein L, Loomba R. Drug Targets in Hepatitis B Virus Infection. Infect Disord - Drug Targets. 2012;9(2):105–16.
6. K U, T T, K M. Three envelope proteins of hepatitis B virus: large S, middle S, and major S proteins needed for the formation of Dane particles. J Virol. 1991;65(7):3521–9.
7. Mehmankhah M, Bhat R, Anvar MS, Ali S, Alam A, Farooqui A, et al. Structure-Guided Approach to Identify Potential Inhibitors of Large Envelope Protein to Prevent Hepatitis B Virus Infection. Oxid Med Cell Longev. 2019;2019:1297484.
8. Wen YM, Wu L, Lin X, Qian GS, Lu PX. Full-length genomic analysis of hepatitis B virus isolates in a patient progressing from hepatitis to hepatocellular carcinoma. J Med Virol. 2001;64(3):299–304.
9. Jones SA, Clark DN, Cao F, Tavis JE, Hu J. Comparative analysis of hepatitis B virus polymerase sequences required for viral RNA binding, RNA packaging, and protein priming. J Virol. 2014;88(3):1564–72.
10. Okamoto H, Yotsumoto S, Akahane Y, Yamanaka T, Miyazaki Y, Sugai Y, et al.

Hepatitis B viruses with precore region defects prevail in persistently infected hosts along with seroconversion to the antibody against e antigen. J Virol. 1990;64(3):1298–303.

11. Slagle BL, Bouchard MJ. Hepatitis B Virus X and Regulation of Viral Gene Expression. Cold Spring Harb Perspect Med. 2016;6(3):a021402.
12. Edwards TC, Ponzar NL, Tavis JE. Shedding light on RNaseH: a promising target for hepatitis B virus (HBV). Expert Opin Ther Targets. 2019;23(7):559.
13. de Clercq E, Férir G, Kaptein S, Neyts J. Antiviral treatment of chronic hepatitis B virus (HBV) infections. Viruses. 2010;2(6):1279–305.
14. Clark DN, Hu J. Hepatitis B virus reverse transcriptase - Target of current antiviral therapy and future drug development. Antiviral Res. 2015;123:132–7.
15. Fernandez-Fernandez B, Montoya-Ferrer A, Sanz AB, Sanchez-Niño MD, Izquierdo MC, Poveda J, et al. Tenofovir nephrotoxicity: 2011 update. AIDS Res Treat. 2011;2011:354908.
16. Fleischer RD, Lok ASF. Myopathy and neuropathy associated with nucleos(t)ide analog therapy for hepatitis B. J Hepatol. 2009;51(4):787–91.
17. Wu D, Ning Q. Toward a Cure for Hepatitis B Virus Infection: Combination Therapy Involving Viral Suppression and Immune Modulation and Long-term Outcome. J Infect Dis. 2017;216(8):S771–7.
18. Ekor M. The growing use of herbal medicines: issues relating to adverse reactions and challenges in monitoring safety. Front Pharmacol. 2013;4:177.
19. Savinaya MS, Patil SS, Narayana J and K V. Traditional medicine knowledge and diversity of medicinal plants in Sharavathi valley region of central western ghats. Int J Herb Med. 2016;4(6):124–30.
20. Block TM, Alter HJ, London WT, Bray M. A historical perspective on the

discovery and elucidation of the hepatitis B virus. Antiviral Res. 2016;131:109–23.

21. Dane DS, Cameron CH, Briggs M. Virus-like particles in serum of patients with Australia-antigen-associated hepatitis. Lancet (London, England). 1970;1(7649):695–8.
22. Seeger C, Mason WS. Molecular biology of hepatitis B virus infection. Virology. 2015;479–480:672–86.
23. Nguyen DH, Ludgate L, Hu J. Hepatitis B virus–cell interactions and pathogenesis. J Cell Physiol. 2008;216(2):289–94.
24. Altinel K, Hashimoto K, Wei Y, Neuveut C, Gupta I, Suzuki AM, et al. Single-Nucleotide Resolution Mapping of Hepatitis B Virus Promoters in Infected Human Livers and Hepatocellular Carcinoma. J Virol. 2016;90(23):10811–22.
25. Tsukuda S, Watashi K. Hepatitis B virus biology and life cycle. Antiviral Res. 2020;182:104925.
26. Dias JD, Sarica N, Neuveut C. Early Steps of Hepatitis B Life Cycle: From Capsid Nuclear Import to cccDNA Formation. Viruses. 2021;13(5):757.
27. Bhattacharya H, Parai D, Sahoo SK, Swain A, Pattnaik M, Mohapatra I, et al. Hepatitis B virus infection among the tribal and particularly vulnerable tribal population from an eastern state of India: Findings from the serosurvey in seven tribal dominated districts, 2021–2022. Front Microbiol. 2023;14:1039696.
28. Niklasch M, Zimmermann P, Nassal M. The Hepatitis B Virus Nucleocapsid-Dynamic Compartment for Infectious Virus Production and New Antiviral Target. Biomedicines. 2021;9(11):1577.
29. Zhao F, Xie X, Tan X, Yu H, Tian M, Lv H, et al. The Functions of Hepatitis B Virus Encoding Proteins: Viral Persistence and Liver Pathogenesis. Front

Immunol. 2021;12:691766.

30. Churin Y, Roderfeld M, Roeb E. Hepatitis B virus large surface protein: function and fame. Hepatobiliary Surg Nutr. 2015;4(1):1.

31. Wei L, Ploss A. Mechanism of Hepatitis B Virus cccDNA Formation. Viruses. 2021;13(8):1463.

32. Guo JT, Guo H. Metabolism and function of hepatitis B virus cccDNA: Implications for the development of cccDNA-targeting antiviral therapeutics. Antiviral Res. 2015;122:91.

33. Liu K, Luckenbaugh L, Ning X, Xi J, Hu J. Multiple roles of core protein linker in hepatitis B virus replication. PLOS Pathog. 2018;14(5):e1007085.

34. Bock CT, Schwinn S, Locarnini S, Fyfe J, Manns MP, Trautwein C, et al. Structural organization of the hepatitis B virus minichromosome. J Mol Biol. 2001;307(1):183–96.

35. Pollicino T, Belloni L, Raffa G, Pediconi N, Squadrito G, Raimondo G, et al. Hepatitis B virus replication is regulated by the acetylation status of hepatitis B virus cccDNA-bound H3 and H4 histones. Gastroenterology. 2006;130(3):823–37.

36. Alexopoulou A, Karayiannis P, George' S. HBeAg negative variants and their role in the natural history of chronic hepatitis B virus infection. World J Gastroenterol. 2014;20(24):7644–52.

37. Wang Y, Cui L, Yang G, Zhan J, Guo L, Chen Y, et al. Hepatitis B e Antigen Inhibits NF-κB Activity by Interrupting K63-Linked Ubiquitination of NEMO. J Virol. 2019;93(2):e00667-18.

38. Ozaki T, Nakagawara A. Role of p53 in Cell Death and Human Cancers. Cancers (Basel). 2011;3(1):994.

39. Gearhart TL, Bouchard MJ. The hepatitis B virus HBx protein modulates cell cycle regulatory proteins in cultured primary human hepatocytes. Virus Res. 2011;155(1):363–7.

40. You H, Qin S, Zhang F, Hu W, Li X, Liu D, et al. Regulation of Pattern-Recognition Receptor Signaling by HBX During Hepatitis B Virus Infection. Front Immunol. 2022;13:438.

41. Zhu M, Guo J, Li W, Xia H, Lu Y, Dong X, et al. HBx induced AFP receptor expressed to activate PI3K/AKT signal to promote expression of Src in liver cells and hepatoma cells. BMC Cancer. 2015;15(1):362.

42. Bouchard M, Giannakopoulos S, Wang EH, Tanese N, Schneider RJ. Hepatitis B Virus HBx Protein Activation of Cyclin A – Cyclin-Dependent Kinase 2 Complexes and G 1 Transit via a Src Kinase Pathway. J Virol. 2001;75(9):4247–57.

43. Gearhart TL, Bouchard MJ. The hepatitis B virus HBx protein modulates cell cycle regulatory proteins in cultured primary human hepatocytes. Virus Research. 2012;155(1):363–7.

44. Sivasudhan E, Blake N, Lu Z, Meng J, Rong R. Hepatitis B Viral Protein HBx and the Molecular Mechanisms Modulating the Hallmarks of Hepatocellular Carcinoma: A Comprehensive Review. Cells. 2022;11(4):741.

45. Guo H, Zhou T, Jiang D, Cuconati A, Xiao GH, Block TM, et al. Regulation of Hepatitis B Virus Replication by the Phosphatidylinositol 3-Kinase-Akt Signal Transduction Pathway. J Virol. 2007;81(18):10072.

46. Xiang K, Wang B. Role of the PI3K-AKT-mTOR pathway in hepatitis B virus infection and replication. Mol Med Rep. 2018;17(3):4713–9.

47. Mani SKK, Andrisani O. Interferon signaling during Hepatitis B Virus (HBV)

infection and HBV-associated hepatocellular carcinoma. Cytokine. 2019;124:154518.

48. Lu X, Chen Q, Liu H, Zhang X. Interplay Between Non-Canonical NF-κB Signaling and Hepatitis B Virus Infection. Front Immunol. 2021;12:730684.
49. Zhao W. Negative regulation of TBK1-mediated antiviral immunity. Febs Lett. 2013;587(6):542.
50. Branda M, Wands JR. Signal transduction cascades and hepatitis B and C related hepatocellular carcinoma. Hepatology. 2006;43(5):891–902.
51. Friedman SL. Liver fibrosis - From bench to bedside. J Hepatol Suppl. 2003;38(1):S38-53.
52. Popper H, Udenfriend S. Hepatic fibrosis. Correlation of biochemical and morphologic investigations. Am J Med. 1970;49(5):707–21.
53. Schaffner F, Klion FM. Chronic hepatitis. Annu Rev Med. 1968;19:25–38.
54. Bataller R, Brenner DA. Liver fibrosis. J Clin Invest. 2005;115(2):209–18.
55. Schaffner F, Popper H. Capillarization of Hepatic Sinusoids in Man. Gastroenterology. 1963;44(3):239–42.
56. Riordan SM, Williams R. The intestinal flora and bacterial infection in cirrhosis. J Hepatol. 2006;45(5):744–57.
57. Schuppan D, Afdhal NH. Liver Cirrhosis. Lancet. 2008;371(9615):838.
58. Noverati N, Bashir-Hamidu R, Halegoua-Demarzio D, Hann HW. Hepatitis B Virus-Associated Hepatocellular Carcinoma and Chronic Stress. Int J Mol Sci. 2022;23(7):3917.
59. Lin J, Wu JF, Zhang Q, Zhang HW, Cao GW. Virus-related liver cirrhosis: Molecular basis and therapeutic options. World J Gastroenterol. 2014;20(21):6457–69.

60. Cholongitas E, Tziomalos K, Pipili C. Management of patients with hepatitis B in special populations. World J Gastroenterol. 2015;21(6):1738.

61. Ward H, Tang L, Poonia B, Kottilil S. Treatment of hepatitis B virus: an update. Future Microbiol. 2016;11(12):1581.

62. Terrault NA, Lok ASF, McMahon BJ, Chang KM, Hwang JP, Jonas MM, et al. Update on prevention, diagnosis, and treatment of chronic hepatitis B: AASLD 2018 hepatitis B guidance. Hepatology. 2018;67(4):1560–99.

63. Brunetto MR, Bonino F. Interferon therapy of chronic hepatitis B. Intervirology. 2014;57(3–4):163–70.

64. Ye J, Chen J. Interferon and Hepatitis B: Current and Future Perspectives. Front Immunol. 2021;12:1–11.

65. Halegoua-De Marzio D, Hann HW. Then and now: The progress in hepatitis B treatment over the past 20 years. World J Gastroenterol. 2014;20(2):401–13.

66. Pol S, Lampertico P. First-line treatment of chronic hepatitis B with entecavir or tenofovir in 'real-life' settings: from clinical trials to clinical practice. J Viral Hepat. 2012;19(6):377.

67. Hu J, Lin YY, Chen PJ, Watashi K, Wakita T. Cell and Animal Models for Studying Hepatitis B Virus Infection and Drug Development. Gastroenterology. 2019;156(2):338.

68. Guo WN, Zhu B, Ai L, Yang DL, Wang BJ. Animal models for the study of hepatitis B virus infection. Zool Res. 2018;39(1):25.

69. Barker LF, Chisari F V., McGrath PP, Dalgard DW, Kirschstein RL, Almeida JD, et al. Transmission of type B viral hepatitis to chimpanzees. J Infect Dis. 1973;127(6):648–62.

70. Allweiss L, Dandri M. Experimental *in vitro* and *in vivo* models for the study of

human hepatitis B virus infection. J Hepatol. 2016;64(1):S17–31.

71. Verrier ER, Colpitts CC, Schuster C, Zeisel MB, Baumert TF. Cell Culture Models for the Investigation of Hepatitis B and D Virus Infection. Viruses. 2016;8(9):261.

72. Du Y, Broering R, Li X, Zhang X, Liu J, Yang D, et al. *In vivo* Mouse Models for Hepatitis B Virus Infection and Their Application. Front Immunol. 2021;12:766534.

73. Ye L, Yu H, Li C, Hirsch ML, Zhang L, Samulski RJ, et al. Adeno-Associated Virus Vector Mediated Delivery of the HBV Genome Induces Chronic Hepatitis B Virus Infection and Liver Fibrosis in Mice. PLoS One. 2015;10(6):e0130052.

74. Sun D, Nassal M. Stable HepG2- and Huh7-based human hepatoma cell lines for efficient regulated expression of infectious hepatitis B virus. J Hepatol. 2006;45(5):636–45.

75. Bhat SA, Ahanger IA, Kazim SN. Forthcoming Developmentsin Models to Study the HepatitisB Virus Replication Cycle, Pathogenesis, and Pharmacological Advancements. ACS Omega. 2023;8(16):14273.

76. Xu R, Hu P, Li Y, Tian A, Li J, Zhu C. Advances in HBV infection and replication systems *in vitro*. Virol J. 2021;18(1):1–15.

77. Tao Y, Wu D, Zhou L, Chen E, Liu C, Tang X, et al. Present and Future Therapies for Chronic Hepatitis B. Adv Exp Med Biol. 2020;1179:137–86.

78. Kaswala D, Shah S, Patel N, Raisoni S, Swaminathan S. Hydroxycut-induced Liver Toxicity. Ann Med Health Sci Res. 2014;4(1):143.

79. Ostapowicz G, Fontana RJ, Schioødt F V., Larson A, Davern TJ, Han SHB, et al. Results of a prospective study of acute liver failure at 17 tertiary care centers in the United States. Ann Intern Med. 2002;137(12):947–54.

80. Gillessen A, Schmidt HHJ. Silymarin as Supportive Treatment in Liver Diseases: A Narrative Review. Adv Ther. 2020;37(4):1279.

81. Wagner H, Diesel P, Seitz M. The chemistry and analysis of silymarin from Silybum marianum Gaertn. Drug Research (formerly Arzneimittelforschung). 1974;24(4):466–71.

82. Bijak M. Silybin, a Major Bioactive Component of Milk Thistle (*Silybum marianum* L. Gaernt.)-Chemistry, Bioavailability, and Metabolism. Molecules. 2017;22(11).

83. Federico A, Dallio M, Loguercio C. Silymarin/Silybin and Chronic Liver Disease: A Marriage of Many Years. Molecules. 2017;22(2):191.

84. Papackova Z, Heczkova M, Dankova H, Sticova E, Lodererova A, Bartonova L, et al. Silymarin prevents acetaminophen-induced hepatotoxicity in mice. PLoS One. 2018;13(1).

85. Arman M, Chowdhury KAA, Bari MS, Khan MF, Huq MMA, Haque MA, et al. Hepatoprotective potential of selected medicinally important herbs: evidence from ethnomedicinal, toxicological and pharmacological evaluations. Phytochem Rev. 2022;21(6):1863–86.

86. Upadhya V, Hegde H V., Mesta D, Belchad S, Hampannavar V, Kholkute SD. Digital database on ethno-medicinal plants of western ghats. Current Science. 2010;99:1658–9.

87. Medicinal Plants of Western Ghats. [cited 2023 Sep 16]. Available from: https://wgbis.ces.iisc.ac.in/biodiversity/sahyadri_enews/newsletter/issue12/mainframe.htm

88. Goyal M, Pareek A, Nagori BP, Sasmal D. *Aerva lanata*: A Review on Phytochemistry and Pharmacological Aspects. Pharmacogn Rev.

2011;5(10):195–8.

89. Srivastav S, Singh P, Mishra G, Jha KK, Khosa RL. *Achyranthes aspera*-An important medicinal plant: A review. J Nat Prod Plant Resour. 2011;1(1):1–14.

90. Cui Y, Ye Q, Wang H, Li Y, Yao W, Qian H. Hepatoprotective potential of *Aloe vera* polysaccharides against chronic alcohol-induced hepatotoxicity in mice. J Sci Food Agric. 2014;94(9):1764–71.

91. Parvez MK, Al-Dosari MS, Alam P, Rehman MT, Alajmi MF, Alqahtani AS. The anti-hepatitis B virus therapeutic potential of anthraquinones derived from *Aloe vera*. Phytother Res. 2019;33(11):2960–70.

92. Europe A, Search A, Europe J. Hepatoprotective activity of andrographolide against galactosamine & paracetamol. Indian J Med Res. 1990:92:284-92.

93. Kapil A, Koul IB, Banerjee SK, Gupta BD. Antihepatotoxic effects of major diterpenoid constituents of *Andrographis paniculata*. Biochem Pharmacol. 1993;46(1):182–5.

94. Jadhav AK, Karuppayil SM. *Andrographis paniculata* (Burm. F) Wall ex Nees: Antiviral properties. Phytother Res. 2021;35(10):5365-5373

95. Atkhuu JB, Attori KH, Akano FT, Ushiya SF, Shiman K ichi O. Suppression of NO Production in Activated Macrophages *in vitro* and ex Vivo by Neoandrographolide Isolated from *Andrographis paniculata*. Biol Pharm Bull. 2002;25:1169–74.

96. Silva FL, Fischer DCH, Tavares JF, Silva MS, De Athayde-Filho PF, Barbosa-Filho JM. Compilation of Secondary Metabolites from *Bidens pilosa* L. Molecules. 2011;16(2):1070–102.

97. Ayub A, Ashfaq UA, Haque A. HBV induced HCC: major risk factors from genetic to molecular level. Biomed Res Int. 2013;2013:810461.

98. Thanigaivel S, Durgadevi H, Balasubramaniam J, Mythily V, Elanchezhiyan M. Comparative evaluation of the anti-Hepatitis B virus activity of *Centella asiatica* and *Camellia sinensis* (green tea). BMC Infect Dis. 2014;14(3):1–1.

99. Puri A, Patil S. Biogenic Synthesis of Selenium Nanoparticles using *Diospyros montana* Bark Extract: Characterization, Antioxidant, Antibacterial, and Antiproliferative Activity. Biosci Biotechnol Res Asia. 2022;19(2):423–41.

100. Venugopal S, Alagesan V. Brief Review of the Genus *Diospyros montana* Roxb: Phytopharmacological Properties. Extensive Rev. 2022;2(1):11–9.

101. Banu S, Bhaskar B, Balasekar P. Hepatoprotective and antioxidant activity of *Leucas aspera* against D-galactosamine induced liver damage in rats. Pharm Biol. 2012;50(12):1592–5.

102. Pourahmad J, Eskandari MR, Shakibaei R, Kamalinejad M. A search for hepatoprotective activity of fruit extract of *Mangifera indica* L. against oxidative stress cytotoxicity. Plant Foods Hum Nutr. 2010;65(1):83–9.

103. Karuppanan M, Krishnan M, Padarthi P, Namasivayam E. Hepatoprotective and Antioxidant Effect of *Mangifera Indica* Leaf Extracts against Mercuric Chloride-induced Liver Toxicity in Mice. Euroasian J Hepato-Gastroenterology. 2014;4(1):18.

104. Jahnavi C, Lakshmi Geetika D, Shrutha Keerthi G, Santhosha D, Ramesh A, Author C, et al. Review on pharmacological activities of *Mangifera indica* and *Zingiber officinale*. J Pharmacogn Phytochem. 2020;9(3):1166–70.

105. Venkateswaran PS, Millman I, Blumberg BS. Effects of an extract from *Phyllanthus niruri* on hepatitis B and woodchuck hepatitis viruses: *in vitro* and *in vivo* studies. Proc Natl Acad Sci U S A. 1987;84(1):274–8.

106. Mathayan M, Jayaraman S, Kulanthaivel L, Suresh A. Inhibition studies of HBV

DNA polymerase using seed extracts of *Pongamia pinnata*. Bioinformation. 2019;15(7):506.

107. Elkousy RH, Said ZNA, Abd El-Baseer MA, Abu El wafa SA. Antiviral activity of castor oil plant (*Ricinus communis*) leaf extracts. J Ethnopharmacol. 2021;271:113878.

108. Atanu FO, Ebiloma UG, Ajayi EI. A review of the pharmacological aspects of Solanum nigrum Linn. Biotechnol Mol Biol Rev. 2011;6(1):1–007.

109. Javed T, Ashfaq UA, Riaz S, Rehman S, Riazuddin S. In-vitro antiviral activity of *Solanum nigrum* against Hepatitis C Virus. Virol J. 2011;8(1):1–7.

110. Patel K, Laloo D, Singh GK, Gadewar M, Patel DK. A review on medicinal uses, analytical techniques and pharmacological activities of *Strychnos nux-vomica* Linn.: A concise report. Chin J Integr Med. 2017;1–13.

111. Patil VS, Harish DR, Vetrivel U, Roy S, Deshpande SH, Hegde H V. Hepatitis C Virus NS3/4A Inhibition and Host Immunomodulation by Tannins from *Terminalia chebula*: A Structural Perspective. Molecules. 2022;27(3):1076.

112. Ajala OS, Jukov A, Ma CM. Hepatitis C virus inhibitory hydrolysable tannins from the fruits of *Terminalia chebula*. Fitoterapia. 2014;99(1):117–23.

113. Patil VS, Harish DR, Vetrivel U, Deshpande SH, Khanal P, Hegde H V., et al. Pharmacoinformatics Analysis Reveals Flavonoids and Diterpenoids from *Andrographis paniculata* and *Thespesia populnea* to Target Hepatocellular Carcinoma Induced by Hepatitis B Virus. Appl Sci. 2022;12(21):10691

114. Dogra NK, Kumar S. A review on ethno-medicinal uses and pharmacology of *Vernonia cinerea* Less. Nat Prod Res. 2015;29(12):1102–17.

115. . DS, . ST, . TK. Vernonia Cinerea: A Review. J Curr Pharma Res. 2014;4(3):1194–200.

116. Kelley LA, Mezulis S, Yates CM, Wass MN, Sternberg MJE. The Phyre2 web portal for protein modeling, prediction and analysis. Nat Protoc. 2015;10(6):845–58.

117. Feig M. Local Protein Structure Refinement via Molecular Dynamics Simulations with locPREFMD. J Chem Inf Model. 2016;56(7):1304–12.

118. Heo L, Park H, Seok C. GalaxyRefine: protein structure refinement driven by side-chain repacking. Nucleic Acids Res. 2013;41:W384.

119. Lansdon EB, Samuel D, Lagpacan L, Brendza KM, White KL, Hung M, et al. Visualizing the Molecular Interactions of a Nucleotide Analog, GS-9148, with HIV-1 Reverse Transcriptase–DNA Complex. J Mol Biol. 2010;397(4):967–78.

120. Fiser A, Sali A. ModLoop: automated modeling of loops in protein structures. Bioinformatics. 2003;19(18):2500–1.

121. Bowers KJ, Chow DE, Xu H, Dror RO, Eastwood MP, Gregersen BA, et al. Scalable Algorithms for Molecular Dynamics Simulations on Commodity Clusters. In: ACM/IEEE SC 2006 Conference (SC'06). IEEE; 2006. p. 43–43.

122. Samdani A, Vetrivel U. POAP: A GNU parallel based multithreaded pipeline of open babel and AutoDock suite for boosted high throughput virtual screening. Comput Biol Chem. 2018;74:39–48.

123. Genheden S, Ryde U. The MM/PBSA and MM/GBSA methods to estimate ligand-binding affinities. Expert Opin Drug Discov. 2015;10(5):449.

124. Liu T, Lin Y, Wen X, Jorissen RN, Gilson MK. BindingDB: A web-accessible database of experimentally determined protein-ligand binding affinities. Nucleic Acids Res. 2007;35:D198-201.

125. Franz M, Lopes CT, Fong D, Kucera M, Cheung M, Siper MC, et al. Cytoscape.js 2023 update: a graph theory library for visualization and analysis. Bioinformatics.

2023;39(1):btad031.

126. Shannon P, Markiel A, Ozier O, Baliga NS, Wang JT, Ramage D, et al. Cytoscape: a software environment for integrated models of biomolecular interaction networks. Genome Res. 2003;13(11):2498–504.

127. Lagunin A, Stepanchikova A, Filimonov D, Poroikov V. PASS: prediction of activity spectra for biologically active substances. Bioinformatics. 2000;16(8):747–8.

128. Ivanov SM, Lagunin AA, Rudik A V., Filimonov DA, Poroikov V V. ADVERPred-Web Service for Prediction of Adverse Effects of Drugs. J Chem Inf Model. 2018;58(1):8–11.

129. Kanehisa M, Furumichi M, Tanabe M, Sato Y, Morishima K. KEGG: new perspectives on genomes, pathways, diseases and drugs. Nucleic Acids Res. 2017;45(D1):D353–61.

130. Szklarczyk D, Gable AL, Nastou KC, Lyon D, Kirsch R, Pyysalo S, et al. The STRING database in 2021: customizable protein–protein networks, and functional characterization of user-uploaded gene/measurement sets. Nucleic Acids Res. 2021;49(D1):D605–12.

131. Eswar N, Webb B, Marti-Renom MA, Madhusudhan MS, Eramian D, Shen M, et al. Comparative Protein Structure Modeling Using MODELLER. Curr Protoc Protein Sci. 2007;50(1):2.9.1-2.9.31

132. Källberg M, Wang H, Wang S, Peng J, Wang Z, Lu H, et al. Template-based protein structure modeling using the RaptorX web server. Nat Protoc. 2012;7(8):1511–22.

133. Dominguez C, Boelens R, Bonvin AMJJ. HADDOCK: A protein-protein docking approach based on biochemical or biophysical information. J Am Chem Soc.

2003;125(7):1731–7.

134. Rebhan M, Chalifa-Caspi V, Prilusky J, Lancet D. GeneCards: a novel functional genomics compendium with automated data mining and query reformulation support. Bioinformatics. 1998;14(8):656–64.

135. Patil PP, Patil VS, Khanal P, Darasaguppe HR, Charla R, Bhatkande A, et al. Network pharmacology and *in vitro* testing of *Theobroma cacao* extract's antioxidative activity and its effects on cancer cell survival. PLoS One. 2022;17(4):e0259757.

136. Rezaee-Khorasany A, Razavi BM, Taghiabadi E, Yazdi AT, Hosseinzadeh H. Effect of crocin, an active saffron constituent, on ethanol toxicity in the rat: histopathological and biochemical studies. Iran J Basic Med Sci. 2020;23(1):51.

137. Thonangi CV, Vedula GS, Bitra VR, Killari KN, Akula A. Bio-Assay Guided Identification of Antioxidant Fractions from Methanolic Extract of *Polyalthia longifolia* Seeds and their Hepatoprotective Effects against Ethanol Induced Oxidative Stress. Indian J Pharm Sci. 2022;84(4):902–9.

138. Hebbani AV, Vaddi DR, DD PP, NCh V. Protective effect of *Terminalia arjuna* against alcohol induced oxidative damage of rat erythrocyte membranes. J Ayurveda Integr Med. 2021;12(2):330–9.

139. Mo Q, Zhou G, Xie B, Ma B, Zang X, Chen Y, et al. Evaluation of the hepatoprotective effect of *Yigan mingmu* oral liquid against acute alcohol-induced liver injury in rats. BMC Complement Med Ther. 2020;20(1):32.

140. Abdel Maksoud HA, Abdel Magid AD, Mostafa YM, Elharrif MG, Sorour RI, Sorour MI. Ameliorative effect of liquorice extract versus silymarin in experimentally induced chronic hepatitis: A biochemical and genetical study. Clin Nutr Exp. 2019;23:69–79.

141. Sedlak J, Lindsay RH. Estimation of total, protein-bound, and nonprotein sulfhydryl groups in tissue with Ellman's reagent. Anal Biochem. 1968;25(1):192–205.

142. Nandi A, Chatterjee IB. Scavenging of superoxide radical by ascorbic acid. J Biosci. 1987;11(1–4):435–41.

143. Ohkawa H, Ohishi N, Yagi K. Assay for lipid peroxides in animal tissues by thiobarbituric acid reaction. Anal Biochem. 1979;95(2):351–8.

144. Sigismund S, Avanzato D, Lanzetti L. Emerging functions of the EGFR in cancer. Mol Oncol. 2018;12(1):3.

145. Gajiwala KS, Feng J, Ferre R, Ryan K, Brodsky O, Weinrich S, et al. Insights into the aberrant activity of mutant EGFR kinase domain and drug recognition. Structure. 2013;21(2):209–19.

146. Buhlig TS, Bowersox AF, Braun DL, Owsley DN, James KD, Aranda AJ, et al. Molecular, Evolutionary, and Structural Analysis of the Terminal Protein Domain of Hepatitis B Virus Polymerase, a Potential Drug Target. Viruses. 2020;12(5):570.

147. Xu X, Thai H, Kitrinos KM, Xia G, Gaggar A, Paulson M, et al. Modeling the functional state of the reverse transcriptase of hepatitis B virus and its application to probing drug-protein interaction. BMC Bioinformatics. 2016;17(Suppl 8):280.

148. Pan SY, Zhou SF, Gao SH, Yu ZL, Zhang SF, Tang MK, et al. New Perspectives on How to Discover Drugs from Herbal Medicines: CAM's Outstanding Contribution to Modern Therapeutics. Evid Based Complement Alternat Med. 2013;2013.

149. Remali J, Aizat WM. A Review on Plant Bioactive Compounds and Their Modes of Action Against Coronavirus Infection. Front Pharmacol. 2021;11:589044.

150. Jones SA, Hu J. Hepatitis B virus reverse transcriptase: diverse functions as classical and emerging targets for antiviral intervention. Emerg Microbes Infect. 2013;2(9):e56.

151. Clark DN, Hu J. Unveiling the roles of HBV polymerase for new antiviral strategies. Future Virol. 2015;10(3):283.

152. Ono-Nita SK, Kato N, Shiratori Y, Masaki T, Lan KH, Carrilho FJ, et al. YMDD motif in hepatitis B virus DNA polymerase influences on replication and lamivudine resistance: A study by *in vitro* full-length viral DNA transfection. Hepatology. 1999;29(3):939–45.

153. Veber DF, Johnson SR, Cheng HY, Smith BR, Ward KW, Kopple KD. Molecular properties that influence the oral bioavailability of drug candidates. J Med Chem. 2002;45(12):2615–23.

154. Alshammari TM. Drug safety : The concept, inception and its importance in patients' health. Saudi Pharm J. 2016;24(4):405–12.

155. Raschi E. Drug- and herb-induced liver injury: Progress, current challenges and emerging signals of post-marketing risk. World J Hepatol. 2015;7(13):1761.

156. Stickel F, Patsenker E, Schuppan D. Herbal hepatotoxicity. J Hepatol. 2005;43:901–10.

157. Chen S, Jiang H, Cao Y, Wang Y, Hu Z, Zhu Z, et al. Drug target identification using network analysis: Taking active components in Sini decoction as an example. Nat Publ Gr. 2016;6:24245.

158. Todorov D, Hinkov A, Shishkova K, Shishkov S. Antiviral potential of Bulgarian medicinal plants. Phytochemistry Reviews. 2014;13:525–38.

159. Herrscher C, Roingeard P, Blanchard E. Hepatitis B Virus Entry into Cells. Cells. 2020;9(6):1486.

160. Iwamoto M, Saso W, Nishioka K, Ohashi H, Sugiyama R, Ryo A, et al. The machinery for endocytosis of epidermal growth factor receptor coordinates the transport of incoming hepatitis B virus to the endosomal network. J Biol Chem. 2020;295(3):800–7.

161. Iwamoto M, Saso W, Sugiyama R, Ishii K, Ohki M, Nagamori S, et al. Epidermal growth factor receptor is a host-entry cofactor triggering hepatitis B virus internalization. Proc Natl Acad Sci U S A. 2019;116(17):8487–92.

162. Chen SW, Himeno M, Koui Y, Sugiyama M, Nishitsuji H, Mizokami M, et al. Modulation of hepatitis B virus infection by epidermal growth factor secreted from liver sinusoidal endothelial cells. Sci Rep. 2020;10(1):14349.

163. Berasain C, Avila MA. The EGFR signalling system in the liver: From hepatoprotection to hepatocarcinogenesis. J Gastroenterol; 2014;49:9–23.

164. Komposch K, Sibilia M. EGFR signaling in liver diseases. Vol. 17, International Journal of Molecular Sciences. 2015;17(1):30

165. Kearney BP, Flaherty JF, Shah J. Tenofovir disoproxil fumarate: clinical pharmacology and pharmacokinetics. Clin Pharmacokinet. 2004;43(9):595–612.

166. Kim TG, Kang SY, Jung KK, Kang JH, Lee E, Han HM, et al. Antiviral activities of extracts isolated from *Terminalis chebula* Retz., *Sanguisorba officinalis* L., *Rubus coreanus* Miq. and *Rheum palmatum* L. against hepatitis B virus. Phytother Res. 2001;15(8):718–20.

167. Lee SJ, Lee HK, Jung MK, Mar W. *In vitro* antiviral activity of 1,2,3,4,6-penta-O-galloyl-beta-D-glucose against hepatitis B virus. Biol Pharm Bull. 2006;29(10):2131–4.

168. Chen H, Ma YB, Huang XY, Geng CA, Zhao Y, Wang LJ, et al. Synthesis, structure–activity relationships and biological evaluation of

dehydroandrographolide and andrographolide derivatives as novel anti-hepatitis B virus agents. Bioorg Med Chem Lett. 2014;24(10):2353–9.

169. Sa-Nguanmoo P, Rianthavorn P, Amornsawadwattana S, Poovorawan Y. Hepatitis B virus infection in non-human primates. Acta Virol. 2009;53(2):73–82.

170. Wieland SF. The Chimpanzee Model for Hepatitis B Virus Infection. Cold Spring Harb Perspect Med. 2015;5(6):1–19.

171. Ortega-Prieto AM, Cherry C, Gunn H, Dorner M. *In vivo* Model Systems for Hepatitis B Virus Research. ACS Infect Dis. 2019;5(5):688.

172. Tan A, Koh S, Bertoletti A. Immune Response in Hepatitis B Virus Infection. Cold Spring Harb Perspect Med. 2015;5(8):1–18.

173. Wu YH, Hu SQ, Liu J, Cao HC, Xu W, Li YJ, et al. Nature and mechanisms of hepatocyte apoptosis induced by D-galactosamine/lipopolysaccharide challenge in mice. Int J Mol Med. 2014;33(6):1498–506.

174. Wills PJ, Asha V V. Protective effect of *Lygodium flexuosum* (L.) Sw. (Lygodiaceae) against D-galactosamine induced liver injury in rats. J Ethnopharmacol. 2006;108(1):116–23.

175. Mondal M, Hossain MM, Hasan MR, Tarun MTI, Islam MAF, Choudhuri MSK, et al. Hepatoprotective and Antioxidant Capacity of *Mallotus repandus* Ethyl Acetate Stem Extract against d-Galactosamine-Induced Hepatotoxicity in Rats. ACS Omega. 2020;5(12):6523.

176. Bag A, Bhattacharyya SK, Chattopadhyay RR. The development of *Terminalia chebula* Retz. (Combretaceae) in clinical research. Asian Pac J Trop Biomed. 2013;3(3):244.

177. Ratha KK, Joshi GC. Haritaki (*Chebulic myrobalan*) and its varieties. Ayu.

2013;34(3):331.

178. Chattopadhyay R, Bhattacharyya S, Bhattacharyya S, Bhattacharyya S. *Terminalia chebula*: An Update. Pharmacogn Rev. 2007;1(1):151-156.

179. Li S, Ye T, Liang L, Liang W, Jian P, Zhou K, et al. Anti-cancer activity of an ethyl-acetate extract of the fruits of *Terminalia bellerica* (Gaertn.) Roxb. through an apoptotic signaling pathway *in vitro*. J Tradit Chinese Med Sci. 2018;5(4):370–9.

180. Shankara BER, Ramachandra YL, Rajan SS, Ganapathy PSS, Yarla NS, Richard SA, et al. Evaluating the Anticancer Potential of Ethanolic Gall Extract of *Terminalia chebula* (Gaertn.) Retz. (Combretaceae). Pharmacognosy Res. 2016;8(3):209–12.

181. Tasduq SA, Singh K, Satti NK, Gupta DK, Suri KA, Johri RK. *Terminalia chebula* (fruit) prevents liver toxicity caused by sub-chronic administration of rifampicin, isoniazid and pyrazinamide in combination. Hum Exp Toxicol. 2006;25(3):111–8.

182. Yang MH, Ali Z KI. Anti-inflammatory activity of the synthetic C-C biflavonoids. JPP. 2006;58:1661–7.

183. Lee Y, Byun HS, Seok JH, Park KA, Won M, Seo W, et al. *Terminalia Chebula* provides protection against dual modes of necroptotic and apoptotic cell death upon death receptor ligation. Sci Rep. 2016 Apr 27;6.

184. Ghosh N, Ghosh R, Mandal V, Mandal SC. Recent advances in herbal medicine for treatment of liver diseases. Pharm Biol. 2011;49:970–88.

185. Seok PR, Kim JH, Kwon HR, Heo JS, Choi JR, Shin JH. Protective effects of *Gastrodia elata* Blume on acetaminophen-induced liver and kidney toxicity in rats. Food Sci Biotechnol. 2018;27(5):1445.

186. Cohen JA, Kaplan MM. The SGOT/SGPT ratio--an indicator of alcoholic liver disease. Dig Dis Sci. 1979;24(11):835–8.

187. McGill MR. The past and present of serum aminotransferases and the future of liver injury biomarkers. EXCLI J. 2016;15:817.

188. Soeters PB, Wolfe RR, Shenkin A. Hypoalbuminemia: Pathogenesis and Clinical Significance. J Parenter Enteral Nutr. 2019;43(2):181.

189. Vitek L, Ostrow JD. Bilirubin Chemistry and Metabolism; Harmful and Protective Aspects. Curr Pharm Des. 2009;15(25):2869–83.

190. Wolf MJ, Beunen G, Casaer P, Wolf B. Extreme hyperbilirubinaemia in Zimbabwean neonates: Neurodevelopmental outcome at 4 months. Eur J Pediatr. 1997;156(10):803–7.

191. Fanjul-Moles ML, López-Riquelme GO. Relationship between Oxidative Stress, Circadian Rhythms, and AMD. Oxid Med Cell Longev. 2016;2016.

192. Das SK, Vasudevan DM. Alcohol-induced oxidative stress. Life Sci. 2007;81(3):177–87.

193. Nordmann R, Ribière C, Rouach H. Ethanol-induced lipid peroxidation and oxidative stress in extrahepatic tissues. Alcohol Alcohol. 1990;25(2–3):231–7.

194. Thurman RG, Bradford BU, Iimuro Y, Knecht KT, Arteel GE, Yin M, et al. The role of gut-derived bacterial toxins and free radicals in alcohol-induced liver injury. J Gastroenterol Hepatol. 1998;13(S1):S39–50.

195. Yin M, Wheeler MD, Kono H, Bradford BU, Gallucci RM, Luster MI, et al. Essential role of tumor necrosis factor α in alcohol-induced liver injury in mice. Gastroenterology. 1999;117(4):942–52.

196. Olleros ML, Martin ML, Vesin D, Fotio AL, Santiago-Raber ML, Rubbia-Brandt L, et al. Fat diet and alcohol-induced steatohepatitis after LPS challenge in mice:

Role of bioactive TNF and Th1 type cytokines. Cytokine. 2008;44(1):118–25.

197. Fabrizi F, Donato FM, Messa P. Association between hepatitis B virus and chronic kidney disease: a systematic review and meta-analysis. Ann Hepatol. 2017;16(1):21–47.

198. Epstein M. Alcohol's Impact on Kidney Function. Alcohol Health Res World. 1997;21(1):84.

# ANNEXURES

Certificate from Institutional Biosafety Committee (IBSC), RCGM-DBT, Govt. of India for the conduct of research on HepG2.2.15 cell line for anti-HBV activity. **Letter No:** BT/IBKP/475/2021**; IBKP TAI No:** C100753.

भारत सरकार
विज्ञान और प्रौद्योगिकी मंत्रालय
जैव प्रौद्योगिकी विभाग
GOVERNMENT OF INDIA
MINISTRY OF SCIENCE & TECHNOLOGY
DEPARTMENT OF BIOTECHNOLOGY

सत्यमेव जयते

स्वच्छ भारत
एक कदम स्वच्छता की ओर

ब्लॉक-2, 7वां तल, सी0जी0ओ0 कम्पलेक्स
लोधी रोड, नई दिल्ली-110003
Block-2, 7th Floor, C.G.O. Complex
Lodhi Road, New Delhi-110003
Tele : 011-24365071 Fax : 011-24362884
Website : http://www.dbtindia.nic.in

**No. BT/IBKP/475/2021** **Dated: 03.11.2021**

**To**

Dr. Harish D R
Scientist B
ICMR- National Institute of Traditional Medicine, Belagavi
Dr Harish D R ICMR National Institute of Traditional Medicine
Belagavi, Belgaum-590010, Karnataka
Email: - drharish49@gmail.com

**Subject:** Applications submitted by ICMR-National Institute of Traditional Medicine, Belagavi for the information and records of Review Committee on Genetic Manipulation (RCGM) on the projects involving recombinant DNA technology.

Sir/Madam,

It is informed that the applications to carry out following research and development work were considered and noted by the Review Committee on Genetic Manipulation (RCGM) in its 217th meeting held on 14.10.2021:

i. To carry out research and development work on Evaluation of anti-hepatitis B virus inhibitory and hepato-protective activity of crude extract / enriched fractions / pure compounds from traditional medicinal plants. (IBKP TAI No: C100753)

ii. To carry out research and development work on Evaluation of anti-Cholera toxin activity of pure herbal compounds or their extracts from traditional medicinal plants. (IBKP TAI No: C100735)

iii. To carry out research and development work on Screening of antimicrobial activity of herbal formulations/or their phytocompounds on highly virulent enteric bacterias isolated from clinical samples and their toxins. (IBKP TAI No: C100738)

2. You are required to comply with the Regulations and Guidelines for Recombinant DNA Research and Biocontainment, 2017.

**Please acknowledge the receipt of the letter.**

Yours faithfully,

(Dr. Nitin K. Jain)
Member Secretary, RCGM &
Scientist-'F', DBT

Approval from IAEC committee of ICMR – National Institute of Traditional Medicine, Belagavi for animal experimentation. Resolution No. IAEC/1CMR-NITM BGM/Apr2022/1).

आई सी एम आर – राष्ट्रीय पारम्परिक चिकित्साविज्ञान संस्थान
स्वास्थ्य अनुसंधान विभाग, स्वास्थ्य एवं परिवार
कल्याण मंत्रालय, भारत सरकार

ICMR - National Institute of Traditional Medicine
Department of Health Research, Ministry of Health and Family Welfare, Government of India

Institutional Animal Ethical Committee

Reg. No. 1388/GO/Re/S/10/CPCSEA DATED 03.02.2022

Resolution No. IAEC/ICMR-NITM BGM/Apr2022/1

Date: 27.04.2022

**CERTIFICATE**

This is to certify that the research project proposed by Dr. Harish D. R. / Mr. Vishal S. Patil entitled "Virtual Screening and Experimental Validation of Bioactive Constituents from Selected Medicinal Plants of Western Ghats Region against Hepatitis B Virus and its Associated Complications" has been approved by IAEC. The approval granted for one year with following number of animals.

| Species | Gender/Age | Number of Animals |
|---|---|---|
| Wistar Rats | Either sex | 72 |
| Wistar Rats | Female | 18 |

The investigator must report the outcome of the experiment to IAEC/CPCSEA. The approved number/species/gender of animals should not be changed without prior permission of IAEC/CPCSEA.

**Dr. Vinay Tikare**
CPCSEA Main Nominee

**Dr. Harish D. R.** 27/01/22.
Member Secretary

**Dr. Banappa S Unger** 27/04/22
Chairman

नेहरू नगर, नेशनल हाईवे नं. 4,
बेलगावी, कर्नाटक – 590 010, भारत
Nehru Nagar, National Highway No. 4,
Belagavi, Karnataka - 590 010, India

आज़ादी का अमृत महोत्सव

Tel: +91-831-2475477
Fax: +91-831-2475479
| director.nitm@icmr.gov.in
| director.nitm.bg@gmail.com | www.icmrnitm.res.in

# PUBLICATIONS

1. Patil VS, Harish DR, Vetrivel U, Deshpande SH, Khanal P, Hegde HV, Roy S, Jalalpure SS. Pharmacoinformatics Analysis Reveals Flavonoids and Diterpenoids from *Andrographis paniculata* and *Thespesia populnea* to Target Hepatocellular Carcinoma Induced by Hepatitis B Virus. Applied Sciences. 2022;12(21):10691. [IF: 2.7].
2. Patil VS, Harish DR, Sampat GH, Roy S, Jalalpure SS, Khanal P, Gujarathi SS, Hegde HV. System Biology Investigation Revealed Lipopolysaccharide and Alcohol-Induced Hepatocellular Carcinoma Resembled Hepatitis B Virus Immunobiology and Pathogenesis. International Journal of Molecular Sciences. 2023;24(13):11146. [IF: 5.6].
3. Patil VS, Harish DR, Charla R, Vetrivel U, Jalalpure SS, Bhandare VV, Deshpande SH, Hegde HV, Roy S. Structural insights into modeling of hepatitis B virus reverse transcriptase and identification of its inhibitors from potential medicinal plants of Western Ghats: an *in silico* and *in vitro* study. Journal of Biomolecular Structure and Dynamics. 2023:1-9. [IF: 4.4]

applied sciences

MDPI

*Article*

# Pharmacoinformatics Analysis Reveals Flavonoids and Diterpenoids from *Andrographis paniculata* and *Thespesia populnea* to Target Hepatocellular Carcinoma Induced by Hepatitis B Virus

**Vishal S. Patil [1,2], Darasaguppe R. Harish [1,*], Umashankar Vetrivel [1,3], Sanjay H. Deshpande [1,4], Pukar Khanal [5], Harsha V. Hegde [1], Subarna Roy [1,*] and Sunil S. Jalalpure [2,*]**

1 ICMR-National Institute of Traditional Medicine, Nehru Nagar, Belagavi 590010, India
2 KLE College of Pharmacy, Belagavi, KLE Academy of Higher Education and Research, Nehru Nagar, Belagavi 590010, India
3 ICMR-National Institute for Research in Tuberculosis, Chetpet, Chennai 600031, India
4 Regional Centre for Biotechnology, NCR-Biotech Science Cluster, Faridabad 121001, India
5 Department of Pharmacology, NGSM Institute of Pharmaceutical Sciences, NITTE Deemed-to-be University, Mangalore 575018, India
* Correspondence: harish.dr@icmr.gov.in (D.R.H.); roys@icmr.gov.in (S.R.); jalalpuresunil@rediffmail.com (S.S.J.)

check for updates

**Citation:** Patil, V.S.; Harish, D.R.; Vetrivel, U.; Deshpande, S.H.; Khanal, P.; Hegde, H.V.; Roy, S.; Jalalpure, S.S. Pharmacoinformatics Analysis Reveals Flavonoids and Diterpenoids from *Andrographis paniculata* and *Thespesia populnea* to Target Hepatocellular Carcinoma Induced by Hepatitis B Virus. *Appl. Sci.* **2022**, *12*, 10691. https://doi.org/10.3390/app122110691

Academic Editors: Snezana Agatonovic-Kustrin, Antonija Tomić and Dejan Agić

Received: 19 September 2022
Accepted: 19 October 2022
Published: 22 October 2022



**Abstract:** Herbs are widely utilized in the Western Ghats region of India to treat liver diseases and viral-like infections. However, such practices lack scientific evidence at the molecular level and may often pose adverse drug reactions. This study intends to identify phytocompounds with druggability and non-toxic profiles with potential activity against hepatitis B virus-induced hepatocellular carcinoma. The details of phytocompounds in traditionally utilized herbs in the Western Ghats region were collated from chemical databases and publications. The druggability and toxicity of these compounds were predicted using MolSoft and ADVERpred, respectively. The probable targets of these phytocompounds were predicted using BindingDB. Moreover, compound-gene set pathways, cellular processes, and functional enrichment analyses were also performed using STRING and KEGG pathway databases. Subsequently, herb–compound–target–disease pathway networks were constructed using Cytoscape. The potential hub protein was virtually screened against the ligand dataset using the POAP pipeline. Finally, molecular dynamics (MD) simulations of the most potential protein–ligand complexes were performed in triplicate using Schrödinger Desmond. Amongst 274 compounds from 16 herbs studied, 36 showed drug-likeness with nontoxic properties and were also predicted to modulate 16 potential targets involved in the pathogenesis of HBV-induced HCC. Among all the molecules screened, flavonoids and diterpenoids from *Andrographis paniculata* and *Thespesia populnea* scored the highest edge count via modulating multiple targets and pathways. Moreover, molecular docking and MD simulation (100ns) also inferred that the top-ranking Andrographin and Gossypetin exhibit stable intermolecular interactions with EGFR protein, which was identified as a highly connected hub protein in the constructed network. All these findings are suggestive of identified moieties as potential therapeutics for targeting HBV-associated HCC sans adverse drug reactions.

**Keywords:** *Andrographis paniculata*; hepatitis B; hepatocellular carcinoma; molecular docking; molecular dynamics; network pharmacology; *Thespesia populnea*

## 1. Introduction

Hepatitis B, caused by the hepatitis B virus (HBV), is a life-threatening chronic liver infection and is one of the major risk factors for the development of hepatocellular carcinoma (HCC), which accounts for 70–90% of all primary liver cancers. HCC is the sixth

International Journal of
*Molecular Sciences*

MDPI

*Article*

# System Biology Investigation Revealed Lipopolysaccharide and Alcohol-Induced Hepatocellular Carcinoma Resembled Hepatitis B Virus Immunobiology and Pathogenesis

**Vishal S. Patil [1,2], Darasaguppe R. Harish [1,*], Ganesh H. Sampat [1,2], Subarna Roy [1,*], Sunil S. Jalalpure [2], Pukar Khanal [2], Swarup S. Gujarathi [1,2] and Harsha V. Hegde [1]**

[1] ICMR-National Institute of Traditional Medicine, Nehru Nagar, Belagavi 590010, India; vishalpatil6377@gmail.com (V.S.P.); ganeshsampat72272@gmail.com (G.H.S.); bhavsargam7744896491@gmail.com (S.S.G.); harshah@icmr.gov.in (H.V.H.)
[2] KLE College of Pharmacy, Belagavi, KLE Academy of Higher Education and Research, Belagavi 590010, India; jalalpuresunil@rediffmail.com (S.S.J.); pukarkhanal58@gmail.com (P.K.)
* Correspondence: harish.dr@icmr.gov.in (D.R.H.); roys@icmr.gov.in (S.R.)

**Abstract:** Hepatitis B infection caused by the hepatitis B virus is a life-threatening cause of liver fibrosis, cirrhosis, and hepatocellular carcinoma. Researchers have produced multiple in vivo models for hepatitis B virus (HBV) and, currently, there are no specific laboratory animal models available to study HBV pathogenesis or immune response; nonetheless, their limitations prevent them from being used to study HBV pathogenesis, immune response, or therapeutic methods because HBV can only infect humans and chimpanzees. The current study is the first of its kind to identify a suitable chemically induced liver cirrhosis/HCC model that parallels HBV pathophysiology. Initially, data from the peer-reviewed literature and the GeneCards database were compiled to identify the genes that HBV and seven drugs (acetaminophen, isoniazid, alcohol, D-galactosamine, lipopolysaccharide, thioacetamide, and rifampicin) regulate. Functional enrichment analysis was performed in the STRING server. The network HBV/Chemical, genes, and pathways were constructed by Cytoscape 3.6.1. About 1546 genes were modulated by HBV, of which 25.2% and 17.6% of the genes were common for alcohol and lipopolysaccharide-induced hepatitis. In accordance with the enrichment analysis, HBV activates the signaling pathways for apoptosis, cell cycle, PI3K-Akt, TNF, JAK-STAT, MAPK, chemokines, NF-kappa B, and TGF-beta. In addition, alcohol and lipopolysaccharide significantly activated these pathways more than other chemicals, with higher gene counts and lower FDR scores. In conclusion, alcohol-induced hepatitis could be a suitable model to study chronic HBV infection and lipopolysaccharide-induced hepatitis for an acute inflammatory response to HBV.

**Keywords:** alcohol; hepatitis B; hepatocellular carcinoma; lipopolysaccharide; network pharmacology; rodent model



**Citation:** Patil, V.S.; Harish, D.R.; Sampat, G.H.; Roy, S.; Jalalpure, S.S.; Khanal, P.; Gujarathi, S.S.; Hegde, H.V. System Biology Investigation Revealed Lipopolysaccharide and Alcohol-Induced Hepatocellular Carcinoma Resembled Hepatitis B Virus Immunobiology and Pathogenesis. *Int. J. Mol. Sci.* **2023**, *24*, 11146. https://doi.org/10.3390/ijms241311146

Academic Editors: Sigrun Lange and Jameel M. Inal

Received: 14 April 2023
Revised: 5 June 2023
Accepted: 7 June 2023
Published: 6 July 2023



## 1. Introduction

Hepatitis B virus (HBV) is a member of the family Hepadnaviridae, possessing a 3.2 kb short genome with largely double-stranded DNA [1]. The human sodium taurocholate co-transporting polypeptide (NTCP) receptor and the viral envelope protein (HBsAg) interact in a remarkably species-specific manner to allow HBV to enter human hepatocytes [2]. Several liver diseases, including cirrhosis, hepatocellular carcinoma, and liver fibrosis, can develop in those with chronic HBV infection [2]. Despite significant advancements in the diagnosis, prevention, and treatment of chronic hepatitis B (CHB), over 296 million individuals worldwide still have the HBV infection and account for an estimated 820,000 deaths, mostly by cirrhosis and hepatocellular carcinoma (HCC) [3]. Injections of interferon and oral nucleoside analogs are used to treat persistent HBV infection [4]. Currently, HIV and HBV polymerase reverse transcriptase inhibitors are licensed treatments for HBV, and only

JOURNAL OF BIOMOLECULAR STRUCTURE AND DYNAMICS
https://doi.org/10.1080/07391102.2023.2264400



# Structural insights into modeling of hepatitis B virus reverse transcriptase and identification of its inhibitors from potential medicinal plants of Western Ghats: an *in silico* and *in vitro* study

Vishal S. Patil[a,b], Darasaguppe R. Harish[a], Rajitha Charla[a], Umashankar Vetrivel[a,c], Sunil S. Jalalpure[b], Vishwambhar Vishnu Bhandare[a,d], Sanjay H. Deshpande[a,e], Harsha V. Hegde[a] and Subarna Roy[a]

[a]ICMR-National Institute of Traditional Medicine, Belagavi, Karnataka, India; [b]KLE College of Pharmacy, Belagavi, KLE Academy of Higher Education and Research, Belagavi, Karnataka, India; [c]ICMR-National Institute for Research in Tuberculosis, Chennai, Tamil Nadu, India; [d]Department of Microbiology, Shivaji University, Kolhapur, Maharashtra, India; [e]Regional Centre for Biotechnology, NCR-Biotech Science Cluster, Faridabad, India

Communicated by Ramaswamy H. Sarma

**ABSTRACT**

The present study was proposed to model full-length HBV-RT and investigate the intermolecular interactions of known inhibitor and libraries of phytocompounds to probe the potential natural leads by *in silico* and *in vitro* studies. Homology modeling of RT was performed by Phyre2 and Modeller and virtual screening of ligands implemented through POAP pipeline. Molecular dynamics (MD) simulation (100 ns) and MM-GBSA calculations were performed using Schrodinger Desmond and Prime, respectively. Phytocompounds probable host protein targets gene set pathway enrichment and network analysis were executed by KEGG database and Cytoscape software. Prioritized plant extracts/enriched fraction LC-MS analysis was performed and along with pure compound, RT inhibitory activity, time-dependent HBsAg and HBeAg secretion, and intracellular HBV DNA, and pgRNA by qRT-PCR was performed in HepG2.2.15 cell line. Among the screened chemical library of 268 phytocompounds from 18 medicinal plants, 15 molecules from *Terminalia chebula* (6), *Bidens pilosa* (5), and *Centella asiatica* (4)) were identified as potential inhibitors of YMDD and RT1 motif of HBV-RT. MD simulation demonstrated stable interactions of 15 phytocompounds with HBV-RT, of which 1,2,3,4,6-Pentagalloyl Glucose (PGG) was identified as lead molecule. Out of 15 compounds, 11 were predicted to modulate 39 proteins and 15 molecular pathways associated with HBV infection. TCN and TCW (500 μg/mL) showed potent RT inhibition, decreased intracellular HBV DNA, and pgRNA, and time-dependent inhibition of HBsAg and HBeAg levels compared to PGG and Tenofovir Disoproxil Fumarate. We propose that the identified lead molecules from *T. chebula* as promising and cost-effective moieties for the management of HBV infection.

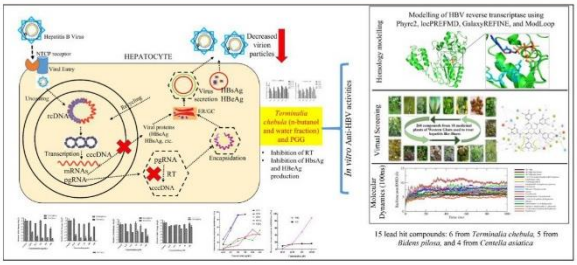


**Abbreviations:** BPHA: *B. pilosa* hydroalcoholic; BPM: *B. pilosa* methanolic; CAHA: *C. asiatica* hydroalcoholic; cccDNA: covalently closed circular DNA; DNA Pol: DNA polymerase; HBeAg: hepatitis B e-antigen; HBsAg: hepatitis B surface antigen; HBV: hepatitis B virus; KEGG: Kyoto Encyclopedia of Genes and Genomes; LC-MS: liquid chromatography-mass spectrometry; locPREFMD: local protein structure refinement *via* molecular dynamics; MD: molecular dynamics; MM-GBSA: molecular mechanics with generalised born and surface area solvation; NTCP: sodium taurocholate co-transporting polypeptide; PCIDB: phytochemical interactions DB; PE: potential energy; PGG: pentagalloylglucose; pgRNA: pregenomic

**ARTICLE HISTORY**
Received 7 July 2023
Accepted 21 September 2023

**KEYWORDS**
Hepatitis B; HepG2.2.15 cell line; molecular modeling; reverse transcriptase; *Terminalia chebula*

**CONTACT** Darasaguppe R. Harish harish.dr@icmr.gov.in ICMR-National Institute of Traditional Medicine, Nehru Nagar, Belagavi, Karnataka, 590010, India; Sunil S. Jalalpure jalalpuresunil@rediffmail.com KLE College of Pharmacy, Belagavi, KLE Academy of Higher Education and Research, Nehru Nagar, Belagavi, Karnataka, 590010, India.

Supplemental data for this article can be accessed online at https://doi.org/10.1080/07391102.2023.2264400.

**9th World Ayurveda Congress & Arogya Expo 2022 organized at Goa. 8th to 11th December 2022**

JSS ACADEMY OF HIGHER EDUCATION & RESEARCH (DEEMED TO BE UNIVERSITY) MYSURU

International Society for Ethnopharmacology

Azadi Ka Amrit Mahotsav

9th SFEC 2022

22nd to 24th April 2022

# International Congress of SOCIETY FOR ETHNOPHARMACOLOGY, INDIA

(Globalizing Local Knowledge and Localizing Global Technologies)

**Theme : Redefining Ethnopharmacology for the Global Health and Wellbeing**

# Certificate of Appreciation

This is to Certify that the Prof./Dr./Mr./Ms ....Vishal S. Patil.....

has been awarded .....PRIZE for the ORAL/POSTER Entitled ..Network biology traced bioactives from traditional medicinal plants of western ghats to target hepatocellular carcinoma induced by hepatitis B virus X protein.

at 9th International Congress of the Society for Ethnopharmacology, India (SFEC-2022) held at JSS College of Pharmacy, JSS Academy of Higher Education & Research, Mysuru, Karnataka, India from 22nd to 24th, April 2022.

| Dr. T.M. Pramod Kumar | Dr. K. Mruthunjaya | Mr. Birendra K. Sarkar |
|---|---|---|
| Organizing Chairman, SFEC - 2022 | Organizing Secretary, SFEC - 2022 | President - SFE - India |

Certificate of International Conference on Drug Discovery- 2022 (ICDD-2022) and presented a poster at BITS Pilani, K K Birla Goa Campus, Organized by Schrodinger/ Date: 10th and 11th November 2022

**Certificate of plants authentication**

*Terminalia chebula*, *Bidens pilosa*, *Centella asiatica*, *Andrographis paniculata*, and *Thespesia populnea* were identified and certified by a qualified plant taxonomist at ICMR-NITM (RMRC), Belagavi and Shri B.M.K Ayurveda Mahavidyalaya (CFR), Belagavi .with voucher specimen number RMRC-1639, RMRC-1640, RMRC-1641, CFR/Auth/06/2023, and RMRC-1714, respectively.

राष्ट्रीय पारम्परिक चिकित्साविज्ञान संस्थान
**ICMR-NATIONAL INSTITUTE OF TRADITIONAL MEDICINE**
(भूतपूर्वक्षेत्रीयआयुर्विज्ञानअनुसंधानकेन्द्रFormerly Regional Medical Research Centre)
Nehru Nagar, Belagavi-590 090

भारतीयआयुर्विज्ञानअनुसंधानपरिषद
**INDIAN COUNCIL OF MEDICAL RESEARCH**
स्वास्थ्यअनुसंधानविभाग, स्वास्थ्यऔरपरिवारकल्याणमंत्रालय, भारतसरकार
Department of Health Research,
Ministry of Health & Family Welfare, Govt. of India

***Dr. Harsha Hegde***
***Scientist-E***
***harshah@icmr.gov.in***

Date: 15-07-2021

**AUTHENTICATION**

This is to authenticate that the plant materials brought by Mr. Vishal Patil, Ph.D. Research Scholar, KLE Academy of Higher Education and Research, Belagavi, are identified as ***Terminalia chebula*** **Retz.** (Combretaceae), ***Bidens pilosa*** **L.** (Asteraceae) and ***Centella asiatica*** **(L.) Urban.** (Apiaceae). The herbarium specimen of the same have been deposited in our herbaria with accession numbers RMRC-1639, RMRC-1640 and RMRC-1641 respectively.

**Harsha Hegde**
**Scientist-E**

राष्ट्रीय पारम्परिक चिकित्साविज्ञान संस्थान
**ICMR-NATIONAL INSTITUTE OF TRADITIONAL MEDICINE**
(भूतपूर्व क्षेत्रीय आयुर्विज्ञान अनुसंधान केन्द्र Formerly Regional Medical Research Centre)
Nehru Nagar, Belagavi-590 010

*Dr. Harsha Hegde*
*Scientist-E*
*harshah@icmr.gov.in*

भारतीय आयुर्विज्ञान अनुसंधान परिषद
**INDIAN COUNCIL OF MEDICAL RESEARCH**
स्वास्थ्य अनुसंधान विभाग, स्वास्थ्य और परिवार कल्याण मंत्रालय, भारत सरकार
Department of Health Research,
Ministry of Health & Family Welfare, Govt. of India

Date: 26-09-2022

## AUTHENTICATION

This is to authenticate that the plant material submitted by Mr. Vishal Patil, Ph.D Student, KAHER, Belagavi is identified as ***Thespesia populnea* (L.) Sol. Ex Correa.** belonging to the family **Malvaceae**. The herbarium specimen of the same has been deposited in our herbaria with accession number RMRC-1714.

**Harsha Hegde**

KLE
EMPOWERING PROFESSIONALS

**SHRI B.M.K. AYURVEDA MAHAVIDYALAYA**
A constituent unit of KLE Academy of Higher Education & Research
Deemed–to-be-University
**Central Research Facility**
**DRUG AUTHENTICATION REPORT**

Outward: - BMK/CRF/12 /2023-24

**Submitted By: K L E Ayurved Pharmacy**
**Submitted Date : 07/01/2023**

**Date of Issue: 12/01/2023**

| SLNo | Sample Name | Scientific Name | Family | Part submitted | CRF Code | Authenticated as | | | |
|---|---|---|---|---|---|---|---|---|---|
| | | | | | | Common Name | Scientific Name | Family | Part Authenticated |
| 1 | Bhunimba | *Andrographis paniculata* Burm. F. | Acanthaceae | Whole Plant | CRF/Auth/06/2023 | Bhunimba | *Andrographis paniculata* Burm. F. | Acanthaceae | Whole Plant |

Signature:
Authentication Expert Name: Dr Divya Khare.
Date: 12/01/2023

CRF
SHAHAPUR, BELGAUM

Signature of Coordinator
ASU Drug Testing Laboratory

# ERRATUM